FRAPCON-3: Modifications to Fuel Rod Material Properties and Performance Models for High-Burnup Application

D. D. Lanning
C. E. Beyer
C. L. Painter

October 1997

Prepared for
the U.S. Nuclear Regulatory Commission

Pacific Northwest National Laboratory
Richland, Washington 99352

Abstract

This volume describes the fuel rod material and performance models that were updated for the FRAPCON-3 steady-state fuel rod performance code. The property and performance models were changed to account for behavior at extended burnup levels up to 65 Gwd/MTU. The property and performance models updated were the fission gas release, fuel thermal conductivity, fuel swelling, fuel relocation, radial power distribution, solid-solid contact gap conductance, cladding corrosion and hydriding, cladding mechanical properties, and cladding axial growth. Each updated property and model was compared to well characterized data up to high burnup levels. The installation of these properties and models in the FRAPCON-3 code along with input instructions are provided in Volume 2 of this report and Volume 3 provides a code assessment based on comparison to integral performance data. The updated FRAPCON-3 code is intended to replace the earlier codes FRAPCON-2 and GAPCON-THERMAL-2.

Glossary

AECL	Atomic Energy of Canada, Ltd.
ANO	Arkansas Nuclear (Commercial nuclear plant from which fuel rod data were taken.)
B&W	Babcock and Wilcox Company
BOL	beginning of life
BR-3	test reactor in Belgium
BWR	boiling water reactor
CEGB	British Central Electricity Generating Board
CRNL	Chalk River National Laboratory (Ontario, Canada)
EOL	end of life
EPMA	electron probe micro analysis
EPRI	Electric Power Research Institute
ESCORE	EPRI Steady-State Core Reload Evaluation (code)- an EPRI steady-state fuel rod performance code
FGR	fission gas release
FRAPT-6	transient analysis code
FRAPCON	steady state fuel rod performance code
FRAPTRAN	new name for former FRAPT codes
GAPCON	An NRC-sponsored fuel performance code series
GT2R2	GAPCON-THERMAL-Revision 2 (Revision 2 of the GAPCON-THERMAL code)
GWd/MTU	Gigawatt day per Metric Ton Uranium
HBEP	High-Burnup Effects Program
IAEA	International Atomic Energy Agency
ID	identification
IFA	instrumented fuel assembly from Halden reactor in Norway
INEEL	Idaho National Environmental and Engineering Laboratory
LHGR	linear heat generation rate
LOCA	loss-of-coolant accident
LWR	light water reactor
NRC	U.S. Nuclear Regulatory Commission
ORIGEN	Oak Ridge Isotope Generation Code
PCI	pellet-cladding interaction
PCMI	pellet-cladding mechanical interaction (same as PCI)
PNNL	Pacific Northwest National Laboratory
PWR	pressurized water reactor
RISO	Danish National Nuclear Laboratory
SIMFUEL	Simulated high-burnup fuel
TD	theoretical density
TVO	A Finnish power utility
XRF	X-ray fluorescence

Contents

Figures

Tables

Executive Summary

Fuel rod material properties and performance models have been updated for the FRAPCON-3 steady-state fuel rod performance code to account for changes in behavior due to extended fuel burnup. Fifteen separate properties and models were reviewed for adequacy at high burnup, and nine were found to need modification. These nine modified properties and models are described in this report volume.

Fission Gas Release: The FRAPCON-3 code has a new two-stage fission gas release (FGR) model. The model was originally developed by Forsberg and Massih where the first stage quantifies the rate of grain-boundary gas accumulation due to diffusion and the concentration levels corresponding to saturation, and the second stage, the kinetics of grain-boundary gas release. Modifications have been made to the model diffusion coefficients with a burnup enhancement term added, and the resolution rate increased to predict high-burnup FGR from fuel rods with both steady-state power and power-bumping operation. The PARAGRASS FGR model has been removed because it underpredicts FGR at moderate to high-burnup levels, and the ANS-5.4 model has been retained because it predicts high-burnup FGR reasonably well for fuel rods operating at steady-state powers. It can calculate the release of volatile radioactive fission products such as iodine, cesium, and tellurium, in addition to xenon and krypton.

Fuel Thermal Conductivity: The MATPRO model for fuel thermal conductivity has been modified to include degradation due to burnup and gadolinia additions based on out-of-reactor simulated, irradiated fuel diffusivity measurements and in-reactor centerline temperature measurements in high-burnup fuel. These changes will help to evaluate commercial fuel operation at higher burnup levels.

Fuel Swelling: The MATPRO model for fuel swelling has been modified. Experimental evidence has suggested that the FSWELL solid fission product-induced swelling rate should be increased. Swelling due to fission-produced gas is not significant at the low fuel temperatures for normal commercial fuel operation to which FRAPCON-3 will be applied, and it has been removed from the swelling model.

Fuel Pellet Cracking and Relocation: The fuel cracking and relocation algorithms in FRAPCON-3 have been modified. The option for *no* crack factor reduction in the pellet thermal conductivity has been retained in FRAPCON-3. The best estimate pellet relocation model developed for GT2R2 has been modified for use in FRAPCON-3 in conjunction with the FRACAS-1 mechanical model.

Radial Power and Temperature Distribution: The power and burnup radial distribution functions in FRAPCON have been modified. A model developed by Lassmann and colleagues at the Institute for Transuranium Elements improves on the original RADAR subroutine for light water reactor applications. Both contain an exponential distribution function that governs the radially dependent buildup of the plutonium and effective cross-sections for the plutonium and uranium isotopes. In order to install and use the TUBRNP sub code, the FRAPCON code has been modified by changing the fuel and cladding temperature calculator from the method of weighted residuals to a more flexible finite-difference scheme. The radial "form factor" (fission rate) arrays generated by TUBRNP are used by both the temperature calculator and the fission gas release subroutines and are mapped into each routine.

Solid-Solid Contact Gap Conductance: The FRAPCON model for solid-solid contact conductance has been modified. As burnup proceeds, the heat conducted through solid-solid fuel pellet to cladding contact increases, and the heat conducted through gases in the gaps decreases. To provide a best-estimate prediction, the contact conductances calculated in subroutine GAPRS are multiplied by 2.9 for contact

pressures greater than 5.9 MPa. In addition the 1.8 multiplier on the roughness sum for closed gaps has been eliminated.

Cladding Corrosion and Hydriding: The MATPRO model for cladding waterside corrosion and hydrogen pickup has been modified. A FORTRAN version of the integrated Electric Power Research Institute ("ESCORE" code) corrosion models for boiling water reactor and pressurized water reactor conditions has replaced the FRAPCON-2 model in subroutine CORROS. The new subroutine's call list is identical to that for the previous subroutine except that it requires the local value of the fast neutron flux. The new subroutine CORROS still provides separate calculations for boiling water reactor and pressurized water reactor types and returns the oxide layer in meters. In addition the hydrogen pickup fraction (subroutine CHUPTK) has been modified to be consistent with high-exposure PWR cladding data.

Cladding Mechanical Properties and Ductility: Mechanical models have been modified. Modifications are provided for the strength coefficient (subroutine CKMN), the strain hardening exponent (subroutine CKMN), and the uniform strain (subroutine CMLIMT) to account for hydriding due to waterside corrosion. The CMLIMT subroutine equations predicting true yield strength and true strain at yield remain unchanged. True uniform strain is calculated using the proposed uniform strain model.

Cladding Axial Growth: The MATPRO model for fuel rod axial growth has been modified. A modified equation replaces the current equation in subroutine CAGROW to bring in fast neutron fluence. The logic for handling the growth strains has been changed to include an accumulation of incremental strains. The cladding growth strains from the array of cladding nodal strains within the mechanical model has been eliminated because this model does not impact the mechanical model predictions.

Each of the above properties and models have been compared to well characterized data and shown to predict these data well up to high-burnup levels. The installation of these properties and models in the FRAPCON-3 along with code input instructions are described in Volume 2 of this report, and Volume 3 provides a code assessment based on comparisons of code predictions to integral performance data.. The updated FRAPCON-3 code is intended to replace the earlier codes FRAPCON-2 and GAPCON-THERMAL-2.

1.0 Introduction

Fuel rod material properties and performance models have been updated in the FRAPCON-3 fuel rod performance code to account for changes in the behavior of materials caused by fuel burnup. A total of 15 material properties and performance models were examined with nine models identified as needing updating to account for high-burnup behavior and operation. These updates are based on in-reactor and ex-reactor experimental results accumulated worldwide over the past decade.

The model updates have been incorporated into the steady-state fuel rod performance code FRAPCON-2 (Berna et al. 1981) to produce FRAPCON-3. The FRAPCON-3 code documentation provided in Volume 2 of this report (Berna et al. 1997) includes the models described in this volume. Some of the models are also applicable to the transient analysis code FRAP-T6 (Siefken et al. 1981) and may be included in future revisions of that code. However, many of the models do not apply to fast transients (on the order of seconds to milliseconds) or to conditions when fuel and cladding temperatures are significantly greater than those experienced in normal fuel rod operation.

The following nine performance models or material properties were updated:

- Fission Gas Release

- Fuel Thermal Conductivity (including effects of burnable absorber additions)

- Fuel Swelling

- Fuel Pellet Cracking and Relocation

- Radial Power Distribution

- Solid-Solid Contact Gap Conductance

- Cladding Corrosion and Hydriding

- Cladding Mechanical Properties and Ductility

- Cladding Axial Growth

The remaining six materials properties or performance models evaluated were assessed to not be significantly impacted by current high-burnup levels, and the models were left unchanged. These six properties or performance models, retained without modification, are discussed in Appendix B. In addition, certain code simplifications and improvements regarding model integration were discovered in the course of model updates and functional assessment. These are documented in this report.

The following sections of this report describe and discuss in turn the nine updated models listed above. For each model, a background for the change is given, the research is summarized that demonstrates the need for model changes, the model changes and their effects are described, and the ranges of application and the estimated uncertainties are stated for the revised model and are compared against the high-burnup data. Some of the original models are referred to as either FRAPCON or MATPRO models (synonymous terms because the FRAPCON code contains a MATPRO materials properties library). Volume 3 of this report assesses these models as they are installed and integrated into the updated FRAPCON-3 code.

2.0 MASSIH: The New Two-Stage Fission Gas Release Model for the FRAPCON-3 Code

2.1 Background

The FRAPCON-2 code contained six fission gas release (FGR) models: PARAGRASS, GRASS, ANS-5.4, MacDonald-Weisman, Beyer-Hann, and Booth Diffusion. Of these, only PARAGRASS (Rest 1980) and ANS-5.4 (ANS-5.4 1982) have been assessed critically against detailed high-burnup experiments and irradiations. Of these FGR models, only ANS-5.4 has been retained in FRAPCON-3. This is because the other models are either too cumbersome and complex (GRASS) or are single-stage and/or empirical models only and are validated only against low-burnup data (Beyer and Hann 1974; Weisman and MacDonald 1969; and Booth 1957). The single-stage models lack treatment of the grain-boundary gas storage mechanism, which has been proven to be significant at burnups greater than 25 GWd/MTU, and the grain boundary gas has been observed to be released during power transients of a few minutes to hours.

The two-stage PARAGRASS FGR model was assessed against high-burnup steady-state fission gas release data by Cunningham and Beyer[a] and found to be unsatisfactory. PARAGRASS also failed to predict high-gas-release data from commercial light water reactor (LWR) rods used in Coleman's (1985) assessment of FRAPCON-2 (VIM5). Therefore, FRAPCON-3 does not contain the PARAGRASS FGR model.

The ANS-5.4 model is an industry standard and compares well to steady-state, high-temperature FGR data at both low and high burnup and can calculate release fractions for radioactive volatile isotopes of xenon, krypton, iodine, cesium, and tellurium. Therefore, the ANS-5.4 model has been retained in FRAPCON-3.

The ANS-5.4 model only includes gas diffusion from the grains as the FGR mechanism, and its temperature and burnup dependent diffusion constants were derived to fit long-term, steady-state FGR data. Therefore, it does not predict the additional FGR that occurs during brief power ramps up to ~50 kW/m at nominal to high burnup (see Figure 2.1). Commercial power reactor fuel can experience such overpower events, occurring hours to days, without shutdown or discharge. The NRC steady-state fuel performance code (and its FGR model options) must be able to predict the fuel behavior from such events, and, therefore, a new or revised FGR model is needed in FRAPCON-3.

(a) Letter report from Pacific Northwest National Laboratory to the Nuclear Regulatory Commission (NRC)/NRR by M. E. Cunningham and C. E. Beyer. *Comparison of FRAPCON-2 to NRC Fuel Performance Data at Intermediate to High Burnup* (1987).
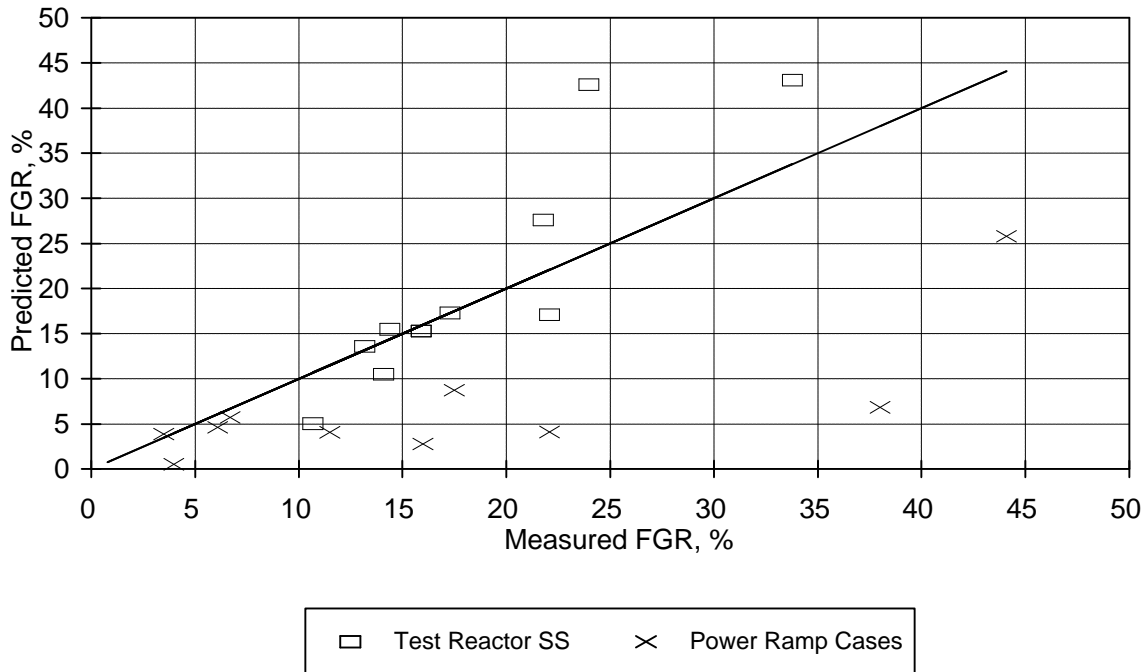
Figure 2.1. ANS-5.4 Model Significantly Underpredicts FGR Data from Power-Ramped Rods

To obtain good FGR predictions for both steady-state and power-ramp performance, it is necessary to recognize the multi-stage nature of thermally activated FGR. This gas diffuses to grain boundaries and precipitates as bubbles on the grain boundaries (intergranular bubbles). In addition, the gas also precipitates as bubbles within the matrix of the grain (intragranular bubbles). The gas atoms can also diffuse to the intragranular bubbles. Fission gas atoms can also be resolved from both types of bubbles back into the matrix due to fission-induced fuel vaporization and condensation at the bubble surface. Bubble coalescence along grain boundaries produces pathways (tunnels) when a "saturation level" (which is temperature dependent due to the temperature dependence of bubble size) by which the grain-boundary gas and perhaps the near-boundary gas is released to the internal void space of the rod during steady-state operation.

It is believed that the inventory of grain-boundary (intergranular) and near-boundary (resolved) gas thus represents additional gas that can also be released rapidly during a power excursion at significant burnup. Thus, a model that recognizes bubble formation on grain boundaries can release the observed "additional FGR" that diffusion alone will not release in the short time of power ramps. Multi-stage gas release models have been proposed by Electric Power Research Institute (EPRI) (Fiero et al. 1987), Argonne National Laboratory (Rest 1980), and the British Central Electricity Generating Board (CEGB) (White and Tucker 1983) among others. The EPRI model was extensively tested at Pacific Northwest National Laboratory against high-burnup cases from pressurized water reactors (PWRs), boiling water reactors (BWRs) and test reactors. The primary cases were from the High-Burnup Effects Program (Barner et al. 1990). Because of the relatively high temperatures required in the model to trigger significant grain-boundary release, the model underpredicted most high-burnup cases. The other two

models listed above (Argonne National Laboratory's GRASS-SST and the related PARAGRASS, and CEGB's model) were considered unnecessarily complex for installation and operation in FRAPCON.

Some previous gas-release models considered that grain growth added to grain-boundary release because the moving grain boundary swept up the bubbles. However, recent power ramping experiments have shown large amounts of FGR resulting from power ramping with very little or no grain growth (Barner et al. 1990). This would indicate that the kinetics for FGR are much faster than grain-growth kinetics.

2.2 Experimental Evidence for Grain-Boundary Gas Storage and Release

Observations of gas accumulation at fuel grain boundaries have long been made. Evidence that the grain-boundary gas is released during power ramps has also been developing for at least a decade.

Attempts to quantify the rate of grain-boundary gas accumulation, the concentration levels corresponding to saturation, and the kinetics of grain-boundary gas accumulation and release are also long standing. Speight (1969) produced one of the early studies on the complexity of resolution at the grain-boundary surface, and Turnbull (1974), White and Tucker (1983), Rest (1980), and Forsberg and Massih (1985) carried this work forward. Lanning and Bradley (1984), Manzel (1993), and Barner et al. (1990) and others have reported attempts to quantify the partition of the produced gas between grain-boundary and matrix fractions in specific fuel samples. Barner et al. (1990) also sought to characterize the release during power ramping, based on detailed microscopy and fission-gas analysis on cross sections from ramped rods and from nonramped siblings with identical pre-ramp irradiation history.

The more recent and better qualified studies point to a consensus regarding the temperature and time dependence of the onset of grain-boundary gas accumulation, for grain-boundary saturation levels, and for rapid grain-boundary release. The simple model of Forsberg and Massih (1985) is attractive because it incorporates all these features while remaining efficient and relatively easy to program. Therefore, a modified version of this model (named MASSIH) was programmed for use in FRAPCON-3.

2.3 Description of the "MASSIH" FGR Model

Appendix A.2 provides detailed descriptions of the Massih/Forsberg model and the modifications to the model incorporated in the MASSIH subroutine. In general, the original MASSIH model is derived from the well-known Booth diffusion model (Booth 1957), which is a solution of the gas-diffusion equation for a spherical grain of fuel with constant temperature, properties, and fission-gas generation. Massih and Forsberg analyzed the accumulation of gas at the grain surface, complicated by the concept of partial resolution of the gas into the grain as it arrives at the boundary. They imposed a saturation criterion for release of gas from the grain boundary to the rod void volume: when the accumulated grain-boundary concentration reaches a 'saturation value' (determined from assumed bubble size and critical areal

coverage of the grain surface by bubbles), the current inventory of grain-boundary gas is released. Following release, the tunnels pinch off because of fuel creep and/or plastic deformation, and the process starts over.

However, Forsberg and Massih do not elucidate what should happen to the gas that is resolved during the accumulation process; it appears to be unavailable for diffusion or release. Furthermore, the resolution fraction proposed by Massih/Forsberg is inversely proportional to the diffusion constant; when the value for the resolution rate proposed by Forsberg et al. (1994) is used, the resolution inventory becomes unrealistically large, and the within-grain inventory unrealistically small at temperatures typical of the outer region of the fuel pellet in normal operation.

These apparent deficiencies have been circumvented, while still retaining Forsberg/Massih's highly efficient solution algorithm, in the following way. The transfer of gas to the grain boundary for a given time step is calculated without regard to resolution (i.e., by using the Forsberg/Massih solution equations with resolution rate set to zero). Then, the gas arriving at the boundary during each time step is partitioned into resolved and grain-boundary accumulation fractions, assuming the same form for the resolution fraction that Massih/Forsberg proposed, but with the resolution rate considered an adjustable parameter.

The adjustment of the model to data then consisted of adjusting the temperature and burnup dependence of the diffusion constant and adjusting the resolution rate until both steady-state and power-ramp data were well predicted. The choices made for these adjustments are described in Appendix A.2.

Because FGR in a given ring of fuel is delayed until the saturation concentration of grain-boundary gas is accumulated or re-accumulated, the FGR versus time for a particular ring proceeds in a sawtooth pattern. See Figures 2.2 and 2.3 where the FGR predicted by MASSIH is shown versus burnup for rings of fuel operating at constant temperatures. The integrated FGR for a number of concentric rings constituting a particular axial section of a rod is a more smooth function of burnup. The predicted integrated FGR behavior vs. burnup for an entire rod is smoother still. In the following section, comparisons are shown between the MASSIH model FGR predictions and high-burnup steady-state and ramp cases for which temperatures can be estimated and FGR has been measured.

2.4 Comparisons Between MASSIH FGR Predictions and Measurements

The modified MASSIH model, with a burnup enhancement on the diffusion constant similar to that for ANS-5.4, was compared to the set of 10 steady-state cases listed in Table 2.1. (The references for these cases are provided in Appendix A.3.) It was found that a large range of correlated pairs of diffusion-constant multipliers and resolution-rate multipliers would result in low-scatter, low-bias matches between predictions and data. The correlated set of parameters resulting in near-zero average deviation corresponds with a minimum in the average deviation plotted against these two variables. This correlation extends all the way from high to low resolution and can be re-generated with varying choices for the activation-energy multiplier.
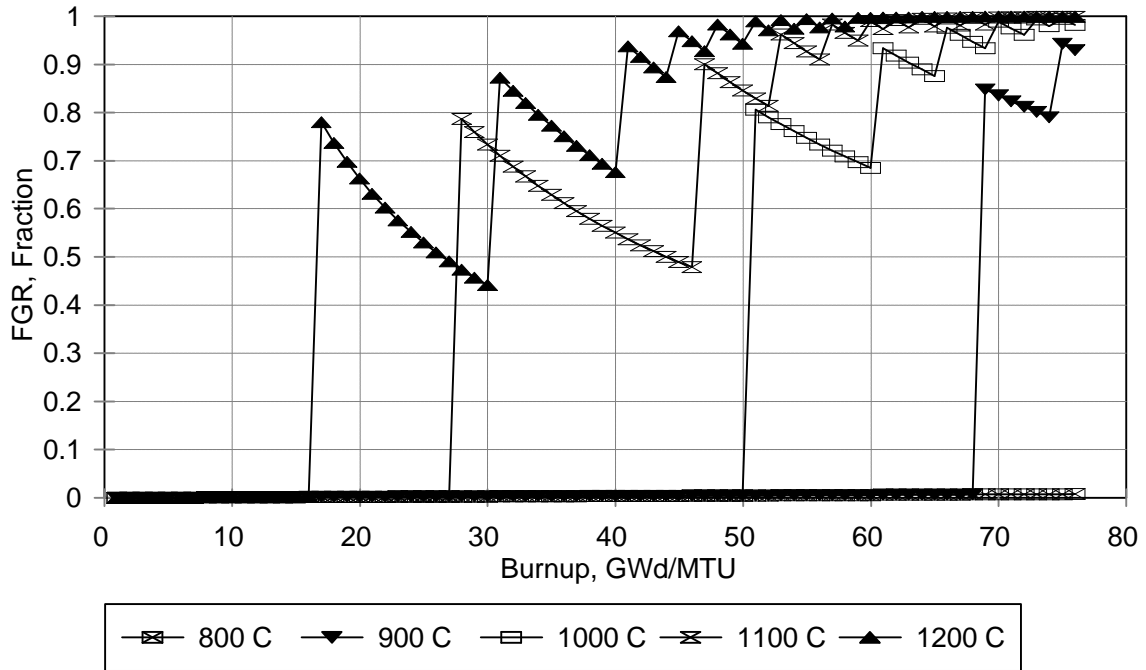
Figure 2.2. Modified MASSIH FGR
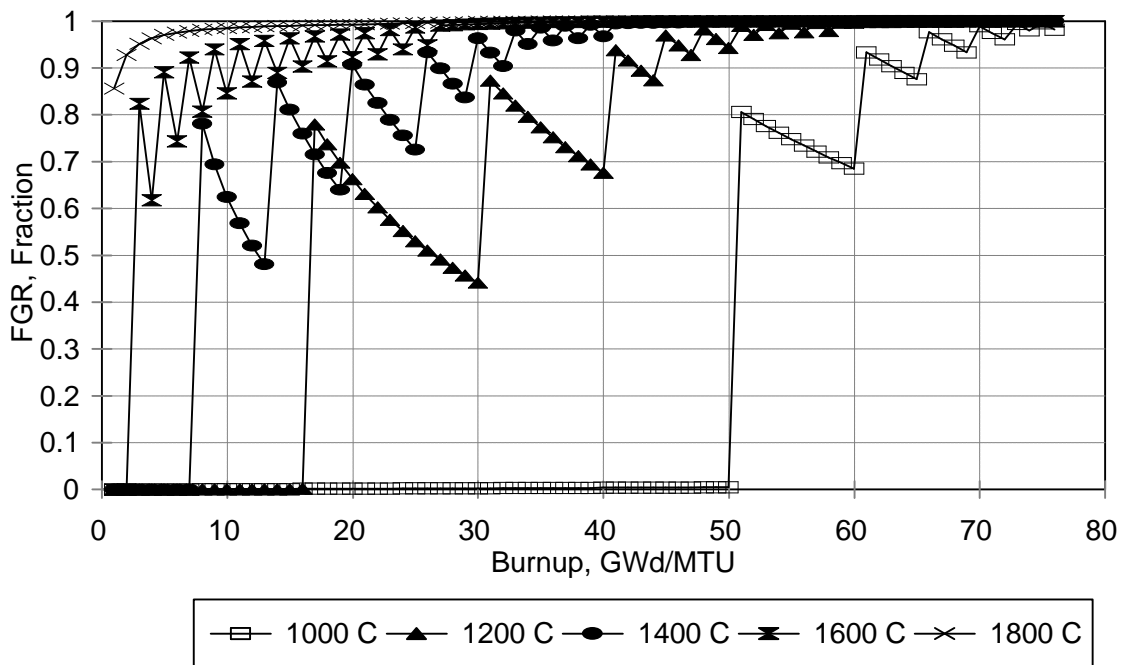
Figure 2.3. Modified MASSIH FGR

Table 2.1. Steady-State Fission Gas Release Case Descriptions (see Appendix A)

Rod Designation	Peak LHGR, kW/m (kW/ft)	Rod-Average Burnup, GWd/MTU	Fission Gas Release, %	Reactor	Fuel Length, Inches
111I5	49.2 (15)	48.6	14.4	BR-3	38.4
36i8	52.5 (16)	61.5	33.8	BR-3	38.4
24i6	55.8 (17)	60.1	21.8	BR-3	38.4
28i6	42.6 (13)	53.3	13.2	BR-3	38.4
LFF	58.4 (17.8)	2.2	17.3	Test	9.57
CBP	55.1 (16.8)	2.7	14.1	Test	6.02
4110-AE2	57.7 (17.6)	6.24	22.1	Test	4.84
4110-BE2	58.4 (17.8)	6.56	15.9	Test	4.84
BNFL Rod DE	42.6 (13)	41.5	10.7	BR-3	39
IFA-429 Rod DH	42.0 (12.8)	73	24	Halden	9.6
(a) IFA = instrument fuel assembly.					

However, when the model was compared to the power-ramp data cases listed in Table 2.2, it was found that only a narrow subset for the activation energy multiplier, the diffusion constant multiplier, and resolution rate was favored. The parameters of the optimzed model are given in Appendix A.2. Figure 2.4 compares the optimized model to the cases from Tables 2.1 and 2.2. As can be seen by comparing Figures 2.1 and 2.4, the MASSIH optimized model predictions are somewhat better than for ANS-5.4 predictions for the steady-state cases and much better for the power-ramp cases. Also, the code-data comparisons as a function of fuel burnup (see Figure 2.5) do not appear to have a bias for steady-state cases. However, the code does appear to underpredict three power-ramp cases where the fuel was known to be densification prone (>2% change in density) and therefore not prototypical of today's low densifying fuel ($\leqslant$1.2% density change). The densification-prone fuel appears to have greater FGR than stable fuel, but has been included for the power ramp cases because of the paucity of power ramp data. The steady-state FGR data do not include densification-prone fuel.

Table 2.2. Description of Selected Power-Ramp FGR Cases (see Appendix A)

Program	Test/Rod Number	Rod-Avg. Burnup, GWd/MTU	Hold Time, Days	RTL,[a] kW/m (kW/ft)	Measured FGR, %
HBEP	D200	25	2.0	41.3 (12.6)	38.0
	D226	44	2.0	43.0 (13.1)	44.1
	PK6-2	35	0.5	40.0 (12.2)	3.5
	PK6-3	35	0.5	43.0 (13.1)	6.7
	PK6-S	35	0.5	41.0 (12.5)	6.1
Inter Ramp	Rod 16	21	1.0	47.9 (14.6)	16.0
	Rod 18	18	1.0	41(12.5)	3.5
RISO FGR	F7-3	35	1.0	38.7 (11.8)	11.4
	F9-3	27	1.0	41.3 (12.6)	17.5
	F14-6	33	3.0	40.7 (12.4)	22.1
(a) RTL = ramp terminal power level.					
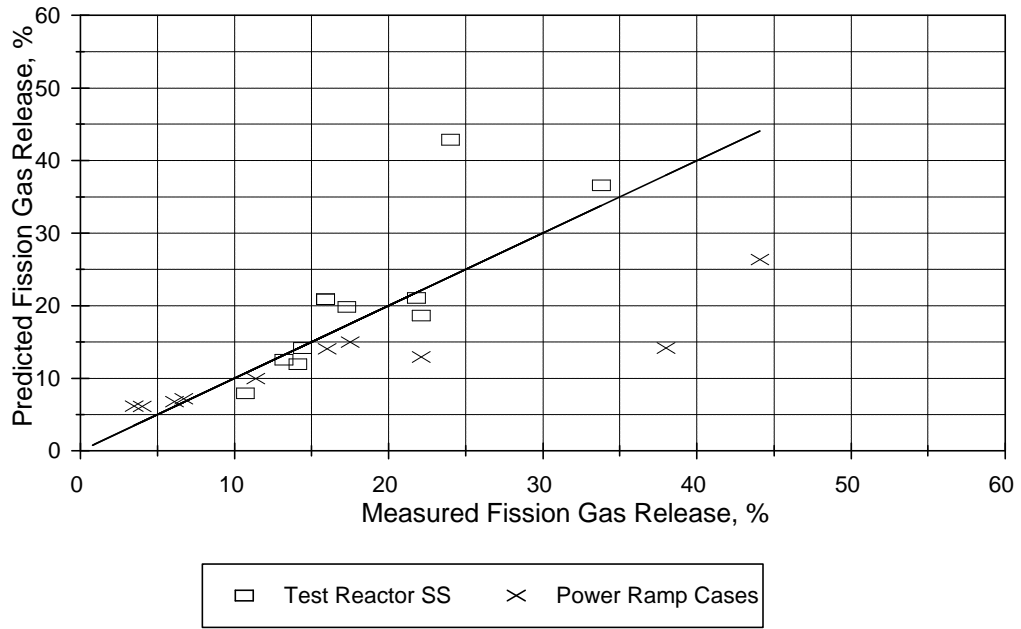
Figure 2.4. Modified MASSIH Model, Compared to High-Burnup Data
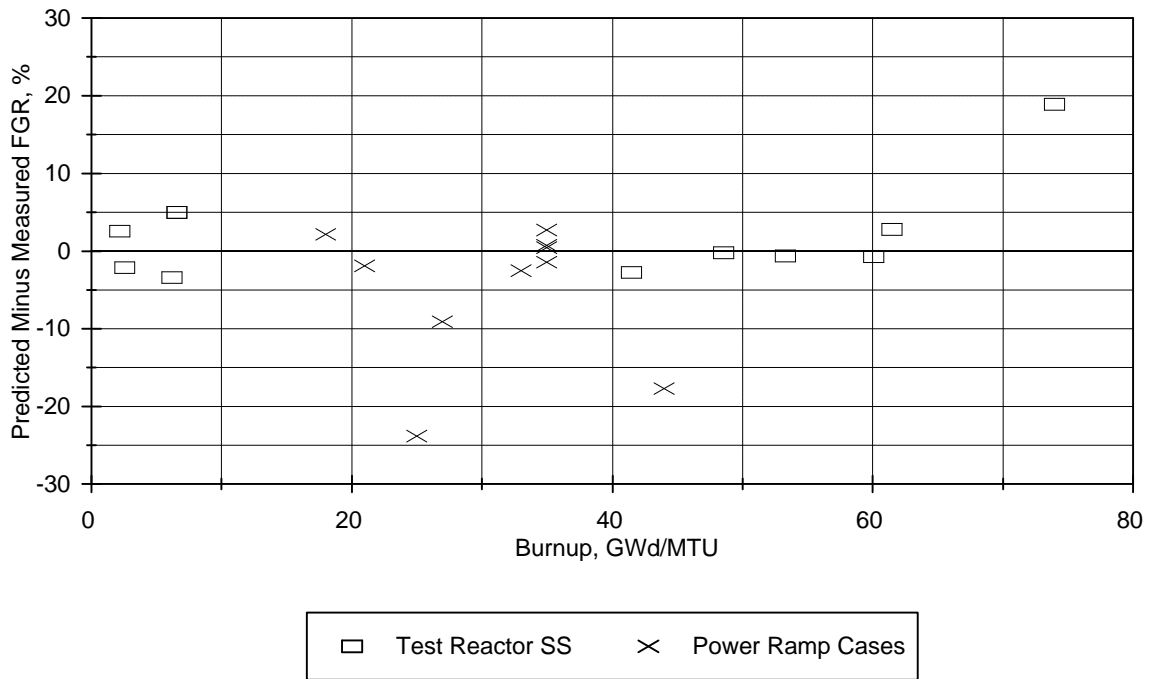
Figure 2.5. Predicted Minus Measured FGR for the Modified MASSIH Gas Release Model

The modified MASSIH model described here has been incorporated into FRAPCON and tested against the integral assessment benchmark cases in Volume 3.

2.4.1 Comparison to Radial Retained Gas Distributions

A more detailed test of the FGR model is to compare the predicted end of life (EOL) radial distribution of retained gas at a selected elevation on a rod to postirradiation measurements of the retained-gas distribution at that elevation. The Third RISØ Fission Gas Release Project (Knudsen et al. 1993) offers such data. These data are not part of the original benchmarking data presented in Tables 2.1 and 2.2 because these data were not available during the development of the models and code. These data are part of an independent data set that was collected after code development was completed and has been used to verify that the code adequately predicts FGR. Further discussion of the independent data set is provided in Beyer et al. 1997. In this program, full-length rods and segmented rods were base-irradiated in various commercial LWRs, then transported to RISØ Laboratories, Denmark. The rods were then refabricated (or in some cases just disassembled) into short segments appropriate for power ramping in the DR-2 test reactor at RISØ. Following ramping, the rods were sectioned and examined. One of the examinations was X-ray fluorescence (XRF) scans of pellet segments extracted from transverse cross-sections, from which the radial distribution of total retained xenon can be deduced.

One rod for which such data were obtained was GE-2. Measured FGR from puncture of this rod was 24.6% following the power ramp and FRAPCON-3 predicted 23%. The design and operating characteristics of this rod are listed in Table 2.3; these were obtained from the OECD/NEA databank (Chantoin et al. 1997). The measured and predicted retained gas distributions for this rod (corresponding to 41.0 kW/m linear heat generation rate [LHGR]) are shown in Figure 2.6. The agreement is excellent in this case except in the low-temperature outermost section of the pellet. It should be noted that the predicted post-ramp integral rod FGR compared well to the measured value. This comparison indicates that the radial distribution of the FGR is well predicted by the MASSIH model, at least when significant release occurs due to a power/temperature ramp at significant burnup.

2.5 Range of Application and Uncertainty of Model

The ranges of application for the MASSIH FGR model based on the range of the data used for benchmarking and independent verification of the code are as follows:

Fuel Center Temperature: 300 to 2200K
Fuel Burnup: 0 to 70 GWd/MTU
Fuel Grain Size: 5 to 30 µm[a]
Time Frames: hours to years (time steps size in the range from 0.1 day to 50 days)

(a) In the modified MASSIH model, the grain size is fixed at 10 µm diameter. For as-fabricated grain diameters greater than 30 µm, the approach may produce somewhat conservative (high) predicted gas release. However, a strong relationship between fuel grain size and fission gas release has not been quantitatively established.

Table 2.3. Characteristics of the GE-2 Test Rod

Fuel Type	UO_2
Fill Gas Type	He
Fill Gas Pressure	97 psia
Cladding Inner/Outer Diameter	0.4185 in./0.4827 in.
Fuel Inner/Outer Diameter	TC hole 0.098 in./0.40984 in.
Base Irradiation Reactor Site	Quad Cities - 1 BWR
Typical Rod Surface temperature in Base Irrad.	550°F
Peak/Average LHGR in Base Irradiation	1.0
Rod-Average Burnup at End of Base Irradiation	42 GWd/MTU
Typical Rod Surface Temp. During Ramping	563°F
Peak-to-Average LHGR Ratio for Ramping	1.05
Peak LHGR During Ramping	42.5 kW/m
Ramp Hold Period	72 hours
FGR at End of Base Irradiation	0.3%
FGR at End of Ramp	24.6%
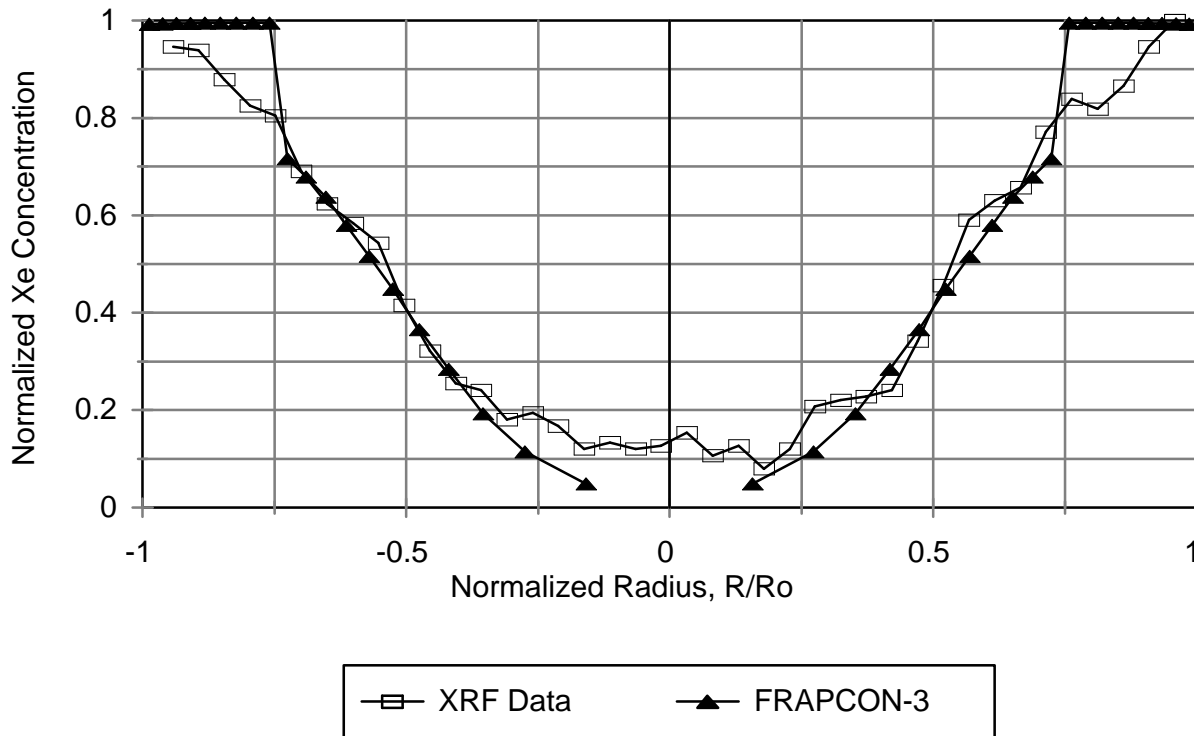
Figure 2.6. Normalized Radial Xenon Distribution in GE-2 Fuel Segment at Terminal Ramped Power of 41 kW/m

The estimated uncertainty (one standard deviation) on fission gas release projections is ± 4.7% absolute FGR for steady-state cases and ± 8% absolute FGR for power-ramp cases when the predicted FGR is in the range from 10 to 30%. These uncertainties are based on comparing statistical analysis of code-data to the 10 steady-state cases listed in Table 2.1 and to the 10 power-ramp cases listed in Table 2.2.

For cases of predicted FGRs greater than 30%, the estimated uncertainty is ± 15% absolute FGR.

The uncertainty for low-release cases (< 10% FGR) is estimated at ± 50% relative; and this increases to ± 100% relative for FGR less than 1%.

2.6 Bibliography

(Note: Bibliographical entries are not called out in the text. For called-out references, see Section 11.0.)

Bagger, C. 1994. "Temperature Measurements in High Burnup UO_2 Nuclear Fuel: Implications for Thermal Conductivity, Grain Growth and Gas Release," *J. Nucl. Mater,* Vol. 211, pp. 11-29.

Bagger, C. 1992. "Experimental Assessment of a Temperature Threshold for Thermally Induced Fission Gas Release in Transient-Tested Water Reactor Fuel with Extended Burnup," from *Fission Gas Release and Fuel Rod Chemistry Related to Extended Burnup,* TECDOC-697, p. 38. Proceedings of a Technical Committee Meeting, Pembroke, Ontario, Canada, International Atomic Energy Agency.

Charles, M. 1992. "Fission Product Behavior and Fuel Rod Chemistry at Extended Burnup," from *Fission Gas Release and Fuel Rod Chemistry Related to Extended Burnup,* TECDOC-697, p. 98. Proceedings of a Technical Committee Meeting, Pembroke, Ontario, Canada, International Atomic Energy Agency.

Charles, M. 1992. "Intergranular Fission Gas Bubbles and Solid Precipitates in UO_2 Irradiated at High Burnup in Various Conditions," *Fission Gas Release and Fuel Rod Chemistry Related to Extended Burnup,* TECDOC-697, p. 172. Proceedings of a Technical Committee Meeting, Pembroke, Ontario, Canada, International Atomic Energy Agency.

Forsberg, K., F. Lindstrom, and A. R. Massih. 1994. "Modeling of Some High Burn up Phenomena in Nuclear Fuel," from *Technical Committee Meeting on Water Reactor Fuel Element Modelling at High Burn up, and Experimental Support*, IWGFPT/41, paper 2.5, 19-23, September 1994 in Windermere, England, International Atomic Energy Agency, Vienna, Austria.

Knudsen, P., C. Bagger, H. Carlsen, I. Misfeldt, and M. Morgensen. 1983. *RISØ Fission Gas Release Project Final Report*, DOE/ET/34033-1, U.S. Department of Energy, Washington, D.C.

Manzel, R. and Eberle. 1991. "Fission Gas Release at High Burnup: Influence of the Pellet Rim," from *ANS/ENS International Topical Meeting on Light Water Reactor Fuel Performance*, Avignon, France, p. 528.

Manzel, R. 1994. "Fuel Rod Behavior at Extended Burnup," from *ANS/ENS International Topical Meeting on Light Water Reactor Fuel Performance*, West Palm Beach, Florida, p. 335.

Manzel, R. and M. Coquerelle. 1997. "Fission Gas Release and Pellet Structure at Extended Burnup," from *Proceedings of the ANS International Topical Meeting on Light Water Reactor Fuel Performance*, Portland, Oregon, March 2-6, 1997.

Nakajime, T. 1985. "FEMAXI-IV: A Computer Code for the Analysis of Fuel Rod Behavior Under Transient Conditions," *Nucl. Eng. Design,* Vol. 88, pp. 69-84.

Smalley, W. R. 1974. *Evaluation of Saxton Core III Fuel Material Performance*. WCAP-3385-57, Westinghouse Electric Corporation, Pittsburgh, Pennsylvania.

U.S. Nuclear Regulatory Commission. 1975. *The Role of Fission Gas Release in Reactor Licensing,* NUREG-75/077, U.S. Nuclear Regulatory Commission, Washington, D.C.

White, R. J. 1994. "A New Mechanistic Code for the Calculation of Fission Gas Release," from *ANS/ENS International Topical Meeting on Light Water Reactor Fuel Performance*, West Palm Beach, Florida, p. 196.

3.0   Fuel Pellet Thermal Conductivity as a Function of Burnup and Gadolinia Content

3.1 Background

It has long been known that irradiation damage and the progressive buildup of fission products (rare earths, gases and volatiles) with increasing fuel burnup in sintered urania and urania-plutonia fuel pellets will progressively reduce their thermal conductivity. The effect is stronger at temperatures less than 800K where the phonon-phonon form of heat transfer dominates. See, for example, the early work on this subject by Daniel and Cohen (1964) and the review by Lokken and Courtwright (1977) that suggested that irradiation damage was the primary mechanism at low temperatures. Until relatively recently, however, this reduction in conductivity with increasing burnup has not been included in fuel performance codes because evidence was inconclusive that the effect was significant. The effect was considered nonsignificant because previously typical end-of-life burnup levels were low for LWR applications (less than 4 atom %), and the pellet operating temperatures were relatively high: 700K or higher at the pellet surface, and 1300K and higher at the pellet center.

Computer code predictions of pellet operating temperatures are typically benchmarked against steady-state fuel centerline thermocouple measurements from instrumented test fuel rods. These data are combined with the test coolant calorimetry and neutron detector data to yield the total thermal resistance from coolant to pellet center, i.e., the increase in center temperature per unit increase in the local LHGR. This resistance can then be correlated to fuel pellet type, fuel rod design and dimensions, and burnup.

However these data are not definitive regarding the *partition* of the total thermal resistance between the pellet and the fuel-cladding gap. Thus, an increase in the measured (total) thermal resistance with increasing burnup, which may in part be due to thermal conductivity degradation due to burnup and fuel cracking, has been typically explained as solely due to an increase in the thermal resistance of the pellet-cladding gap. The gap resistance can certainly increase because of pellet densification (which increases the gap size) and/or degradation of the helium-gap gas conductivity by the addition of noble fission gases (xenon and krypton) released from the fuel pellets. Fuel swelling and cladding creepdown decrease the thermal resistance with increasing burnup. Fuel center temperature data also fail to define the partition of thermal resistance within the fuel pellet; e.g., the low and high temperature regions.

Thus, fuel performance codes have typically been benchmarked by retaining fuel thermal conductivity applicable to uncracked pellets and then tuning the gap closure mechanisms to acheive agreement with in-reactor measurements of pellet center temperature. This approach yields conservative (high) estimates for the pellet surface and average temperatures, and hence for the stored energy associated with a given combination of LHGR and center temperature (see Lanning 1982). One major use of code-calculated fuel temperatures is to estimate the fuel-stored energy and gap conductance as initial conditions for analyzing loss-of-coolant accidents (LOCAs). Furthermore, the limiting LOCA initial conditions generally occur at

very low burnup for PWRs and within 10- to 20-GWd/MTU burnup for BWRs. Thus, for this important code application, the error produced by ignoring burnup-induced degradation from fuel thermal conductivity was deemed both small and acceptable.

In the past decade, however, requests to NRC have been made for commercial fuel operation to ever higher uranium burnup levels, exceeding 7 atom %, and this has resulted in renewed interest in the degree and nature of burnup-induced degradation from pellet thermal conductivity. At the same time, better experimental evidence, both in-reactor and ex-reactor, has been obtained to define the conductivity degradation as a function of burnup and temperature.

In addition, higher levels of burnable absorber addition (approaching 8 wt% gadolinia) are needed to provide early-in-life power peaking control for the higher-enriched fuel needed to achieve the higher burnups. The degrading effects of these burnable absorber material additions to the urania fuel pellet thermal conductivity are both significant and clearly present from beginning of life (BOL) onward. At the same time, publicly-accessible data on these effects have become available.

The evidence for burnup-induced degradation of fuel thermal conductivity is reviewed in Section 3.2, and the changes implemented in FRAPCON-3 to account for these effects are given in Section 3.3. The data and implemented code changes to pellet thermal conductivity degradation due to gadolinia addition are summarized in Section 3.4. The ranges of application and the uncertainties for the upgraded thermal conductivity functions are given in Section 3.5.

3.2 Experimental Evidence for Burnup Degradation

An instrumented assembly referred to as the Halden Ultra-High-Burnup Experiment has indicated a steady degradation in urania fuel thermal conductivity (averaged over the temperature range from ~750 to 1200K) of ~5 to 7% relative per 10 GWd/MTU, for burnups up to 88 GWd/MTU (Wiesenack 1997). These measurements are described in the open literature (see Kolstad 1992; Kolstad et al. 1991; Wiesenack 1995). These data are supplemented by results from other Halden instrumented tests involving small-gap rods operated to significant burnup with surviving centerline thermocouples. The degradation rate initially reported (Kolstad et al. 1991) is qualitatively consistent with the results of laser-flash diffusivity measurements on unirradiated simulated high-burnup fuel performed at Chalk River National Laboratory (CRNL), Ontario, Canada (Lucuta et al. 1991; Lucuta et al. 1992). These two experimental programs are described below.

3.2.1 Thermal Diffusivity Measurements on SIMFUEL

P. G. Lucuta at CRNL measured thermal diffusivity in pellets with simulated burnups of 0, 3, and 8 atom % (i.e., 0, 28, and 75 GWd/MTU). For the simulation, he added a mixture of 11 rare earth oxides to the urania before pressing and sintering, as described in Lucuta et al. (1991). He selected the mixture on the basis of ORIGEN code calculations for water reactor fuel, and the resulting sintered material was thoroughly characterized microstructurally (see Lucuta et al. 1992 and 1995). Diffusivity was measured over the temperature range of 500 to 1800K by both laser-flash and sine-wave techniques, and the specific

heats were measured on companion samples over a similar temperature range using a differential scanning calorimeter. The rare earth additions changed the specific heat very little (less than 2%). This finding simplified and reduced the uncertainty in Lucuta's reduction of the diffusivity data (D) to conductivity (K) via the relationship:

$$K = d \, c \, D \tag{3.1}$$

where d = as fabricated SIMFUEL density and c = specific heat.

In the temperature range of the measurements, the phonon-phonon heat transfer mechanism dominates, and the conductivity, K, as a function of temperature, T, has the form

$$K = 1 / (A + BT) \tag{3.2}$$

where A and B are constants.

When Lucuta reduced his diffusivity data to conductivity and plotted the inverse of the conductivity versus temperature, he obtained parallel straight lines, with the offsets (increases) in the curves for simulated-burnup materials (relative to the "0 burnup" samples) being proportional to their simulated burnup level. (This is consistent with the results from diffusivity measurements on urania containing rare earth additions; see, for example, Fukushima et al. [1982] and Hirai and Ishimoto [1991].) This led Lucuta to a simple representation of the burnup degradation effect:

$$R = 0.053 + (0.016 \pm 0.0015) \, b + 0.00022 \, T \tag{3.3}$$

where   R   =   inverse conductivity (1 / K) in m-K/W
             b   =   fuel burnup in atom %
             T   =   temperature in K.

The accuracy of the diffusivity measurements (better than 5% relative standard deviation) combined with the extremely accurate specific heat measurements indicates conductivity-measurement accuracy of better than 6% relative standard deviation. Indeed, that is the level of precision in comparing the above expression to the data (see Figure 3.1). Furthermore, the uncertainty assigned to the burnup multiplier (about 10% relative standard deviation) is consistent with the magnitude of the burnup term relative to the average total inverse conductivity and its uncertainty.

3.2.2 The Halden Ultra-High-Burnup Experiment

The Halden Reactor Project designed an instrumented test fuel assembly specifically to measure the effects of burnup-induced degradation of fuel thermal conductivity. The basic design and operating parameters of this test are listed in Table 3.1. The pellets were small diameter with large annular holes to accommodate accurate, rugged elongation temperature sensors that measure the axially averaged value
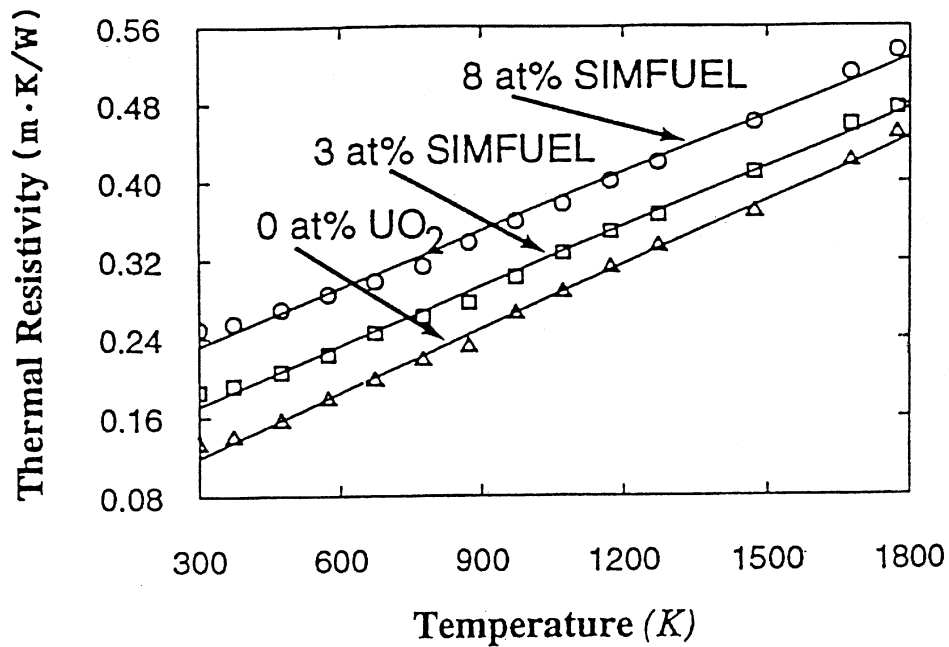
Figure 3.1. Lucuta Expression (Lines) and SIMFUEL Data (Symbols)

Table 3.1. Design Parameters of the Halden "Ultra-High-Burnup" Instrumented Test Fuel Assembly

Parameter and Units	Value
Number of Rods	6
Rod Diameter, mm	7
Cladding Thickness, mm	0.50
Diametral Gap, mm	0.10
Fuel Outer Diameter, mm	5.9
Fuel Inner Diameter, mm	2
Fuel Rod Length, mm	443
Plenum Length, mm	32.5
Rod Pressure, MPa (Helium)	10
Fuel Enrichment, % ^{235}U	13
Grain Size, μm	10 to 20

of the fuel central temperature by calibrated thermal expansion of a central rod. The power and temperature levels were kept low to avoid the confounding thermal effects of fission gas release, and the rods were pressurized with helium for similar reasons.

Fuel rod internal-pressure measurements and postirradiation rod-puncture results on companion rods in the assembly confirmed that, up through 60-GWd/MTU burnup, the fission gas release and the degradation of fill gas thermal conductivity were negligible. The fuel and cladding were highly stable dimensionally as a function of irradiation. Thus, in their analysis of the center temperature measurements, Halden found that the gap thermal resistance quickly stabilized at a relatively constant value, reduced slowly by fuel swelling. The trends have continued to a rod-average burnup of 88 GWd/MTU (Wiesenack 1997).

Various analysis tools were used to confirm that, in the absence of thermal conductivity degradation, the fuel temperatures should have quickly equilibrated or slowly decreased at a given LHGR. Instead, the center temperatures (normalized to a common LHGR) slowly increased with increasing burnup (see Figure 3.2). This is taken as an indication of the magnitude of conductivity degradation caused by burnup. The center temperature at 25 kW/m increased from about 1000K at BOL to 1125K by a burnup of 60 GWd/MTU. Since the fuel pellet surface temperature is estimated to have decreased from 675 to
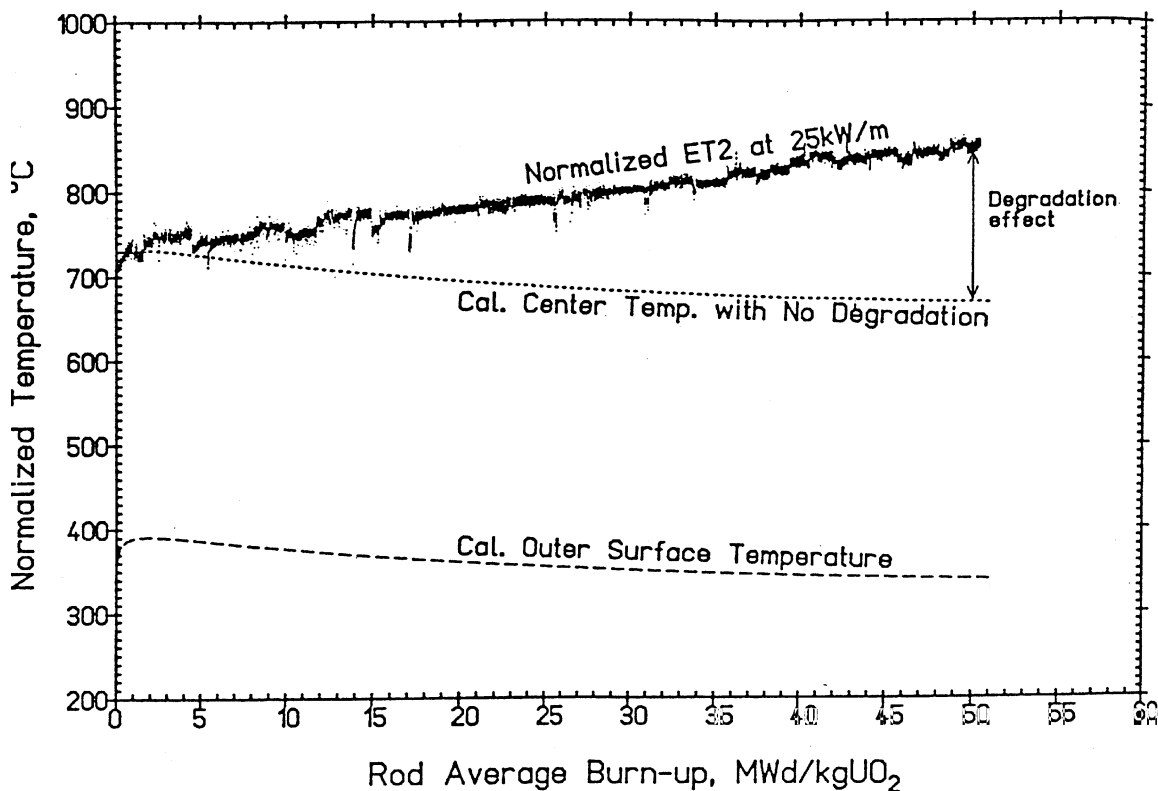
Figure 3.2. Normalized Ultra-High Burnup Experiment Temperature Data (all figures normalized to 25 kW/m)

625K, the 125K rise in the center temperature constitutes a change of about 125 + (675 - 625) = 175K. The BOL center-to-surface temperature difference is about 750-400 = 350K (see Figure 3.2). Therefore, the 175K net increase in center temperature corresponds with a thermal conductivity change of 175/350 = 50% or about 8% per 10 GWd/MTU. This is fairly consistent with the Lucuta degradation, averaged over the Halden surface-to-center temperature ranges. The uncertainty on the burnup degradation rate must reflect the uncertainty on temperature measurement (~2%), heat generation rate (10%), and on the analysis (~10%) and is therefore about 15% relative standard deviation, which is higher than the estimated uncertainty in the SIMFUEL measurements.

Following scrutiny of temperature data trends with burnup in small-gap xenon-filled rods, Halden now proposes that the thermal gap resistance becomes very small (smaller than previously thought) when fuel swelling and cladding creepdown closes the gap and that, therefore, the observed trend in the Ultra-High-Burnup fuel temperatures indicates even stronger degradation.

3.3 Experimental Evidence for the Effect of Gadolinia Additions

Gadolinia additions to reactor fuel provide a burnable neutron absorber for power peaking control early in the life of a fuel assembly because of the high cross section of two gadolinium isotopes. The additions are typically limited to less than 8 wt%. Because of the similar magnitude and temperature dependence for urania and gadolinia specific heats, the impact of limited gadolinia additions on the specific heat of urania fuel is very small (< 5% relative), and a standard mixing rule has been shown to be adequate (see Massih et al. 1992).

The impact of limited gadolinia additions on the fuel thermal diffusivity is more profound due to its disturbance of the lattice and its consequent effect on phonon-type heat transfer. Various commercial fuel vendors have their own diffusivity data sets and proprietary thermal conductivity modeling approaches. In FRAPCON-3, it will suffice to have an "evaluation" type model that captures the effect in a conservative way. The FRAPCON-3 modeling of the gadolinia effect is provided in Section 3.4.2.

Experimental thermal diffusivity data in the open literature have been reported by Newman et al. (1984), Hirai and Ishimoto (1991) and Fukushima (1982). The Newman data were taken using the laser-flash method at concentrations of 2.98 wt%, 5.66 wt%, and 8.5 wt% gadolinia at temperatures up to 1880°C. Hirai and Ishimoto (1991) measured thermal conductivities by the laser-flash diffusion method on sintered samples containing 0, 3, 5, 7, and 10 wt% gadolinia over the temperature range from 20 to 1750°C. By using a special form for the phonon term that includes point-defect interactions, and adding a high-temperature term, they fit their data with a standard error of only 6% relative. In an earlier study, Fukushima et al. measured thermal diffusivities and deduced conductivities in the temperature range from 400 to 1335°C for gadolinia contents of 0 to 10.3 wt%.

The Newman data, Hirai and Ishimoto model, and Fukushima model are shown in Figure 3.3 in terms of thermal conductivity as a function of temperature at 8.5 wt% gadolinia. As demonstrated, the
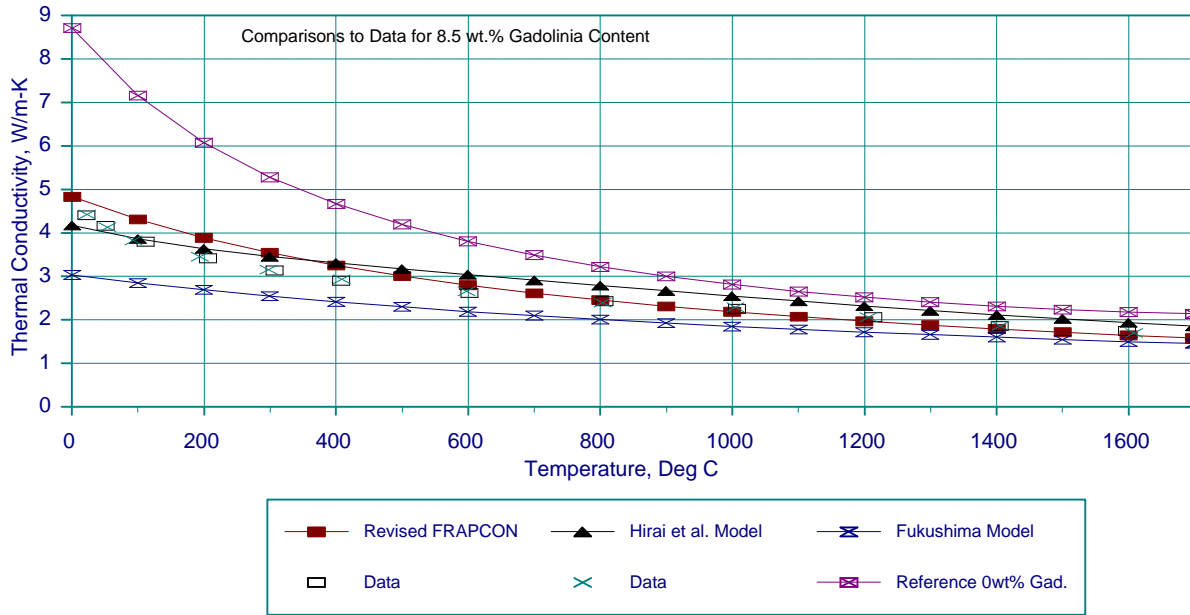
Figure 3.3. Thermal Conductivity for 95% TD 8.5% Gadolinia-Urania Fuel: Revised
FRAPCON, Literature Models, and B&W Data

Fukushima data are low relative to results of other investigations, such as that of Hirai and Ishimoto. Therefore, the Fukushima results have been ignored in the effect of gadolinia on thermal conductivity for FRAPCON-3.

3.4 Modifications to the MATPRO Equations

The conductivity formula for sintered, stoichiometric uranium dioxide as proposed recently by Lucuta et al. (1996) has been evaluated and incorporated in FRAPCON-3 in place of the MATPRO-11 function of temperature and porosity. This formula includes the effects of temperature, radiation (environment), fuel burnup, and porosity. It is described in Section 3.4.1 below. A modification for the effect of limited gadolinia additions has been added by Pacific Northwest National Laboratory, based on published ex-reactor data, and a modification for limited plutonia additions has also been added. These are described in Sections 3.4.2 and 3.4.3.

3.4.1 Burnup-Dependent Conductivity for Urania

In Lucuta et al. (1996), a revised fuel thermal conductivity model is presented that correlates the SIMFUEL data as well as the previous model (Lucuta et al. 1992), but also correlates the irradiated fuel data from Daniel and Cohen, plus comparing well to low-burnup, low-temperature irradiated fuel data from early Atomic Energy of Canada, Ltd. (AECL) experiments. In addition, this revised model has improved the comparison between FRAPCON-3 predictions and the in-pile fuel temperature data to high

burnup from the Halden Ultra-High Burnup Experiment. The revised Lucuta model also compares well to thermal conductivity values determined from thermal diffusivity measurements on high-burnup fuel as demonstrated by Lucuta et al. (1996). Therefore, this new model has been implemented in FRAPCON-3 instead of simply introducing a burnup enhancement factor into the existing (MATPRO-11 derivative) fuel thermal conductivity model.

Lucuta's new formula uses the expression developed by Harding and Martin (1989) for the conductivity ("K_o") of unirradiated, fully dense urania:

$$K_o = \frac{1}{0.0375 + 2.165 \times 10^{-4} T} + \left[\frac{4.715 \times 10^9}{T^2}\right] \exp\left[-\frac{16361}{T}\right] \tag{3.4}$$

where K_o = conductivity of unirradiated urania (W/m-K)
          T = Temperature (K)

The effect of burnup is to build dissolved and precipitated fission products into the matrix. The effect of the dissolved fission products is reflected by a burnup and temperature-dependent factor, "FD," which multiplies K_o:

$$FD = \left[\frac{1.09}{B^{3.265}} + \frac{0.0643}{\sqrt{B}}\sqrt{T}\right] \arctan\left[\frac{1}{\dfrac{1.09}{B^{3.265}} + \dfrac{0.0643}{\sqrt{B}}\sqrt{T}}\right] \tag{3.5}$$

where B = Burnup in atom% (1 atom% = 9.383 GWd/MTU at 200 MeV/fission)
          T = Temperature, K

The effect of the precipitated fission products is reflected by the factor FP given by

$$FP = 1 + \left[\frac{0.019B}{3 - 0.019B}\right]\left[\frac{1}{1 + \exp(-\dfrac{T-1200}{100})}\right] \tag{3.6}$$

The effect of porosity is accounted for by the well known Maxwell factor, FM, given by FM =

$$FM = \frac{1 - p}{1 + (s-1)p} \tag{3.7}$$

where p = porosity fraction (as-fabricated plus swelling)
          s = shape factor (= 1.5 for spherical pores)

The radiation effect (applied at all times in-reactor is given by the factor FR:

$$FR = 1 - \frac{0.2}{1 + \exp(\frac{T-900}{80})}$$

(3.8)

This factor has a significant effect at temperatures below 900K, but a sharply decreasing effect as temperatures increase above 900K. Finally then, the conductivity K for irradiated urania is given by

$$K = K_o \bullet FD \bullet FP \bullet FM \bullet FR$$

(3.9)

A plot of this conductivity as a function of temperature and burnup appears as Figure 3.4.
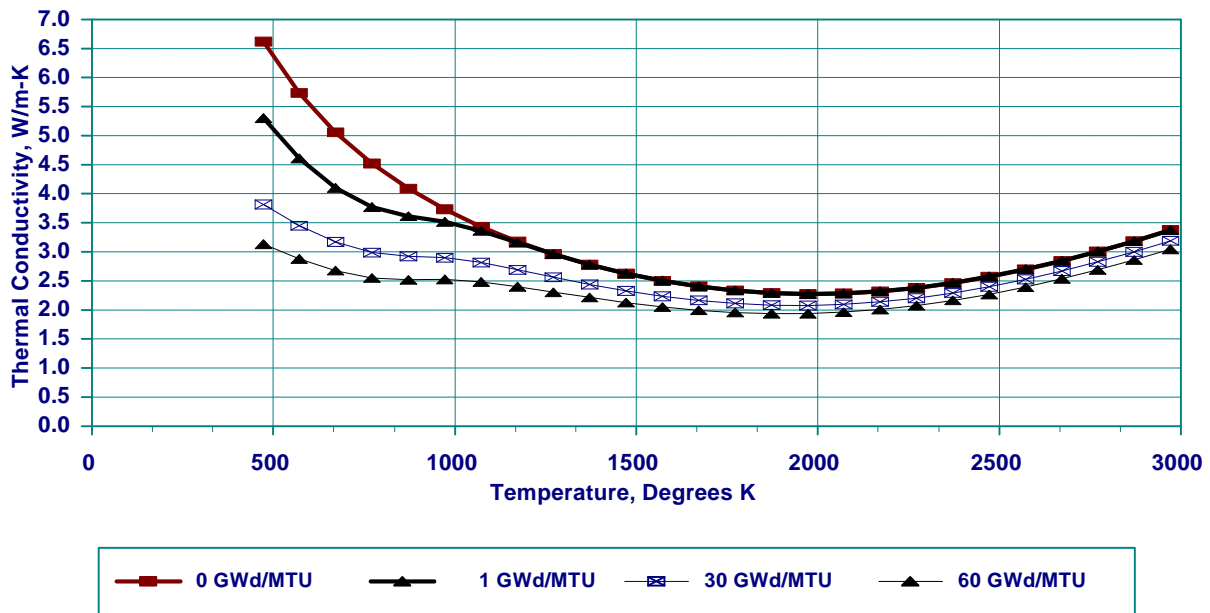
Figure 3.4. Fuel Thermal Conductivity as a Function of Temperature, Degraded by Burnup

3.4.1.1 Verification of Burnup Dependence

   The most recently reported temperature/LHGR data from Rod 18, the Ultra-High Burnup Experiment, and the data from Rod 3 of instrumented fuel assembly (IFA)-432, have been used for comparison with the FRAPCON-3 code predictions. Lucuta's recommended new burnup dependent degradation factor that accounts for irradiation effects has been incorporated for FRAPCON-3 for this comparison together with the fuel pellet relocation changes described in Section 5.0. The comparison between FRAPCON-3 predictions and the measured data is shown in Figure 3.5. The overprediction of
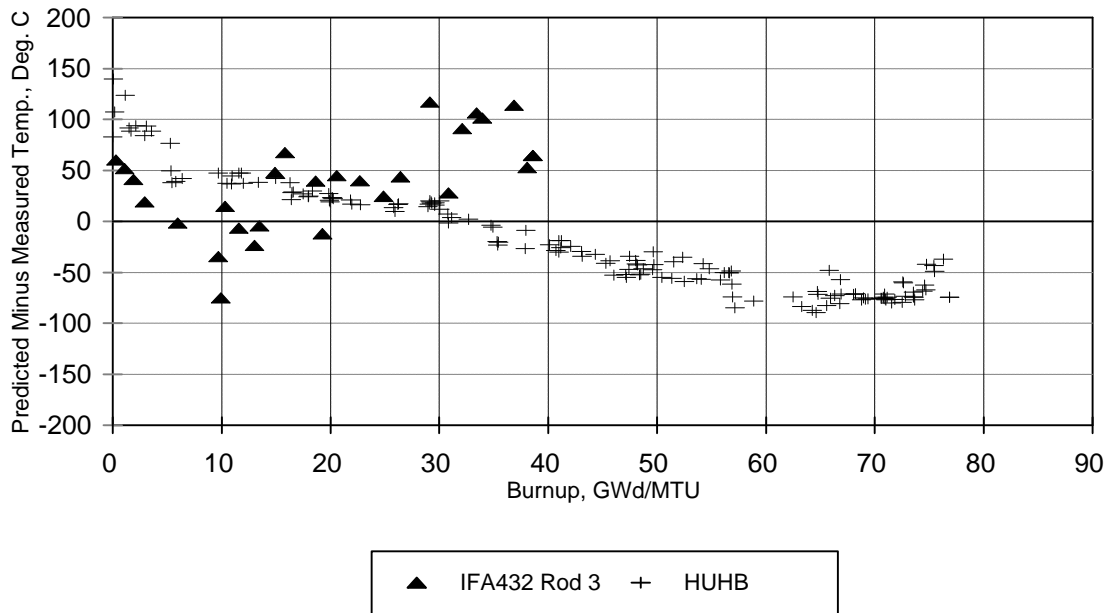
Figure 3.5. FRAPCON-3 Thermal Conductivity Model, Compared to Fuel Temperature Data from the Ultra-High Burnup Experiment and the IFA-432 Experiment

the Ultra-High Burnup Halden data at low burnups is considered to be an anomaly of this experiment due to the large hole, small pellet diameter, and the thermal expansions. Thermometers in the annular hole influence the pellet relocation towards the cladding differently than normal fuel with a large pellet and no hole. There is still a small underprediction of the Halden Ultra-High Burnup data at high burnups, but the model appears to predict well against thermal diffusivity data (Lucuta et al. 1996) from high-burnup fuel. Therefore, until further in-reactor thermal data and thermal diffusivity data become available for high-burnup fuel, a large uncertainty will be used for burnups >40 GWd/MTU (±10%) and for burnups greater than 60 GWd/MTU (±15%). On the basis of this optimized comparison, Lucuta's new (1996) burnup-dependent urania thermal conductivity function is used in FRAPCON-3.

3.4.2 Modification for Gadolinia Additions

The phonon term in the unirradiated urania-only equation for fuel pellet thermal conductivity was reduced, for the case of urania-gadolinia fuel, by adding a term to the denominator of the phonon term. It was found that adding a degradation term equal to 0.0150 m-K/W per weight percent gadolinia achieved an acceptable match to ex-reactor conductivity measurements. The performance of the revised model (with no neutron flux and 0 burnup) is shown as a function of both temperature and gadolinia content in Figure 3.6, over the full temperature range (i.e., from room temperature up to the fuel melting temperature).
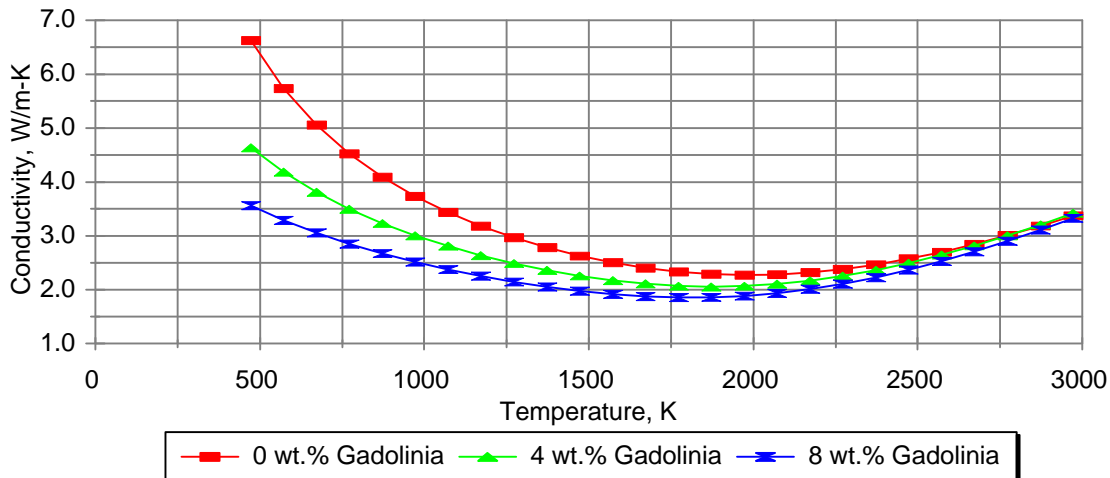
Figure 3.6. New Lucuta Thermal Conductivity as a Function of Temperature and Gadolinia Content

3.4.2.1 Check Against Diffusivity Data

  To further check the validity of the modified FRAPCON-3 thermal conductivity, thermal diffusivity data in Newman et al. (1984) for 2.98, 5.66, and 8.5 wt% gadolinia samples were reduced to thermal conductivity values and then compared to the recommended modified MATPRO model. These comparisons are shown in Figures 3.7 to 3.9. The modifications to the MATPRO model recommended here fit the original Babcock and Wilcox Company (B&W) data set as well as the original MASSIH model, based on a statistical analysis of the comparisons of both models to this data set. The data are slightly overpredicted at high temperatures ($> 1600°C$) because of the shift in dominance from the phonon term to the electronic term at those temperatures. Because of this shift, the alteration of the phonon term has minimal effect at the higher temperatures.

  It should be noted that comparison of the FRAPCON-3 code with this model against Halden instrumented fuel rods with centerline thermalcouples and 8 wt% gadolinia demonstrated a code overprediction in centerline temperature of 120 to 150°C. The code overpredicted a sister fuel rod with UO_2 by only 25°C to 50°C (Beyer et al. 1997). This would indicate that the out-of-reactor data and the FRAPCON-3 thermal conductivity dependence for gadolinia may be greater than the in-reactor conductivity dependence. However, this needs to be confirmed with additional in-reactor testing and varying urania-gadolinia fabrication techniques.
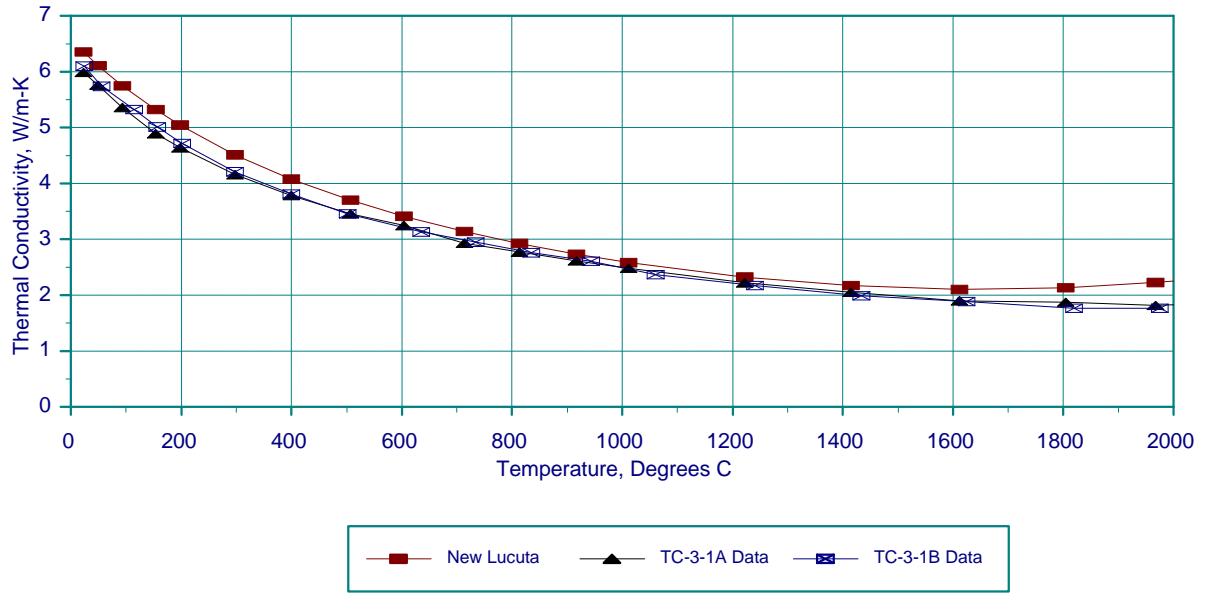
Figure 3.7. Comparison of Modified New Lucuta Model and Data for 2.98 wt% Gadolinia Fuel
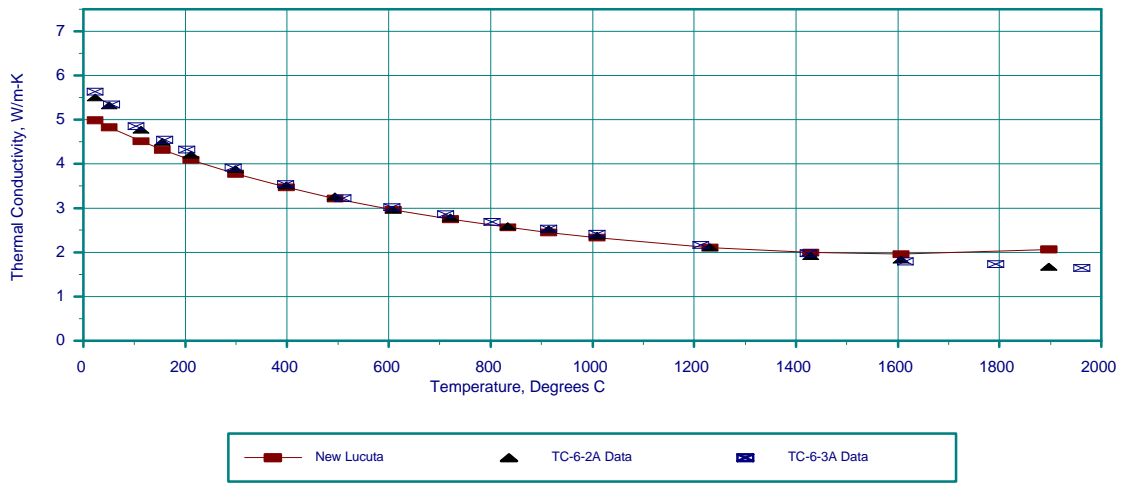
Figure 3.8. Comparison of Modified New Lucuta Model and Data for 5.66 wt% Gadolinia Fuel
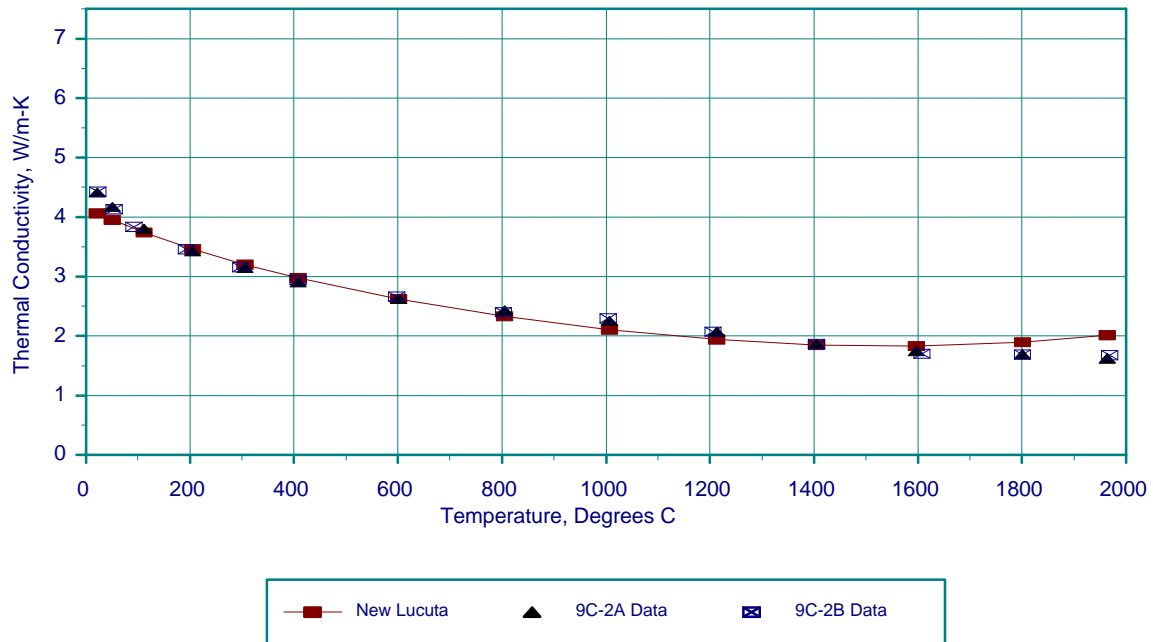
Figure 3.9. Comparison of Modified New Lucuta Thermal Conductivity and Data for 8.5 wt% Gadolinia Fuel

3.4.3 Adjustment for Plutonia Additions

The MATPRO version 11 Rev.2 fuel thermal conductivity function was used in FRAPCON-2. This MATPRO model (Hagrman et al. 1981) provided an adjustment for limited plutonia additions, and this has been re-established in FRAPCON-3. The heat-capacity functions for plutonia and urania were used via mass-weighting to calculate these functions for the mixed oxide, and the conductivity is corrected by the ratio of mixed oxide heat capacity to that of pure urania.

In Figure 3.10, the revised model is shown as a function of temperature and plutonia content for unirradiated mixed oxides. As can be seen, the adjustment caused by the limited plutonia additions (up to 7 wt%) expected for LWR fuel is minimal.

3.5 Range of Application and Uncertainty of the Model

The ranges of application for the fuel thermal conductivity expression are as follows:

Temperature: 300 to 3000K
Burnup: 0 to 8 atom% (0 to 75 GWd/MTU)
Gadolinia Content: 0 to 8 wt%
Plutonia Content: 0 to 7 wt%.
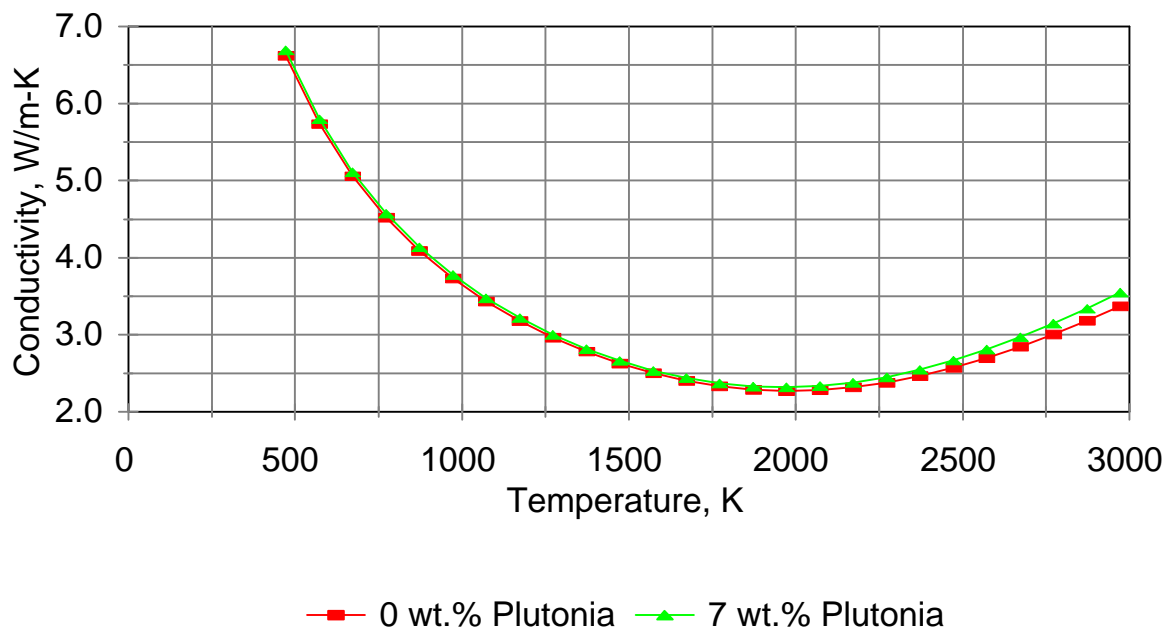
Figure 3.10. New Lucuta Thermal Conductivity as a Function of Temperature and Plutonia Content

The estimated uncertainties (one standard deviation) for the fuel thermal conductivity are based on statistical analysis of ex-reactor and in-reactor data at low burnups (< 40 GWd/MTU) and professional judgment for burnups > 40 GWd/MTU, and are listed in Table 3.2. In general, the relative uncertainty increases with increasing temperature, increasing burnup and increasing gadolinia content.

Table 3.2. Uncertainties for Fuel Thermal Conductivity

Fuel Type and Burnup	Uncertainty in Temperature Range 300 to 2000 K, ± % Relative	Uncertainty in Temperature Range 2000 to 3000 K, ± % Relative
Urania Burnups < 40 GWd/MTU	7	7
Urania Burnups 40 to 60 GWd/MTU	10	10
Urania Burnups > 60 GWd/MTU	15	10
Urania-Gadolinia Burnups < 40 GWd/MTU	7	7
Urania-Gadolinia Burnups > 40 GWd/MTU	10	10
Urania-Plutonia	Not defined; verification not yet performed	

3.6 Bibliography

(Note: Bibliographical entries are not called out in the text. For called-out references, see Section 11.0.)

Matzke, H. J. 1995. "Oxygen Potential Measurements in High Burn up LWR UO$_2$ Fuel," *J. Nucl. Mater.,* Vol. 223, pp. 1 to 5.

4.0 Modifications to the MATPRO Model for Fuel Swelling

4.1 Background

The progressive buildup of fission products (rare earths, gases, and volatiles) with increasing burnup in urania and urania-plutonia sintered fuel pellets will reduce their density and increase their specific volume. The swelling is countered early in life by as-fabricated fine porosity loss and pellet densification due to irradiation enhancement of the sintering process; however, this densification is normally completed by 5-GWd/MTU burnup and has little effect thereafter (Freshley et al. 1976). The effects have been studied for over 20 years (see, for example, Anselin 1969; Freshley et al. 1976; Hargreaves and Collins 1976; Stehle and Lassmann 1974; and Zimmermann 1978). Two components to the swelling are now identified: 1) a low-temperature (or athermal) swelling, connected to the buildup of solid fission products and limited to approximately 0.5 to 1.0% $\Delta V/V$ per 10 GWd/MTU and 2) a temperature-dependent, high-temperature swelling connected to gas pressure in fuel pores. The demarcation between the high-temperature and low-temperature (athermal) regimes is approximately 1000°C. In the high-temperature regime, the fuel is also progressively plastic at higher temperatures; hence the gas-induced swelling in constrained situations can lead to plastic flow of fuel into pores and into pellet end dishes.

Modern LWR fuel pellets operate predominantly in the athermal swelling regime. A survey by Franklin et al. (1984) established that the athermal swelling rate remains constant at approximately 1% $\Delta V/V$ per 10 GWd/MTU up to a burnup of 11×10^{20} fissions/cm^3 or 44.5 GWd/MTU. More recent density measurements on high-burnup fuel extend this trend out to 60 GWd/MTU, but indicate a lower average swelling rate.

On the other hand, Chubb et al. (1972), Turnbull and Tucker (1974), and Zimmermann (1978) reported much higher rates for high-temperature (but isothermal), unrestrained UO_2 samples subject to gas-induced swelling. These conditions are atypical for fuel in commercial power reactors because the fuel pellets in power reactor rods are non-isothermal, are constrained by the cladding, and operate at low to moderate temperatures. Indeed, studies involving non-isothermal constrained fuel have shown limited net fuel swelling even at high temperatures (Baroch and Rigdon 1973; Nelson et al. 1971).

4.2 Experimental Evidence for Modified Solid Fission Product Swelling Rate

The present solid fission product-induced swelling rate ($\Delta V/V$) in the MATPRO subroutine FSWELL is 7.74E-9 per MW-s/kgU for 95% TD fuel, which corresponds to 0.669% per 10 GWd/MTU. Estimates of the solid swelling rate have been derived from density stack elongation measurements from instrumented fuels tests in the Halden Reactor[a] at about 1% $\Delta V/V$ per 10 GWd/MTU. Fuel pellets irradiated in commercial PWRs to pellet burnups ranging from 20 to 70 GWd/MTU have been measured

---

(a) Personal communication with Halden.

for density (Newman 1986; Smith et al. 1994; Dideon 1983; Garde 1986). The estimated swelling rates range from 0.7 to 1.0 % ΔV/V per 10 GWd/MTU.

A linear least-squares fit of the data compiled from these PWR references (as a function of sample burnup) yields a line with a slope of 0.77% per 10 GWd/MTU with an uncertainty of approximately 1.2% in absolute volumetric swelling (See Figure 4.1). In Figure 4.1, data below 10 GWd/MTU are not shown because they are still strongly influenced by early in-life fuel densification and hence were excluded from the linear least-squares fitting procedure. FRAPCON-3 simulations of the power histories for the PWR rods from which these data were taken indicate a negligible expected contribution from the gas-swelling function as demonstrated in the following section. On this basis, the FSWELL solid fission product-induced swelling rate has been increased by the factor (0.77/0.669) = 1.15.

4.3 Experimental Evidence for Eliminating the Gaseous Fission Product Swelling Rate for LWR Fuel in Normal Operation

The present gas-induced swelling rate in MATPRO and FRAPCON-2 is a complex function of temperature multiplied by an exponentially decreasing function of burnup. When this function is integrated with respect to burnup, the resulting cumulative swelling is found to exponentially approach a plateau level that is temperature dependent. The plateau is essentially reached by 10-GWd/MTU burnup. The plateau levels increase with increasing temperature, but constitute a negligible fraction of the solid swelling until a temperature of 1500K is exceeded. The plateau level (the ultimate swelling of unrestrained samples) then is predicted to increase rapidly with temperature, reaching 30% at 2100K, beyond which it decreases to negligible values by 2700K.
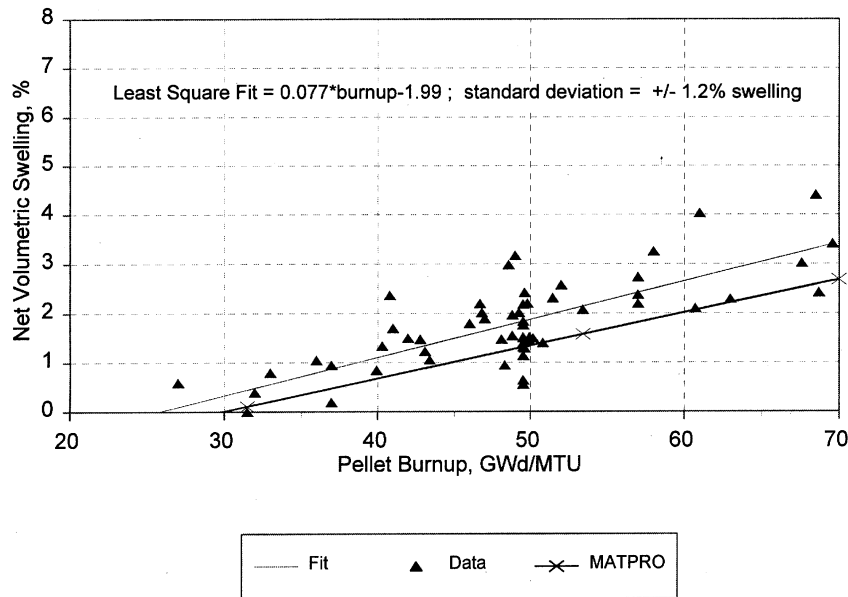
Figure 4.1. PWR Swelling Data and Least Squares Fit Compared to MATPRO Model

These plateau values of ultimate cumulative gas-induced swelling are plotted as a function of temperature in Figure 4.2. The basis for this function is out-of-reactor swelling induced in heated but unconstrained samples (Chubb et al. 1972; Turnbull and Tucker 1974).

For cases where a significant fraction of the pellet volume exceeds 1500K, the total swelling is predicted to be much greater than that predicted by solid-swelling alone. A test of the validity of this increase would be to compare measured and predicted pellet densities from rods that were confirmed by in-reactor fuel temperature measurements to have attained the temperatures and burnups sufficient to cause significant (predicted) gas swelling.

Rod number 1 from the NRC-sponsored IFA-432 test assembly in the Halden Reactor (Lanning and Bradley 1984) offers such a test. The early-in-life LHGRs along this rod ranged from 10 to 15 kW/ft, and, because of thermal feedback in this non-pressurized high-powered BWR type test rod, the measured center temperatures exceeded 1800K in the solid pellets in the first 10-GWd/MTU burnup.

FRAPCON-3 was used to simulate the IFA-432 rod 1 power history, reasonably matching the measured temperatures. The fuel volume change predicted by the code with gas-induced swelling included is shown in Figure 4.3 together with the measured postirradiation volume change from two locations in the pellet column. Also shown in the figure is the prediction without gas-induced swelling, but with the proposed solid fission product swelling. The over prediction by the present model in this case, coupled with the adequate prediction by the revised solid swelling only, suggests that the present gas-swelling function does not apply well to fuel pellets constricted by their own thermal stresses and constrained by the cladding.
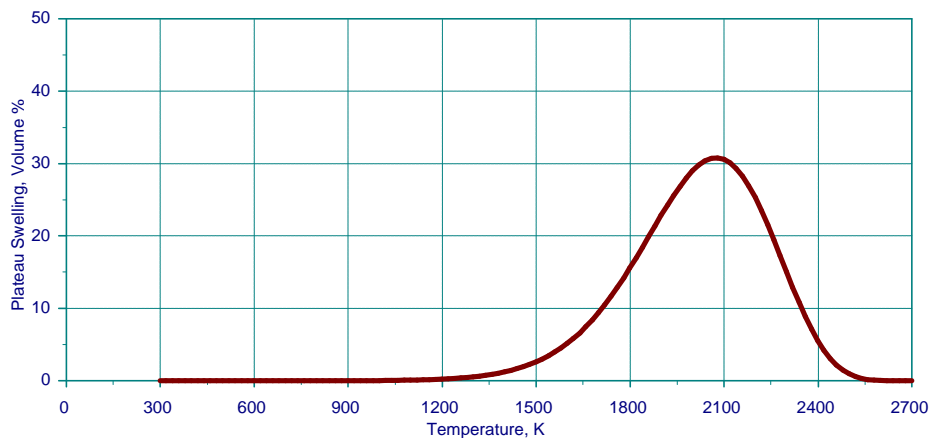
Figure 4.2. Plateau Swelling from the MATPRO Gas-Induced Fuel Swelling Model
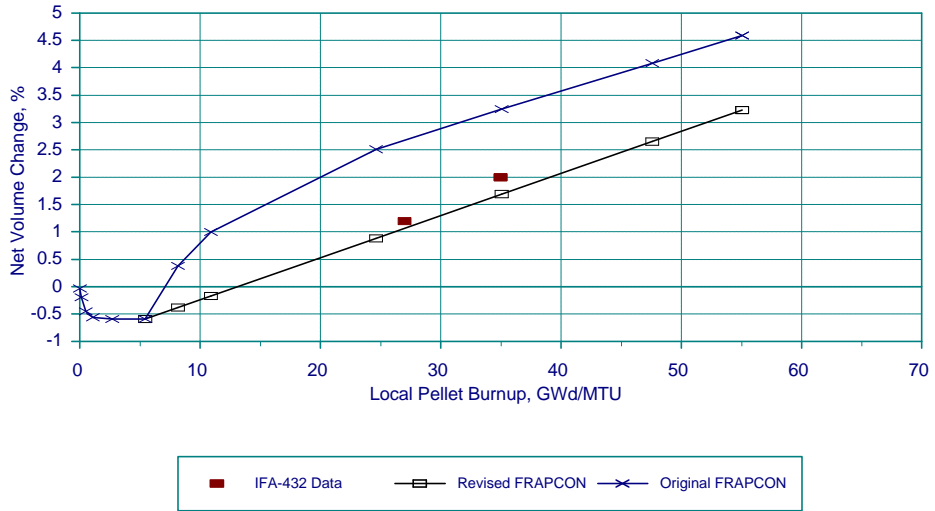
Figure 4.3. Original and Modified FRAPCON Models Compared to Pellet Swelling Data from IFA-432 Rod 1

Swelling data from BWR rods, which may experience higher fuel temperatures than PWR rods due to thermal feedback, still lie within the scatter band of the PWR data (see Figure 4.4). Thus the uncertainty bounds derived on solid-swelling rate alone will bound the available swelling data, for both PWRs and BWRs, without having to add a gas-swelling term. The current gas-swelling term has been eliminated from the MATPRO model for application in FRAPCON-3.
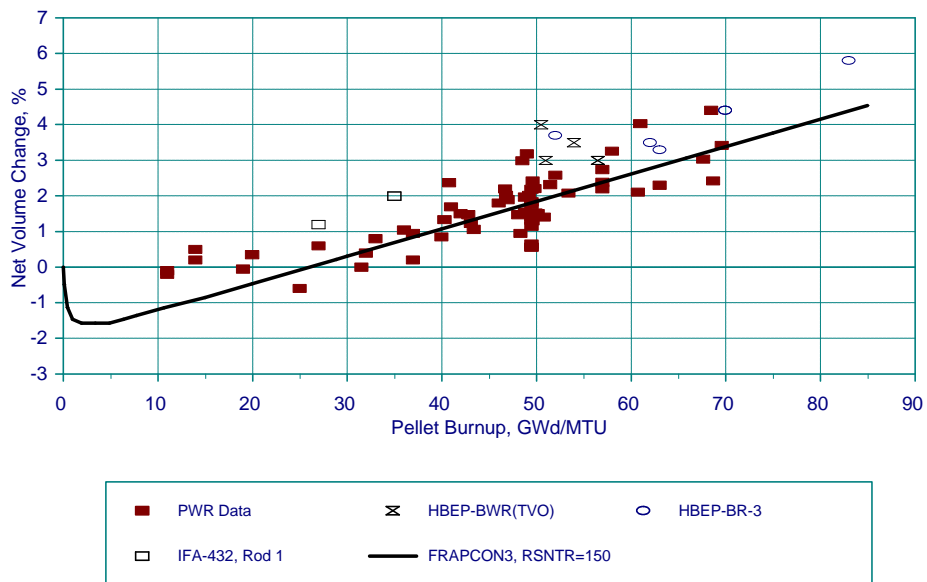
Figure 4.4. Pellet Swelling Data from PWR Rods, IFA-432, and High-Burnup Effects Program (HBEP), Compared to Nominal Application of the FRAPCON-3 Swelling Model

This is not to say that gas swelling does not occur under some circumstances. Pellet dish filling was observed for PWR rodlets irradiated to 45 GWd/MTU and then ramp-tested to 45 kW/m with a 48-hour hold, under the High-Burnup Effects Program (Barner et al. 1990). However, practically no dish filling was noted for identical rods similarly ramp tested under the same program, but with pre-ramp burnups of only 25 GWd/MTU. This implies that the gas swelling may be burnup dependent at burnups greater than 25 GWd/MTU. The present MATPRO model contains no such dependence.

Also, it should be noted that high-temperature fuel performance data, including fuel swelling data, are sparse at burnup levels greater than 45 GWd/MTU. A concern at high burnup, > 55 GWd/MTU, is that gas swelling may become more dominant during power transients because of the additional gas within grains and on grain boundaries. This additional gas-induced swelling at higher burnups could lead to significant cladding stresses and strains during power transients and possibly to lower thresholds for cladding failure. Therefore, to evaluate cladding loadings due to swelling, fuel rod power ramp tests are needed on rods with >55-GWd/MTU burnup to obtain fuel swelling and cladding strain data. A future version of FRAPCON-3 should incorporate the porosity and dish filling and enhanced fuel and cladding strain associated with high-LHGR operation at high burnup as the data for these effects become better defined.

4.4 Changes to the FRAPCON Model (Subroutines FSWELL and SWELL)

To reflect the revised (15% greater) solid-fission product induced swelling rate of 0.77%ΔV/V per 10 GWd/MTU, the line in Subroutine FSWELL that read

$$\text{SOLDSW} = 2.5e\text{-}23*\text{BUS} \tag{4.1}$$

has been changed to read

$$\text{SOLDSW} = 2.875E\text{-}23*\text{BUS} \tag{4.2}$$

To eliminate the gas-induced swelling, all references to "GASWL" in both subroutines FSWELL and SWELL have been eliminated.

The current logic in subroutine SWELL, which delays the onset of solid swelling (until 2.13-GWd/MTU local burnup), has been retained. This delay is mechanistically related to partial porosity filling and is qualitatively substantiated by the swelling data.

Finally, the adjustment to fuel porosity due to swelling in subroutine SWELL has been eliminated. The porosity does not really change without gas-induced swelling, and the impact of solid fission products on the fuel thermal conductivity will be handled explicitly in the revised code and not through a pseudo increase in the porosity. Thus, the line in subroutine SWELL that read

$$\text{POROS2(I,J)} = \text{POROS1(I,J)} + \text{DENPOR} + (\text{SOLDSW} + \text{GASWL})/3.0 \tag{4.3}$$

has now been changed to read

$$POROS2(I,J) = POROS1(I,J) + DENPOR \qquad (4.4)$$

Similarly the line that read

$$IF(POROS2(I,J).LE.0.0) \; DELDEN = POROS1(I,J) - (GASWL+SOLDSW)/3 \qquad (4.5)$$

has now been changed to read:

$$IF(POROS2(I,J).LE.0.0) \; DELDEN = POROS1(I,J) \qquad (4.6)$$

FRAPCON-2 did not originally allow the fuel to densify to the input value of density change (RSNTR) input by the code user. FRAPCON-3 has been changed so that fuel density change calculated by the code due to densification is equal to the user-specified value for RSNTR.

4.5 Range of Application and Uncertainty

The revised fuel pellet swelling model has the following ranges of application:

    Burnup: 0 to 70 GWd/MTU (pellet burnup)
Temperature: 300 to 2000K
  Fuel types: Constrained (clad) urania and urania-plutonia sintered pellets.

The uncertainty on the swelling (one standard deviation) is estimated at $1.2\%\,\Delta V/V$ absolute, based on the least-squares fitting to the recent data sets.

4.6 Bibliography

(Note: Bibliographical entries are not called out in the text. For called-out references, see Section 11.0.)

Lassmann, H. and R. Manzel. 1977. "The Matrix Swelling Rate of UO_2", *J. Nucl. Mater.,* Vol. 68, p. 360 -364.

Hagrman, D. L., G. A. Reymann, and G. E. Mason. 1981. *A Handbook of Materials Properties for Use in the Analysis of Light Water Reactor Fuel Rod Behavior*. MATPRO Version 11 (Revision 2).

NUREG/CR-0479 (TREE-1280), Prepared by EG&G Idaho, Inc., Idaho Falls, Idaho for the U.S. Nuclear Regulatory Commission, Washington, D.C.

Meyer, R. O. 1976. *The Analysis of Fuel Densification*, NUREG-0085, U.S. Nuclear Regulatory Commission, Washington, D.C.

5.0 Modifications to the Fuel Cracking and Relocation Algorithms in FRAPCON-3

5.1 Background

Fuel pellet center temperatures measured at BOL in instrumented test rods have repeatedly been found to be lower than values predicted by thermal performance computer programs when the predicted fuel-cladding gap in operation is calculated only on the basis of fuel and cladding thermal expansion (Lanning 1982).[a] It has long been concluded, on the basis of microscopic examination of fuel cross sections (Galbraith 1973; Cunningham and Beyer 1984), that fuel pellet cracking promotes an outward relocation of the pellet fragments that causes additional gap closure. This process begins at BOL and quickly reaches an equilibrium. Oguma (1983) characterized this approach to equilibrium based on his analysis of BOL test rod elongation data from Halden instrumented test assemblies.

The fuel pellet cracking that promotes relocation is predominantly radial; however, some circumferential components to these crack patterns exist, and they could alter the fuel thermal conductivity. Thus, cracking and relocation will to some degree increase the thermal resistance in the pellet while reducing the thermal resistance of the pellet-cladding gap by reducing its effective size.

5.2 Experimental Evidence for Crack-Induced Relocation and Thermal Conductivity Degradation

In a series of tests in the Power Burst Facility (PBF) reactor at Idaho National Engineering Laboratory (INEL) (Garner et al. 1978) entitled the "Gap Conductance" (GC) series GC-1,2, and 3, test rods of varying gap size and fill gas compositions were instrumented with both centerline thermocouples and multiple coplanar off-center thermocouples in an attempt to quantify this transfer of thermal resistance from gap to fuel. The results indicated a major effect; according to INEL's analysis, the BOL gap size is reduced to much less than 50% of its unrelocated value, and the pellet thermal conductivity is significantly reduced to a degree that varies with the LHGR and thus with the degree of "soft" pellet-cladding mechanical interaction (PCMI).

"Soft" PCMI occurs when the cracked (and highly deformable) pellet interacts mechanically with the cladding, producing fuel-cladding contact and limited enhanced axial rod elongation, but not the steep elongation vs. LHGR and bamboo ridging associated with "hard" PCMI. A rod evidencing soft PCMI in operation also evidences pellet deformability in rod radial compression tests. The occurrence of "soft"

(a) Kjaerheim, G. and E. Rolstad. 1967. In-Pile Determination of UO_2 Thermal Conductivity, Density Effects and Gap Conductance, HPR-80. Halden Reactor Project, Halden, Norway.

PCMI is consistent with the results of several experiments in the Halden Reactor, including NRC-sponsored tests, in which fuel temperature and rod elongation were simultaneously measured as a function of burnup and LHGR (Williford et al. 1980).

However, the PBF tests are difficult to analyze thermally; the off-center thermocouples create complex heat transfer solutions and also complex and atypical pellet cracking patterns. Therefore, the degree to which the thermal resistance transfers from gap to pellet by cracking/relocation remains largely undefined.

5.3 New Relocation Model for FRACAS-1

It is certain that cracking and relocation serve to reduce measured fuel-center temperatures at a given LHGR from what they are predicted to be when differential fuel/cladding thermal expansion is the sole gap closure mechanism (Lanning and Cunningham 1981). It is also certain that predicted fuel-stored energy (for a given combination of LHGR and centerline temperature) is maximized by assuming *no* "crack factor" reduction of the fuel thermal conductivity (Lanning 1982). Therefore, since calculation of the initial BOL stored energy for LOCA analysis initialization is one major application of the NRC fuel performance code, the option for *no* crack factor on the pellet thermal conductivity (in combination with an explicit, best-estimate relocation/gap closure model) is preserved in FRAPCON-3.

In conjunction with the FRACAS-1 model, the original FRAPCON-2 used a lower-bound version of the GT2R2 model for gap closure due to relocation (Cunningham and Beyer 1984). This model, called EMRLOC, resulted in very large overestimates of BOL fuel temperatures for the standard IFA-432/513 cases, on the order of 100 to 200 K (see Figure 5.1). The best-estimate version of GT2R2 relocation is as follows:

$$\Delta G/G(\text{in \%}) = 30 + 5 \bullet \text{FBU for LHGR} < 20 \text{ kW/m}$$

$$= 30 + \text{PFACTOR} + (5 + \text{PFACTOR}) \bullet \text{FBU for LHGR} < 40 \text{ kW/m}$$

$$= 35 + 10 \bullet \text{FBU for LHGR} > 40 \text{ kW/m} \tag{5.1}$$

where   FBU = BURNUP/5, for BURNUP < 5 GWd/MTU
              = 1.0 for BURNUP $\geq$ 5 GWd/MTU

and   PFACTOR = (LHGR - 20) $\bullet$ 5/20
         BURNUP = fuel nodal burnup in GWd/MTU
             LHGR = Nodal LHGR in kW/m.
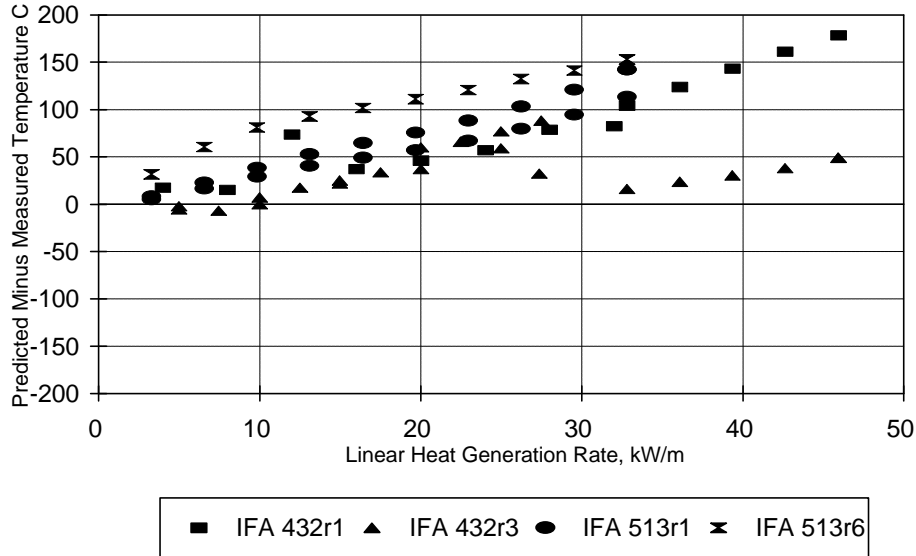
Figure 5.1. Comparison of FRAPCON-3 Predictions with EMRELOC Relocation Against BOL Measured Fuel Center Temperatures from Halden Instrumented Fuel Experiments vs. LHGR

This best-estimate GT2R2 relocation model was altered slightly to provide a best estimate prediction of fuel temperatures for FRAPCON-3. This GT2R2 model is a function of LHGR and burnup that is similar to Oguma's model, but less complex in form. The gap closure due to relocation as a fraction of the as-fabricated pellet-cladding gap is given by

$$\Delta G/G = 30 + 10 \bullet FBU \text{ for LHGR} < 20 \text{ kW/m}$$

$$= 28 + PFACTOR + (12 + PFACTOR) \bullet FBU \text{ for LHGR} < 40 \text{ kW/m}$$

$$= 32 + 18 \bullet FBU \text{ for LHGR} > 40 \text{ kW/m} \tag{5.2}$$

where FBU, BURNUP, and PFACTOR have the same meaning as above.

A plot of this model (subroutine GTRLOC) as a function of burnup and LHGR is shown in Figure 5.2.

5.3.1 Verification of the Revised Model

The FRAPCON-3/FRACAS-I combination, in conjunction with the above revised relocation model, (and the other major model changes described in this report), has been evaluated against in-reactor fuel
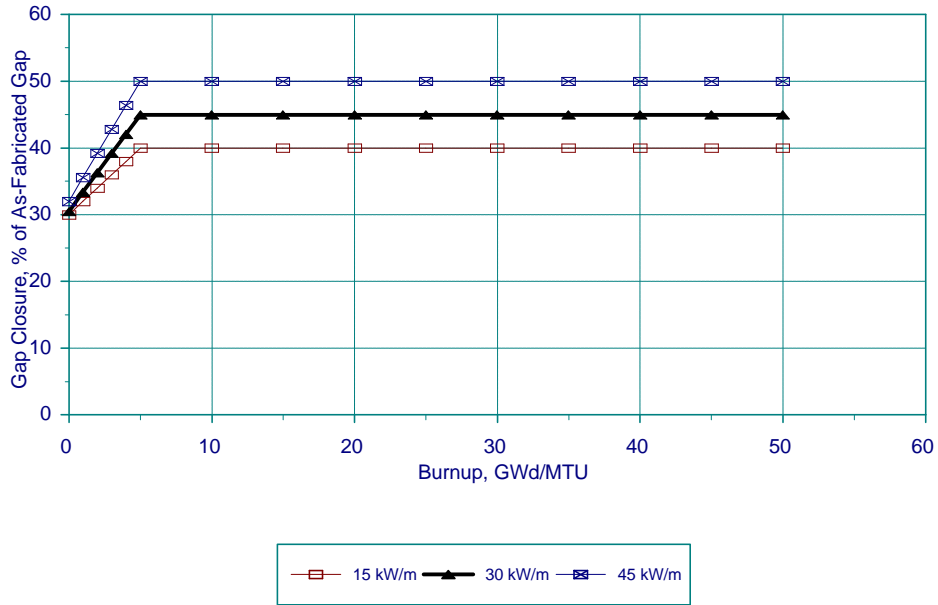
Figure 5.2. Power and Burnup Dependence of the FRAPCON-3 Relocation Model

temperature measurements from the IFA-432 and IFA-513 test rods described in Table 5.1, at BOL. The predicted-minus-measured temperature differences at BOL are plotted vs LHGR in Figure 5.3. Inspection of this figure confirms that bias does not exist in the temperature deviations,

Table 5.1. Design Variations Among the Selected Test Rods[a]

Halden Assembly	Rod Number	Fuel Cladding Diametral Gap, μm (mils)	Fill Gas Composition, Vol. %
IFA-432	1	230(9)	100% He
IFA-432	2	380(15)	100% He
IFA-432	3	76(3)	100% He
IFA-513	1	230(9)	100% He
IFA-513	6	230(9)	23% Xe 77% He[b]

(a) For all these rods, cladding ODxID = 1.2789/1.0909 cm (0.5035/0.4295 inches), and pellet ID in the thermocouple region = 0.1753 cm (0.069 inch); and fuel density = 95%, TD (stable against in-reactor densification).
(b) Gas thermal conductivity = ~50% that of helium.
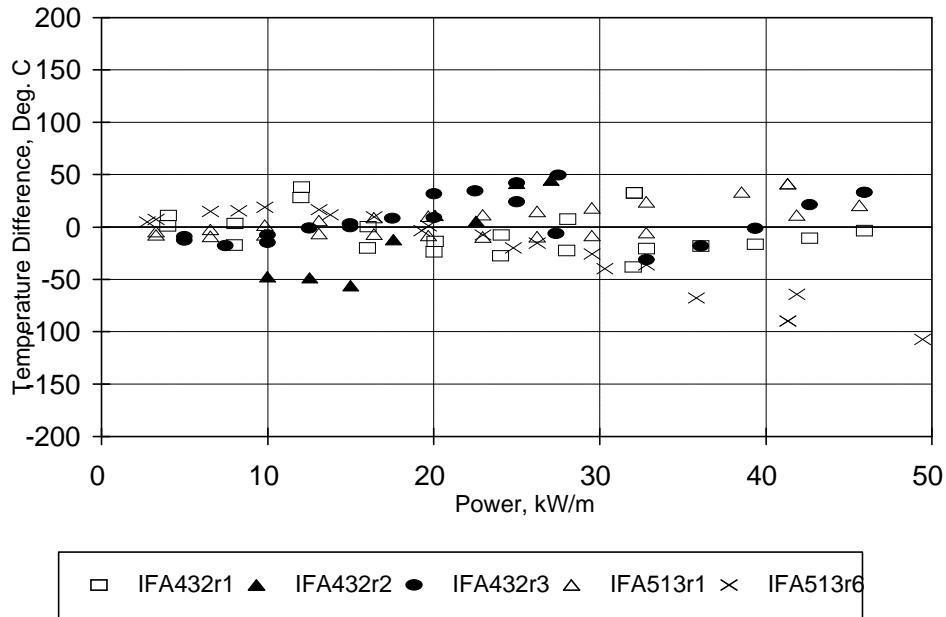
Figure 5.3. Comparison of FRAPCON-3 Predictions with GTRLOC Relocation against BOL Measured Fuel Center Temperatures from Halden Instrumented Fuel Experiments, vs. LHGR

as a function of LHGR, and that the code predictions are within ± 50K of measured values at BOL for rods with 100% helium fill gas. This close correspondence is considered to be state-of-the-art for such comparisons and, therefore, is verification of the adequacy of the combined pellet relocation and fuel thermal conductivity models in FRAPCON-3.

5.4 Range of Application and Uncertainty

The GTRLOC model has its greatest effect at burnups less than 10 GWd/MTU; nevertheless, it is assumed to apply throughout fuel life. The LHGR range is that of the original database. Therefore, the application ranges are taken to be as follows:

  Burnup: 0 to 65 GWd/MTU Rod-Average
  LHGR: 9 to 60 kW/m

The uncertainty on the relocation model is proportional to the LGHR, and is ± 0.3 degree K per W/m (one standard deviation), based on a combination of uncertainty on center temperature measurements and uncertainty on BOL gap closure. The latter is estimated from the data scatter of 15 μm (one standard deviation) in Oguma's paper.

5.5 Bibliography

(Note: Bibliographical entries are not called out in the text. For called-out references, see Section 11.0.)

Berna, G. A., M. P. Bohn, W. N. Rausch, R. W. Williford, and D. D. Lanning. 1981. *FRAPCON-2: A Computer Code for the Calculation of Steady State Thermal-Mechanical Behavior of Oxide Fuel Rods*, NUREG/CR-1845, Nuclear Regulatory Commission, Washington, D.C.

Kjaerheim, G. and E. Rolstad. 1967. In-Pile Determination of UO_2 Thermal Conductivity, Density effects and Gap Conductance, HPR-80 (Halden Reactor Project, Halden, Norway). Not publicly available.

Lanning, D. D., B. O. Barnes, and R. E. Williford. 1979. *Manifestations of Nonlinearity in Fuel Center Thermocouple Steady-State and Transient Data: Implications for Data Analysis*, NUREG/CR-0220, PNL-2692, Pacific Northwest Laboratory, Richland, Washington.

Lanning, D. D. and M. E. Cunningham. 1981. "Trends in Thermal Calculations for Light Water Reactor Fuel (1971-1981)." In proceedings of the *Ninth Water Reactor Safety Research Information Meeting*, Gaithersburg, Maryland, October 26-30, 1981.

Williford, R. E., C. L. Mohr, D. D. Lanning, M. E. Cunningham, W. N. Rausch, and E. R. Bradley. 1980. *Interim Report: The Analysis of Fuel Relocation for the NRC/PNL Halden Assemblies IFA-431, IFA-432, and IFA-513*, NUREG/CR-0588, PNL-2709. Pacific Northwest Laboratory, Richland, Washington.

6.0 Modifications to the Power and Burnup Radial Distribution Functions in FRAPCON

6.1 Background

The volumetric heat generation (W/m^3) at any point within a fuel pellet is proportional to the effective thermal neutron flux multiplied by the sum of the fissile isotope concentrations times their effective fission cross sections. At BOL, the typically low enrichment of the [235]U isotope (3 to 5%) constitutes the only fissile isotope, and the radial distribution of [235]U is uniform. The thermal neutron flux level is only slightly depressed in the center relative to the edge, resulting in a nearly uniform radial distribution of volumetric heat generation.

As burnup proceeds, fission consumes [235]U, but [238]U captures resonance energy neutrons, resulting in a limited buildup of plutonium, including the fissile plutonium isotopes [239]Pu and [241]Pu. Because of the large value of the capture cross section at resonance energies, this plutonium buildup occurs preferentially, but not exclusively, at the pellet edge. The plutonium content in the pellet builds asymptotically towards approximately 1% pellet average and 3 to 4% in the pellet rim. Thus the fissile plutonium concentration at the rim begins to significantly exceed that in the remainder of the pellet as burnup accumulates, and the radial distribution of the volumetric heat generation becomes progressively edge-peaked. The radial distribution of fuel burnup (in relation to the initial concentration of heavy metal atoms) also becomes progressively edge-peaked.

Accurate calculations of the evolution of neutron flux distribution and fissile isotope concentrations within a fuel rod require detailed neutronics codes that account for all the interactions and the specific time-dependent neutronic environment of the rod. However, the environments and fuel designs in standard LWR cores are sufficiently similar to permit approximate, one-dimensional one-group calculations, using effective values for fission and capture cross sections. The RADAR subroutine (Palmer et al. 1982) represents one such approximate solution that contains an exponential distribution function that governs the radially dependent buildup of the plutonium and an effective cross-section for the plutonium. Matsamura and Kameyama (1988) published another algorithm, based on interpolation within tabulated specific neutronics results. Shann (1991) produced a similar algorithm.

Lassmann et al. (1994) from the Institute for Transuranium Elements, Karlsruhe, Germany, wrote the TUBRNP code, which improves upon RADAR by modifying the parameters for the plutonium-distribution function and accounting for the plutonium isotopes explicitly. The result is a somewhat more edge-peaked distribution function at nominal to high fuel burnups, which is supported by comparison to detailed neutronics calculations and to detailed electron microprobe data on the distribution of both plutonium and stable fission products (Lassmann et al. 1994; Lassmann et al. 1995).

Figures 6.1 and 6.2 show an example of the plutonium buildup and its consequences, which apply to a C-E 14 × 14 type fuel rod with 4.5% ^{235}U enrichment. Figure 6.1 shows the radial distributions of heat generation and burnup at 60-GWd/MTU pellet-average burnup. Figure 6.2 shows the ratios of the edge (outermost 1%) to volume-average values for heat generation and for burnup. The edge-peaking becomes significant from 20-GWd/MTU burnup onward.

Lassmann's model has demonstrated good comparisons to detailed data on burnup distribution while retaining more generality than the specific-case interpolations by Matsamura or Shann; it is therefore chosen for application in FRAPCON-3.
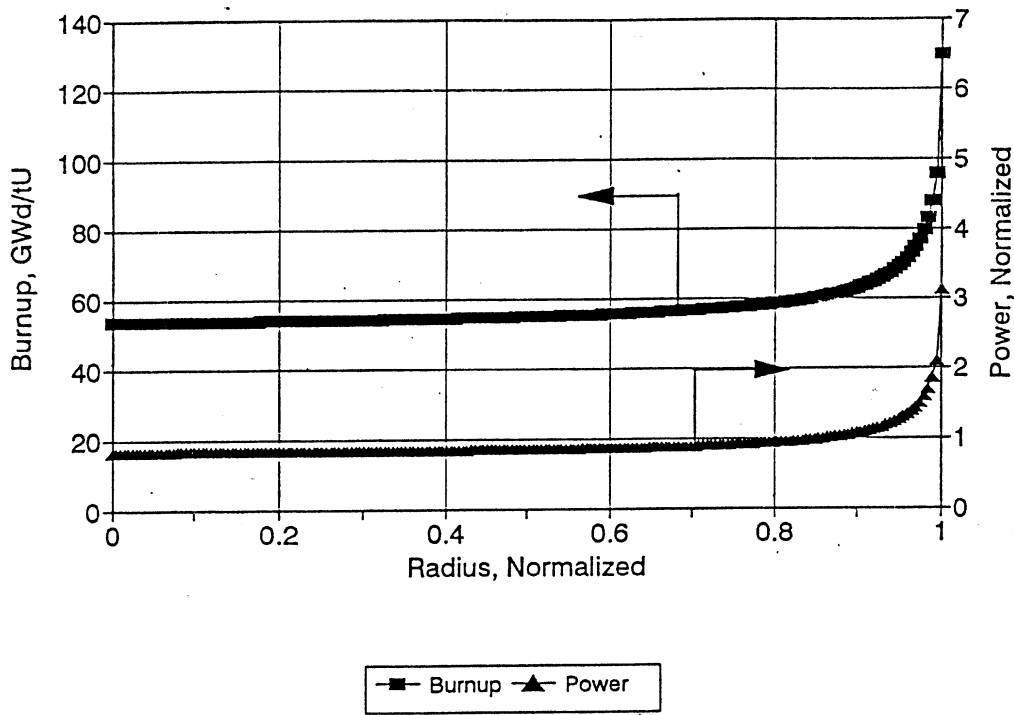
Figure 6.1. Edge Burnup and Power vs. Radius for an Average Burnup of 60 GWd/MTU

6.2 Experimental Evidence for Edge-Peaking of Burnup and Heat Generation in LWR Fuel Pellets

Electron microprobe scans across transverse cross sections cut from irradiated fuel pellets reveal the relative radial distribution of selected fission products. If the selected fission product is extremely stable (i.e., stays fixed at the position of creation throughout the irradiation), then its relative radial distribution indicates the radial distribution of the fuel burnup. This is only indirect evidence for the radial distribution of the heat generation, which of course is changing throughout the irradiation. However,
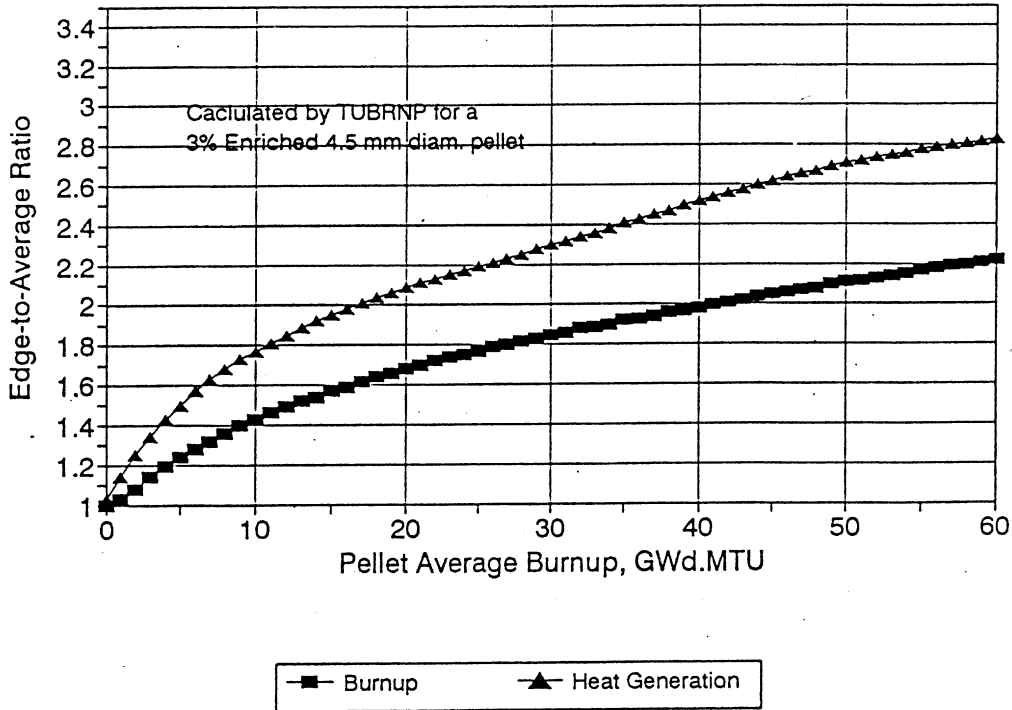
Figure 6.2. Ratio of Heat Generation and Burnup in Outermost 1% of Pellet Radius to Average

comparative radial scans on burnup indicators at different burnup levels for the similar fuel types, subjected to similar irradiation histories, give detailed evidence about the evolution of the radial power distribution.

The fission product neodymium, a rare-earth metal, has been proven to be extremely stable chemically and thermally within the fuel; it is therefore a reliable burnup distribution indicator. In the High-Burnup Effects Program (Barner et al. 1990; Cunningham 1992), electron microprobe scans for neodymium were performed on urania LWR test fuel and urania pellets from BWR rods, with pellet burnups ranging from 25 to 55 GWd/MTU. Table 6.1 lists the pertinent parameters for these rods (pellet dimensions, enrichment, and burnup). Figures 6.3 to 6.7 show HBEP neodymium distributions measured by electron probe micro analysis (EPMA), together with the radial burnup distribution predicted by TUBRNP. To make this comparison on radial distribution, the neodymium concentrations have been transformed to burnups, and the predicted and measured values have been forced to have the same volume-averaged value.

These code-data comparisons are excellent regarding the general shape of the radial burnup distribution at various burnup levels. The predicted value of the relative burnup at the surface of the pellet consistently exceeds the measurements near the surface; however, it is very difficult in this steeply changing region to position the EPMA analysis area (the 2- to 10-μm-diameter "spot") at the exact surface of the fuel without overlapping into the gap region that contains no fuel and hence biases the

Table 6.1. Description of the Selected HBEP Rods Used for Code-Data Comparisons for Radial Burnup Distributions

Rod Number	Pellet Inner/Outer Radii, mm	U-235 Enrichment, %	EOL Burnup, GWd/MTU	Reactor Name and Type
A3/6-4	5.22/0.0	3.08	55	TV0-1 BWR (1.5-m Elevation)
H8/36-4	4.97/0.0	1.39	55	TVO-1 BWR (2.2-m Elevation)
BK-365	4.09/1.27	6.97	83	BR-3 PWR Test Reactor
D200	4.52/0.0	3.2	25	Obrigheim PWR
D226	4.56/0.0	3.2	45	Obrigheim PWR
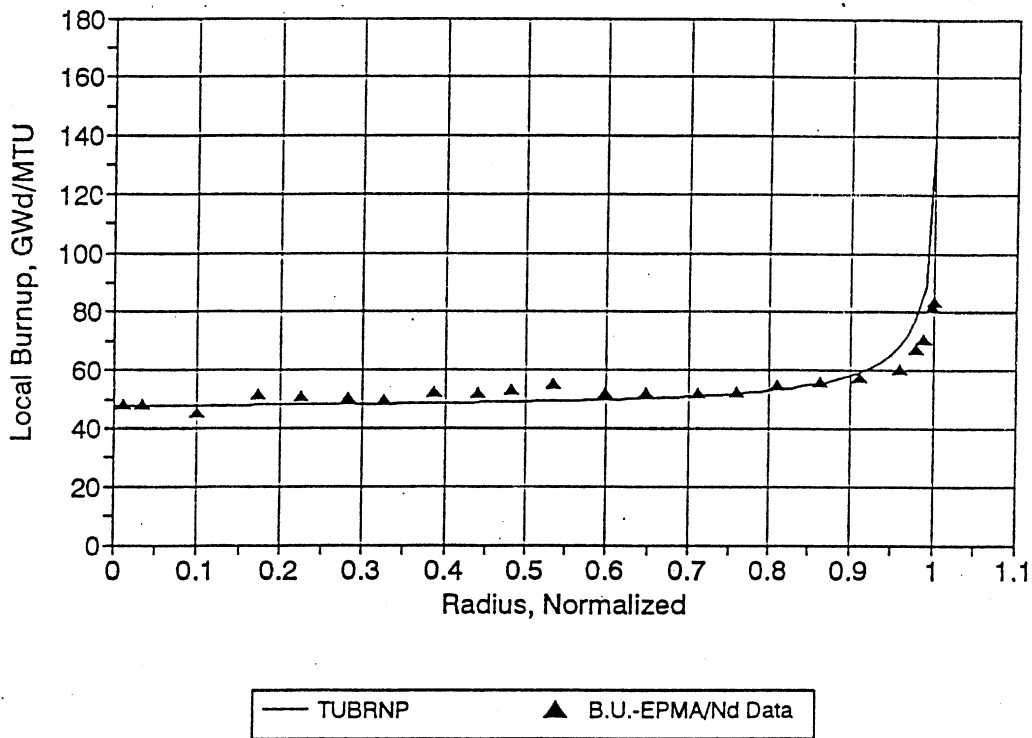
Figure 6.3. TUBRNP Compared to HPEP Data for Rod A3/6-4 at 55 GWd/MTU
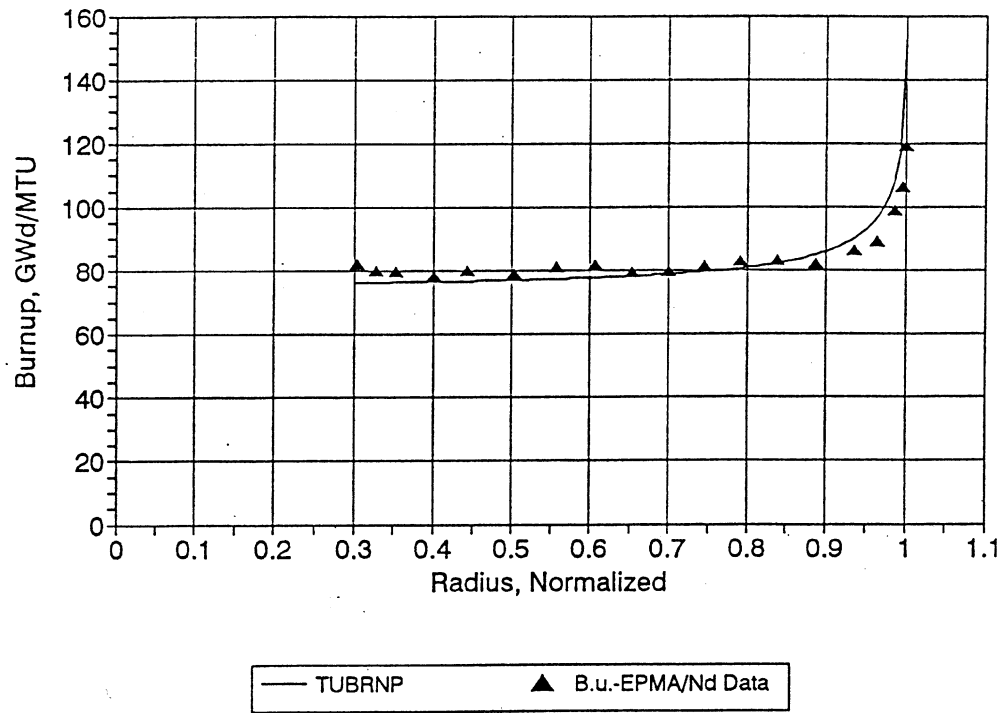
Figure 6.4. TUBRNP Compared to HBEP Data for TVO Rod H8/36-4 at 55 Gwd/MTU
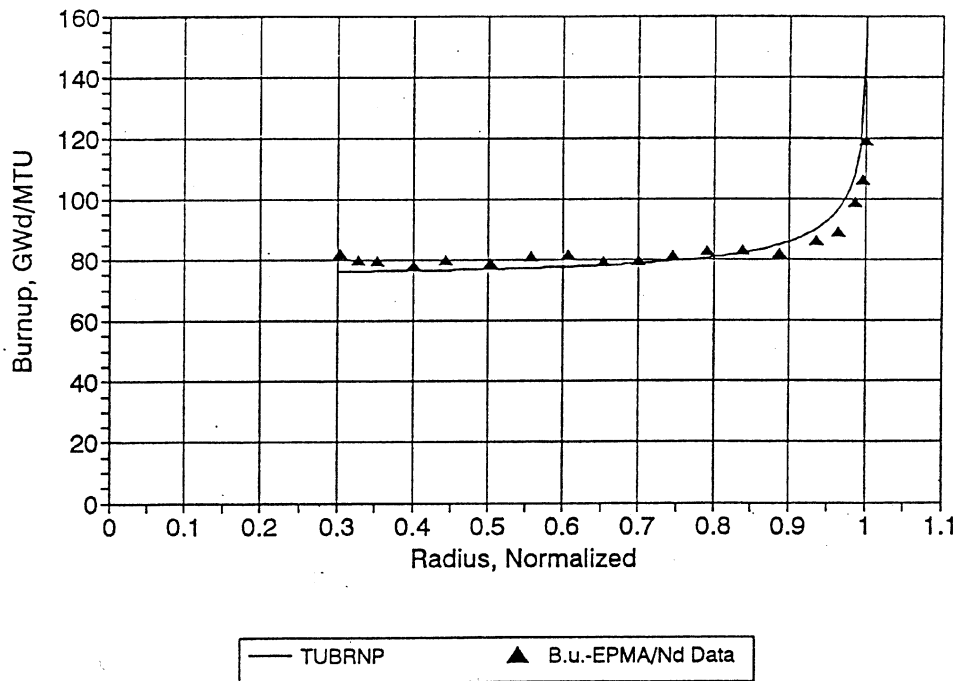
Figure 6.5. TUBRNP Compared to HBEP Data for Rod BK365 at 83 GWd/MTU
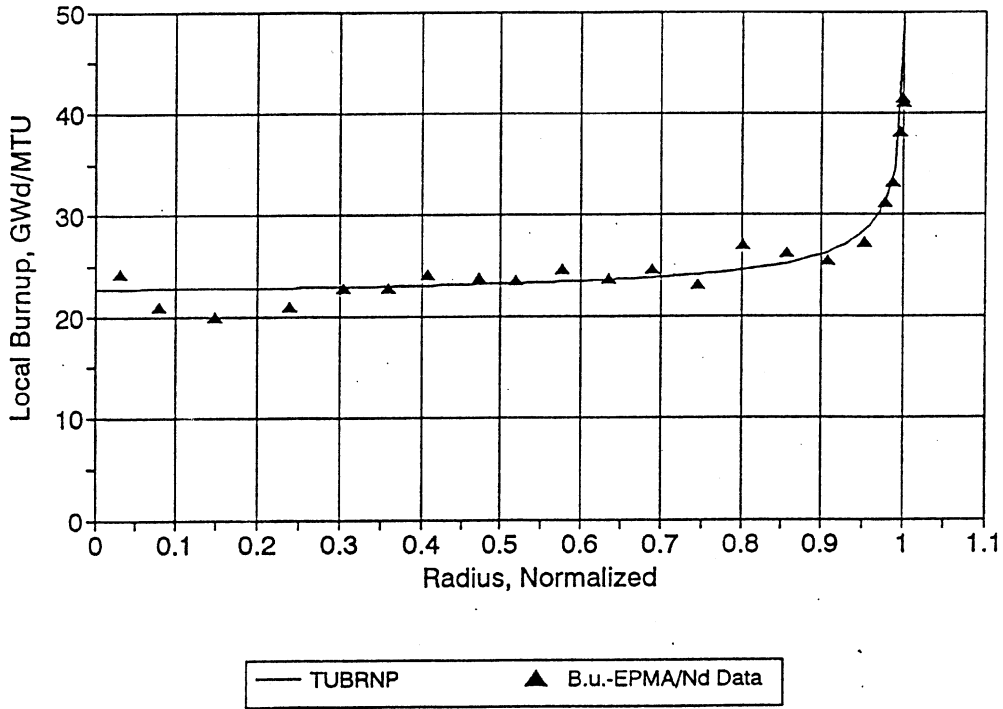
Figure 6.6. TUBRNP Compared to HBEP Data for Rodlet D226 at 45 GWd/MTU
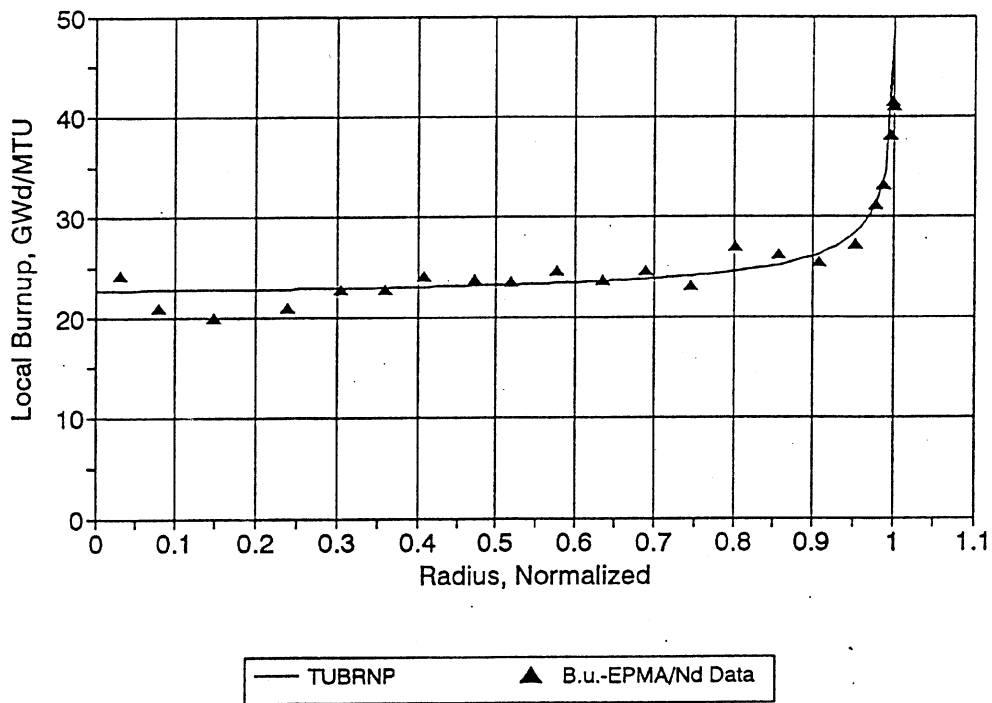
Figure 6.7. TUBRNP Compared to HPEP Data for Rodlet D200 at 25 GWd/MTU

measurement downward. Therefore, because the predicted shape of the distribution does follow the measurements closely out to very nearly the pellet surface, the predicted surface values are considered realistic.

6.3 Description of the TUBRNP Subcode

The neutron flux distribution $\phi(r)$ within the fuel pellet is described in TUBRNP by the solution of one-group, one-dimensional diffusion theory applied to cylindrical fuel:

$$\phi(r) = CI_0(\kappa r) \tag{6.1}$$

for solid pellets, and

$$\phi(r) = C \left(I_0(\kappa r) + \left[\frac{I_1(\kappa r_0)}{K_1(\kappa r_0)} \right] K_0(\kappa r) \right) \tag{6.2}$$

for annular pellets

where

$$\kappa = \sqrt{\Sigma_a/D}, \ \Sigma_a = \sum_k \sigma_{a,i} \overline{N}_i, \ D = \frac{1}{3\Sigma_s} = \frac{1}{3\sigma_s \overline{N}_{tot}}$$

and I,K = Modified Bessel functions
    C = a constant
    σ_a, σ_s = absorption and scattering cross sections
    $\overline{N}$ = pellet-average atom concentration
    r_0 = the pellet outer radius
    I = subscript indicating all U and Pu isotopes

The evolution of average uranium and plutonium isotope concentrations in the fuel through time can be described as a coupled set of differential equations, which are coupled because the loss of one isotope by neutron capture leads in some cases to some production of the next higher isotope. These equations are summarized as follows:

$$\frac{d\overline{N}_{235}}{dt} = -\sigma_{a,235} \overline{N}_{235} \phi \tag{6.3}$$

$$\frac{d\overline{N}_{238}}{dt} = -\sigma_{a,238}\overline{N}_{238}\phi \qquad (6.4)$$

$$\frac{d\overline{N}_j}{dt} = -\sigma_{a,j}\overline{N}_j\phi + \sigma_{c,j-1}\overline{N}_{j-1}\phi \qquad (6.5)$$

where $\quad j \quad = \quad ^{239}Pu, ^{240}Pu, ^{241}Pu,$ and ^{242}Pu

$\qquad \sigma_a, \sigma_c \quad = \quad$ absorption and capture cross sections.

Because, in fuel performance codes, the LHGR and time step duration are input values, the burnup increment for the time step is prescribed and can be related to the flux, the fission cross sections, and the concentrations of fissile isotopes. Thus flux-time increment dt can be replaced by the burnup increment "dbu," via the relation

$$dbu = \frac{q'''dt}{\rho_{fuel}} = \frac{\alpha}{\rho_{fuel}}\sum_k \sigma_{f,k}\overline{N}_k\phi dt \qquad (6.6)$$

where $\quad q''' \quad = \quad$ Volumetric heat generation rate

$\qquad \rho_{fuel} \quad = \quad$ fuel density

$\qquad \sigma_f \quad = \quad$ fission cross section

$\qquad \alpha \quad = \quad$ a conversion constant

Furthermore, the distribution of plutonium production is described by an empirical function f(r), the parameters for which are to be selected on the basis of code-data comparisons on plutonium concentrations as a function of burnup. Thus, the equations for isotope distribution N(r) become

$$\frac{dN_{235}(r)}{dbu} = -\sigma_{a,235}\,N_{235}(r)\,A \qquad (6.7)$$

$$\frac{dN_{238}(r)}{dbu} = -\sigma_{a,238}\overline{N}_{238}\,f(r)A \qquad (6.8)$$

$$\frac{dN_{239}(r)}{dbu} = -\sigma_{a,239}N_{239}(r)A + \sigma_{c,238}\overline{N}_{238}\,f(r)A \qquad (6.9)$$

$$\frac{dN_j(r)}{dbu} = -\sigma_{a,j}N_j(r)A + \sigma_{c,j-1}N_{j-1}A \qquad (6.10)$$

where, in this case, j = the 240, 241, and 242 isotopes of plutonium,

$$A = 0.8815 \ \rho_{fuel}/\alpha \ \sum_i \sigma_{f,i}\overline{N}_i$$

$$f(r) = 1 + p_1 \exp[-p_2(r_{out}-r)^{P3}],$$

and p_1, p_2, and p_3 are empirically determined constants.

The function f(r) is constrained to have a volume-averaged value of 1.0.

At the end of each time step, the isotope concentrations are updated based on the burnup increment, using the above equations. These equations are solved and the concentrations evaluated at every input radial boundary. Because the flux and plutonium deposition distribution functions are prescribed, and the solutions are carried out at ring boundaries, the solution is independent of the radial nodalization scheme; it is also quite stable with respect to time-step size, within the limits dictated by other processes, such as cladding creep and fission gas release.

The TUBRNP subcode provided by the Institute for Transuranium Elements carries with it an associated subroutine (bes.f) for calculating the modified Bessel functions used to distribute the reactions implied by each burnup step.

Users of the FRAPCON-3 code must reference the Lassmann et al. 1994 citation in published calculational results in which the TUBRNP model is employed.

6.4 Changes to FRAPCON-3 to Include and Accommodate the TUBRNP Subcode

The changes to the FRAPCON-3 code to install and use the TUBRNP subcode provided by the Institute for Transuranium Elements, Karlsrulhe, Germany (Lassmann et al. 1994), are extensive. They involve, first of all, changing the fuel and cladding temperature calculator from the method of weighted residuals to a finite-difference scheme defined in Berna et al. 1997.

Next, the radial "form factor" arrays generated by TUBRNP and used by both the temperature calculator and the fission gas release subroutines have been properly mapped into each routine. The form-factor arrays are two-dimensional arrays of normalized current local fission rates and the radial boundaries

at which they are defined; the fission rates are normalized to have a volume (i.e., area) averaged value of 1.0. A power array is calculated by TUBRNP for each axial node every time step. The use of the TUBRNP array for the fission gas release subroutines MASSIH and ANS-5.4 are defined in Berna et al. (1997). The radial burnup array generated by TUBRNP is not currently used except for optional output. The burnup and fission gas production arrays needed by each FGR subroutine are built up incrementally within the respective routines, using the form factor arrays from TUBRNP.

6.5 Range of Application and Uncertainty

The revised fuel pellet radial power distribution model has the following ranges of application:

        Burnup: 0 to 80 GWd/MTU
 Temperature: 300 to 3000K
   Fuel types: Urania and urania-plutonia sintered pellets (but not urania-gadolinia pellets)

In addition, users of the FRAPCON-3 code must reference the Lassmann et al. 1994 citation in published calculational results in which the TUBRNP model is employed.

The uncertainty on the localized (ring) burnup (one standard deviation) varies with the position in the pellet and with pellet burnup. Based on statistical analysis of the code-data comparisons presented herein, Table 6.2 provides estimated uncertainties for localized burnup and power (one standard deviation) for pellets with average burnups greater than 25 GWd/MTU (see Table 6.3 for individual analyses on specific samples). It should be noted that these uncertainties apply to UO_2 fuel only, and the code has not been validated against urania-plutonia fuel and uncertainties, which are unknown.

Table 6.2. Estimated Uncertainties

Position within the Pellet (normalized radius where 1.0 is outer surface)	Relative Uncertainty on Burnup (1 standard deviation), %	Relative Uncertainty on Heat Generation, %
0.0 to 0.9	7	8
0.9 to 0.98	12	15
0.98 to 1.0	50	50

Table 6.3. Results of Statistical Analyses of Code-Data Comparison: TUBRNP Model vs.
Selected HBEP EPMA Data for Burnup Determined from Nd

Rod Number	Overall Standard Deviation, %	Std. Dev. from 0 to 90% of Pellet Radius	Std. Dev. from 90 to 98% of Pellet Radius	Std. Dev. from 98 to 100% of Pellet Radius
A3/6-4	29.7	6.7	16	100
H8/36-4	36.6	11.5	23	80
D200	9.9	6.8	7.6	12
D226	16.5	4.0	5.0	25
BK365	13.5	4.6	7.0	20
Averages	21	6.7	11.7	~50

7.0 Modifications to the FRAPCON-3 Model for Solid-Solid Contact Conductance

7.1 Background

When the pellet-cladding gap closes for various reasons, heat is conducted through the points of solid-solid contact between the rough and cracked pellet and relatively smoother cladding. This "contact conductance" is typically about 1/5 of the total gap conductance when helium gas fills the spaces between the contact points. As the fill gas becomes progressively contaminated with the noble fission gases, the gas conductivity decreases, and the contact conductance will represent a much greater fraction of the total gap conductance. Furthermore, as burnup proceeds, the cladding will creep to conform more closely with the pellet surface, and the interstitial space may fill with condensed volatile fission products, notably cesium and iodine and their compounds. These effects enhance the contact conductance even more.

Because of its importance to late-in-life heat conduction from the rod, contact conductance has been the subject of numerous ex-reactor and even in-reactor studies in the past 30 years (for example, Ross and Stoute [1962], Dean [1962], and Fenech and Rohsenow [1959]). Todreas and Jacobs (1973) published a summary of their own and earlier ex-reactor experimental results. The Todreas model was modified slightly by Lanning and Hann (1975) for use in the GAPCON-THERMAL-2 code (Beyer et al. 1975), and this version was also used in FRAPCON-2. However, this model underpredicts the contact conductance at high-contact pressure on the basis of definitive measurements obtained in an NRC-sponsored ex-reactor series of tests on Zircaloy:sintered urania interfaces. This is discussed in the next section.

7.2 Experimental Evidence for Modifying Contact Conductance

Lanning and Hann (1975) noted that considerable scatter existed in contact conductance data available at that time, with the available data taken under widely varying surface and ambient conditions. Therefore, NRC initiated a program to make ex-reactor controlled measurements of gap conductance, including contact conductance; Garnier and Begej (1979) reported their findings from this program.

Garnier and Begej measured solid-solid conductance by measuring the steady-state temperature gradients within contacting pairs of UO_2 and Zircaloy samples (having precharacterized contacting surfaces). The contact pressure was varied as the samples conducted heat longitudinally along their length and across their interface while residing in a vacuum atmosphere. The contact conductance data obtained by Garnier and Begej are summarized by the points labeled ISM-II Block 0 and ISM-II Block 1 data in Figure 7.1, taken from their report. The ISM-II compacts had representative roughness values (1.6 µm for the UO_2, 0.4 µm for the Zircaloy) but differed in the amplitude of the UO_2 surface waviness, as described in Table 11 in the Garnier/Begej report. The Block 1 compact had the higher amplitude
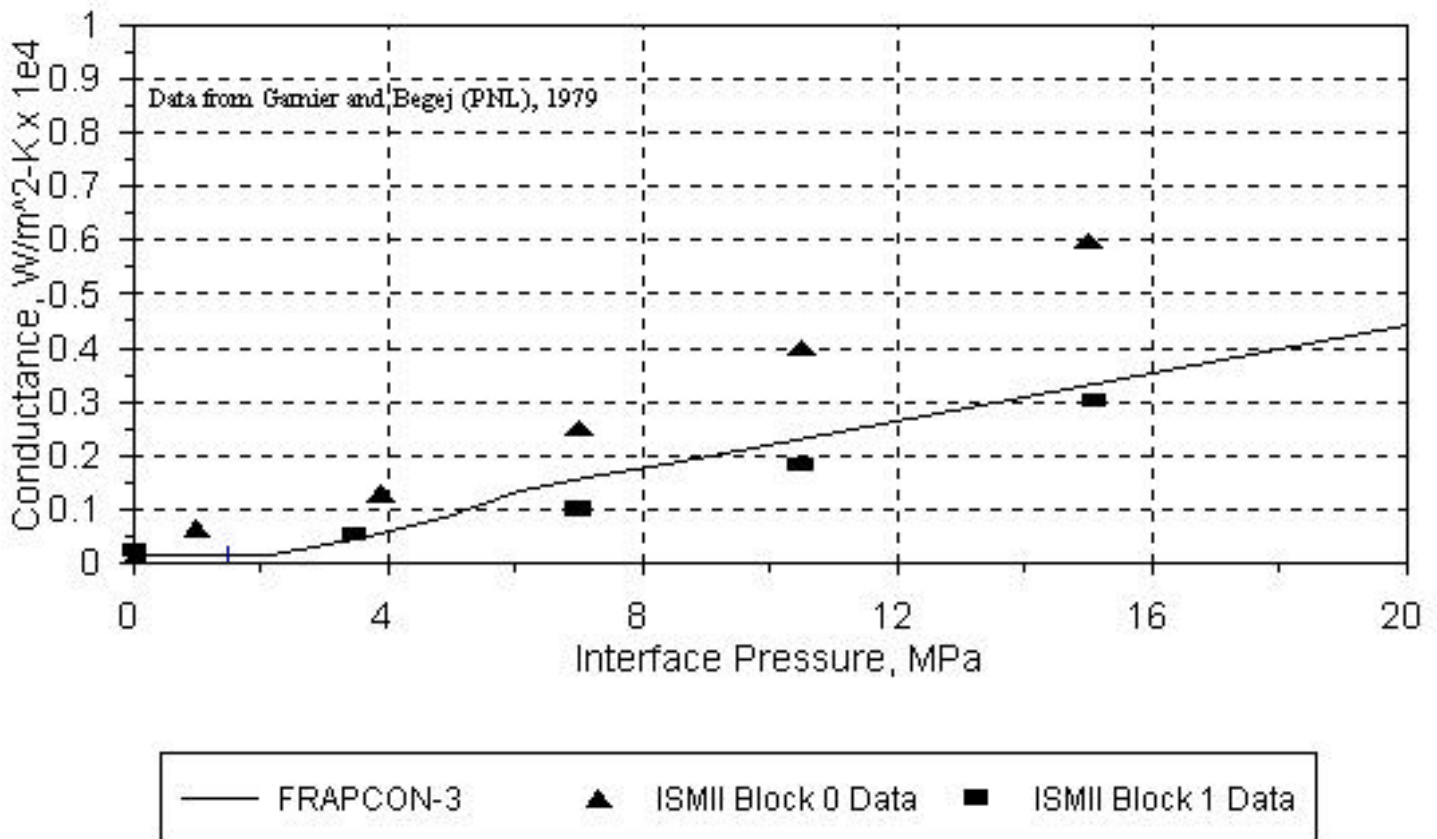
Figure 7.1. Solid-Solid Conductance from FRAPCON-3 Compared to Data by Garnier and Begej

and hence the lower conductance values than the Block 0 compact. The range of contact conductance values represented by these data sets was originally considered typical of the possible range (because of variations in surface waviness) to be encountered in commercial reactor fuel.

In this same plot, the result of multiplying the contact conductances calculated from FRAPCON-2 by 2.9 is shown, as implemented in FRAPCON-3, for relative contact pressures greater than 0.0087 (5.9 MPa). Without this modification, the contact conductance model underpredicts both the ISM-II Block 0 and Block 1 data sets. This change preserves the roughness, conductivity, and pressure dependencies of the original Mikic-Todreas model in FRAPCON-3, but provides a best estimate prediction for the contact conductances measured by Garnier and Begej. It was elected to provide a best estimate prediction for this data because it compared the better against in-reactor temperature measurements of small gap rods, with fuel-cladding contact.

Description of the Model

The contact conductance model is a modification of the Mikic-Todreas model that preserves the roughness, conductivity, and pressure dependencies while providing a best-estimate for the range of contact conductances measured by Garnier and Begej. The GAPRS subroutine uses expressions for h_{solid} that are dependent on both the fuel-cladding interfacial pressure and the microscopic roughness, R, as follows

$$h_{solid} = \frac{0.4166 \ k_m P_{rel} R_{mult}}{R \ E} \quad , \text{if } P_{rel} > 0.003$$

$$= \frac{0.00125 \ k_m}{R \ E} \quad , \text{if } 0.003 > P_{rel} > 9E{-6}$$

$$= \frac{0.4166 \ k_m P_{rel}^{0.5}}{R \ E} \quad , \text{if } P_{rel} < 9E{-6} \tag{7.1}$$

where h_{solid} = solid-solid conductance in W/m^2-K
$\quad\quad P_{rel}$ = ratio of interfacial pressure to cladding Meyer hardness (approximately 680 MPa)
$\quad\quad k_m$ = mean conductivity (W/m-K),
$\quad\quad\quad$ = $2K_f K_c/(K_f + K_c)$
$\quad\quad\quad\quad$ where K_f, K_c = fuel and cladding thermal conductivities,
$\quad\quad\quad\quad$ evaluated at the surface temperature
$\quad\quad R$ = $\sqrt{R_F^2 + R_C^2}$ (m), where R_f, R_c = roughness of fuel and cladding(m)
$\quad R_{mult}$ = 333.3 P_{rel}, if $P_{rel} \leq 0.0087$
$\quad\quad\quad$ = 2.9 $\quad\quad$, if $P_{rel} > 0.0087$
$\quad\quad E$ = exp[5.738 - 0.528 ln (R_f *3.937x10^7)]

7.4 Range of Application and Uncertainty

The revised contact conductance model has the following ranges of application:

$\quad\quad\quad\quad$ Burnup: Not specifically limited
$\quad\quad\quad$ Temperature: Normal LWR operating temperature range
$\quad$ Contact Pressures: 0 to 4000 psia

The materials are Zircaloy and urania (or urania-plutonia). (However, within the broad uncertainty in the measured data, this correlation is also expected to be applicable to stainless steel: urania interfaces.)

The uncertainty on the contact conductance (one standard deviation) is estimated as ± 50% relative, based on comparing the model with the Garnier-Begej contact conductance data at low pressure, and based on their error analysis of the modified longitudinal design measurement technique.

At sustained contact pressures higher than 4000 psia, the model is expected to yield low results because localized creep or plastic deformation of the cladding will, over time, decrease the average separation of the surfaces and increase the points of contact, therefore increasing the contact conductance.

7.5 Bibliography

(Note: Bibliographical entries are not called out in the text. For called-out references, see Section 11.0.)

Cetinkale, T. N. and M. Fishenden. 1951. *Thermal Conductance of Metal Surfaces in Contact*. Institute of Mechanical Engineers, London.

Cooper, M. G., B. B. Mikic, and M. M. Yavanovich. 1969. "Thermal Contact Conductance." *Internatl. J. Heat Mass Trans.* 12: pp. 279-300.

Rapier, A. C., T. M. Jones, and J. E. McIntosh. 1963. "The Thermal Conductance of Uranium Dioxide/Stainless Steel Interfaces." *Internatl. J. Heat Mass Trans.* 51:277-279.

Shlykov, Y. L. 1966. "Thermal Contact Resistance." *Thermal Engineering* 12:102.

8.0 Modifications to the MATPRO Model for Cladding Waterside Corrosion and Hydrogen Pickup

8.1 Background

Fuel rod cladding corrodes (oxidizes) very slowly on the water side during service because the zirconium alloys developed for cladding have high corrosion resistance. Nevertheless, over the long exposure times associated with extended fuel burnup, this corrosion will become significant, and in the case of Zircaloy cladding, hydrogen will be absorbed and appear as zirconium hydrides. The hydrides are concentrated preferentially near the oxidation layer, and the corrosion significantly reduces the cladding wall thickness at high burnup. In addition, the hydrides when in sufficient quantity can embrittle the cladding, reduce its ductility, and enhance its susceptibility to mechanical failure, acting as crack initiation points.

The interrelated processes of cladding corrosion and hydriding are described more fully below.

8.1.1 Corrosion Rates

Waterside corrosion of the Zircaloy cladding for LWR fuel rods has been studied for over 30 years, along with the associated hydrogen pickup and hydride formation in the cladding. See, for example, the extensive literature survey on in-reactor cladding corrosion published by the International Atomic Energy Agency (IAEA 1993) and the earlier reviews by Garzarolli et al. (1982) and Johnson (1987). The uniform corrosion rates in PWR systems differ from BWR systems. Three major reasons are 1) the relatively higher uniform corrosion resistance of the Zircaloy-2 used in BWRs as opposed to the Zircaloy-4 used in PWRs, 2) the lower operating coolant temperature in the BWR as opposed to the PWR, and 3) the lower heat flux of BWR rods as opposed to PWR rods. The uniform corrosion in PWR rods becomes significant at high-burnup levels. Waterside corrosion levels of 100 µm and greater have been observed at rod average burnup levels $\geq$ 60 GWd/MTU in plants with relatively high coolant outlet temperatures $\geq 327°$C (620°F). This extent of corrosion, with the associated hydriding, corresponds to effective wall thinning of greater than 10% and to the onset of oxide layer spallation and associated localized high-hydride concentrations.

A model revision is clearly needed for PWR normal-operation applications to high burnups and long exposures because the current MATPRO model predicts oxide layer thickness a factor of four to five lower than the measured values for high-burnup PWR rods (see Figure 8.1 as an example).

The improved model should reflect the observed differences in uniform corrosion between BWRs and PWRs. It should also reflect the proper temperature sensitivity for the post-transition linear corrosion rate and thus should include the effect of heat flux and current oxide-layer thickness upon the oxide-metal interface temperature, which is understood to be the controlling temperature for the corrosion.
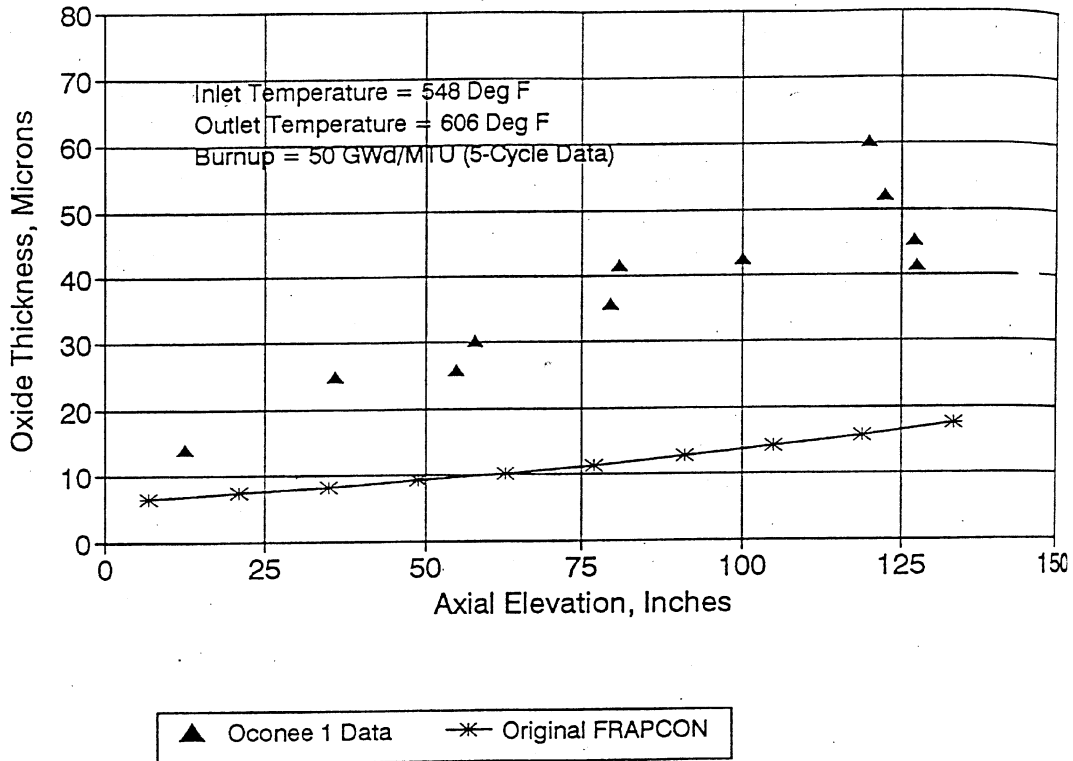
Figure 8.1. Comparison of Original FRAPCON Oxidation to Oconee-1 5-Cycle Data

Garzarolli proposed a model for corrosion of PWR fuel rods that fulfills these criteria, and EPRI used it for their ESCORE steady-state fuel rod performance code (Fiero et al. 1987). To stabilize the model calculation and follow the relatively large time steps typical of fuel performance codes, the EPRI equations were integrated across the time step. Garzarolli et al.'s (1980) guidance for this integration was followed. This integrated form was then compared to well-characterized high-burnup LWR data (see Section 8.2) with satisfactory results. This time-step integrated EPRI model is proposed as an improvement over the current MATPRO model.

Staff at EPRI have recently published a revised PWR corrosion model, which includes cladding annealing and alloying effects, hydride layer effects, and coolant chemistry history effects (Cheng et al. 1996). This model will be evaluated as a possible future improvement to the FRAPCON-3 code; however, the coefficients of this model are not publicly available at this time.

Further adjustment will also be made in the future for the differing uniform corrosion rates among standard BWR and PWR cladding types (these, however, are very sensitive to cladding manufacturing routes), and the vendors' models will be assessed in the course of code reviews by installing those models as options within FRAPCON-3.

In addition to the Garzarolli model for PWRs, the current update to FRAPCON-3 uses the EPRI-developed ESCORE BWR oxidation model (Fiero et al. 1987). This model has been compared to Monticello and TVO-1 medium-to-high burnup rod data, with reasonable success, as described in Section 8.2.

8.1.2 Corrosion Layer Thermal Conductivity

The thermal conductivity of the zirconium oxide corrosion layer is an important parameter in the heat-flux dependent oxidation model and is the subject of ongoing research. The current MATPRO function (for zirconium dioxide) for this parameter will be retained at this time; it produces values of approximately 2.0 W/m-K at normal LWR operating cladding temperatures. An EPRI-sponsored Halden Reactor experiment (Wiesenack 1995) gives indications that the value for this conductivity may be much lower, i.e., near 1.0 W/m-K. This lower value has not been substantiated by ex-reactor measurements on irradiated cladding, and no adjustment will be made at this time to the MATPRO corrosion layer thermal conductance model (ZOTCON). A change to this model may be advisable in the future, however.

8.1.3 Hydrogen Pickup Fraction

Hydrogen uptake in LWR cladding has been found to be consistently in the range of 10 to 25% of the calculated "nascent hydrogen" born in the apparent reaction between the Zircaloy and the water, based on oxide layer thickness (Limback 1994; Susuki et al. 1994). The current MATPRO model does not predict this level of hydrogen uptake (see Figure 8.2). Accordingly, the hydrogen pickup model has been altered to return a value given by a proportionality constant times the calculated local oxide-layer thickness. This proportionality constant was chosen on the basis of several high-burnup PWR irradiated rod examinations. The current MATPRO pick-up fraction for BWR cladding material has not been altered as yet, pending the evaluation of adequate open-literature data upon which to base the change.

8.1.4 Hydrogen Migration and Concentration

Hydrogen concentration due to migration to localized colder cladding regions, such as oxide spallation spots and abnormal pellet-pellet axial gaps, is a recognized mechanism (for example, see Versterlund and Corsetti [1994]). At all axial locations, the hydrogen concentration has a radial distribution that quickly becomes edge-peaked at the outer surface because of the double effect that this surface is the major hydrogen source and also the cooler surface. However, these localized effects of high-hydrogen concentration must be accounted for by a separate analysis (outside the FRAPCON-3 code) because the code will not generate the localized cladding temperature gradients needed for these analyses.
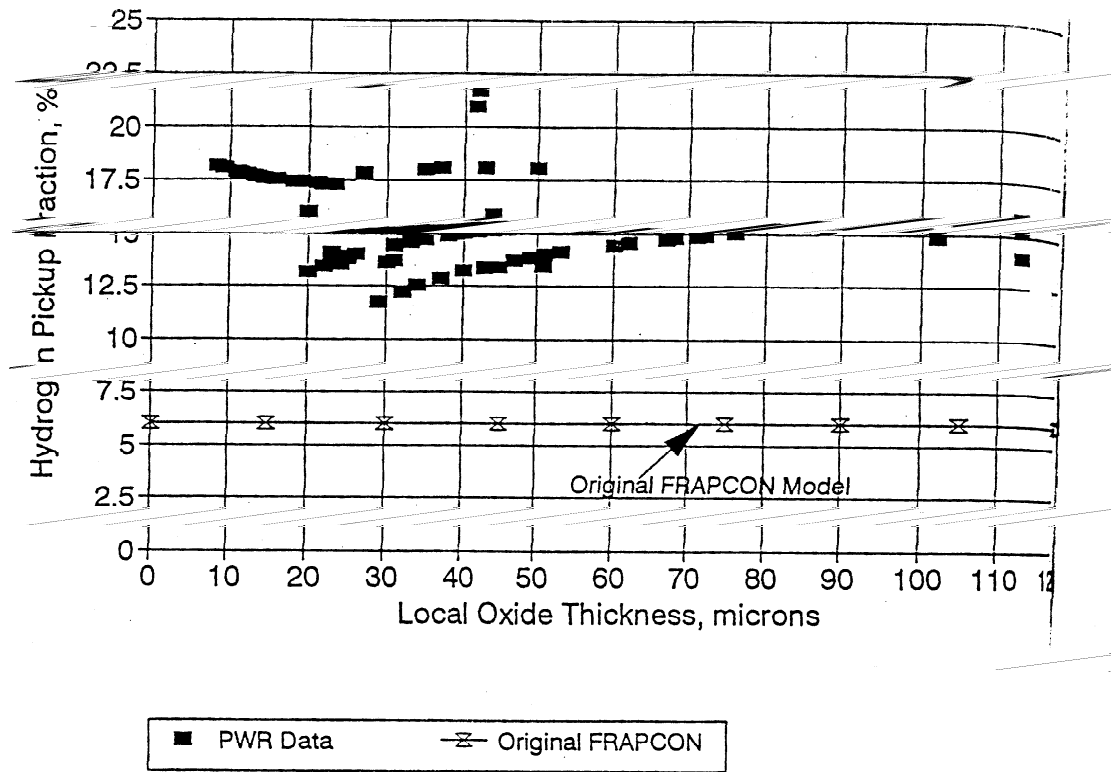
Figure 8.2. Comparison of Original FRAPCON Hydrogen Pickup Model to PWR Data with Burnups Greater than 30 GWd/MTU

8.2 Experimental Evidence for Modified Oxidation Rates

8.2.1 Corrosion Data and Modeling for PWR Fuel Rods

Corrosion data from PWR rods with rod-average burnups up to 65 GWd/MTU (70-GWd/MTU peak pellet) and maximum corrosion layer thicknesses up to and exceeding 100 µm have been published from various fuel performance surveillance and examination programs (Smith et al. 1994; Peyecha 1985; Newman 1986; Balfour 1982b; Dideon 1983, and Garde 1986). These data have been used to verify the adequacy of the proposed revised FRAPCON-3 PWR oxidation model; Figure 8.3 illustrates the spread and trend of the code-to-data comparisons. Figures 8.4 to 8.6 compare the data to the revised FRAPCON model for specific cases.

These same data sets contain total hydrogen-content measurements (via hot vacuum extraction) from samples taken near those used for the corrosion-layer determinations. From these hydrogen extraction data, the wall-average hydrogen concentration can be calculated and also the apparent pick-up fraction
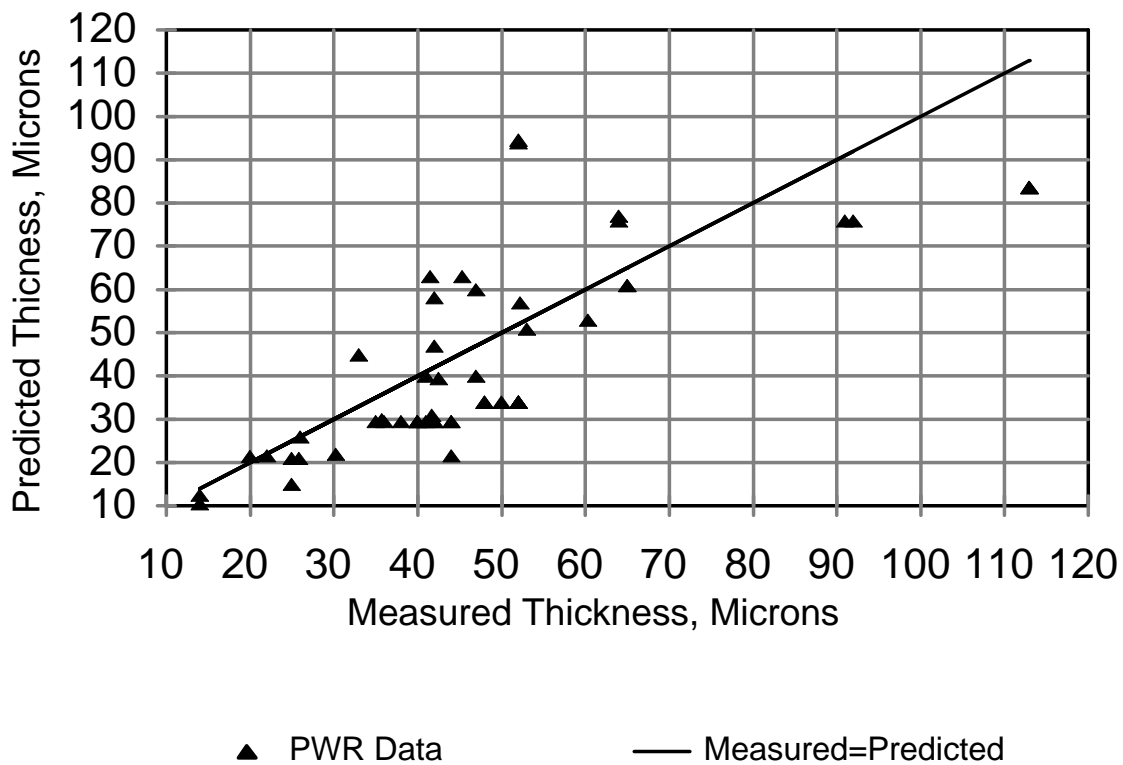
Figure 8.3. PWR Data Compared to Revised MATPRO Oxidation Model

(i.e., the fraction of the hydrogen liberated in the apparent formation of zirconium oxide that is found in the metal). The hydrogen pickup appears to be ~15% with limited uncertainty at oxide thicknesses exceeding 30 µm (see Figures 8.2 and 8.7).

8.2.2 Corrosion Data and Modeling for BWR Fuel Rods

The BWR portion of the revised FRAPCON-3 model has been compared to data from the Monticello reactor (West et al. 1983) and the TVO-1 reactor (Barner et al. 1990). The results were satisfactory and similar to the PWR comparisons presented above.

8.3 Description of the Model

The oxidation models are different in the PWR and BWR environments, and the applicable model is selected based on the relationship of the local coolant temperature to the saturation value of the coolant.
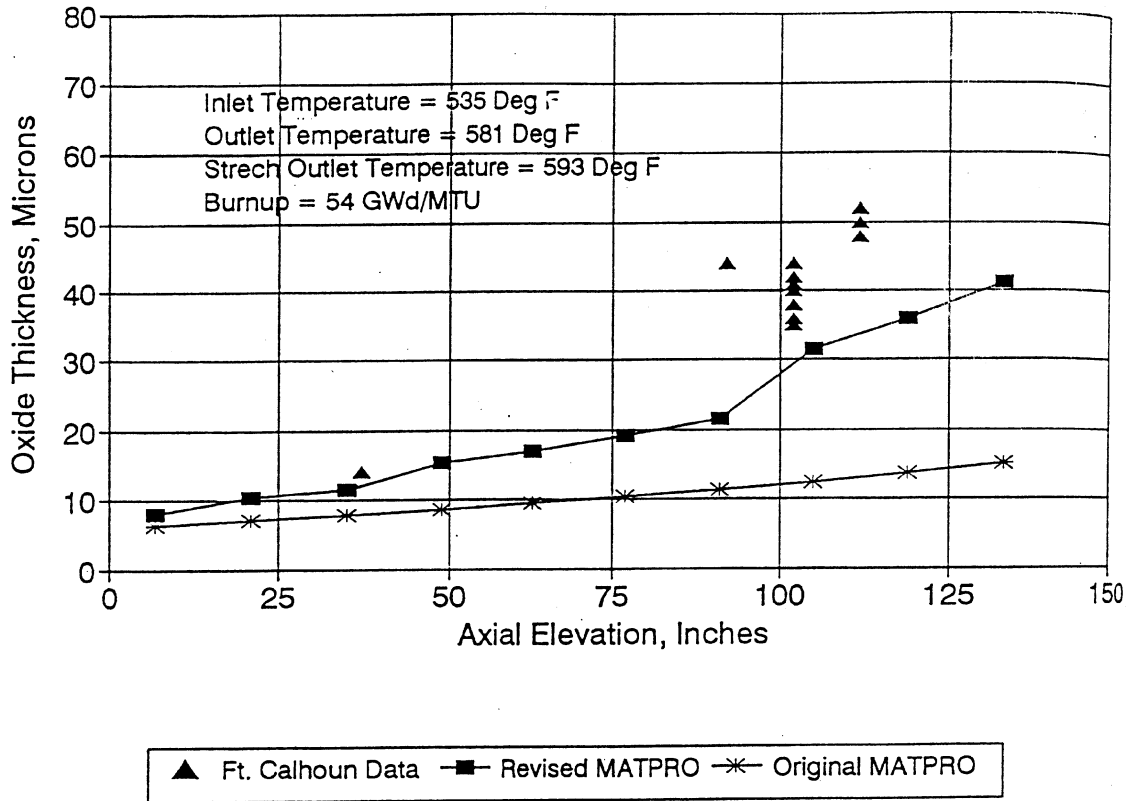
Figure 8.4. Original and Revised MATPRO Oxidation Models Compared to Fort Calhoun Data

8.3.1 The PWR Oxidation Model

The oxidation proceeds via a cubic rate law until the transition thickness (taken to be 2.0 µm) is accumulated. That is,

$$\frac{ds}{dt} = (A/s^2)\ \exp(-Q_1\ /RT_I) \tag{8.1}$$

After transition, the oxidation proceeds according to a linear rate law; that is,

$$\frac{ds}{dt} = [C_0\ +\ U\ (M\phi)^P]\ \exp(-Q_2\ /RT_I) \tag{8.2}$$

where,

ds/dt = Oxidation rate (µm/day)
T_1 = metal-oxide interface temperature, K
ϕ = fast neutron flux (E>1 MeV), n/cm^2/s
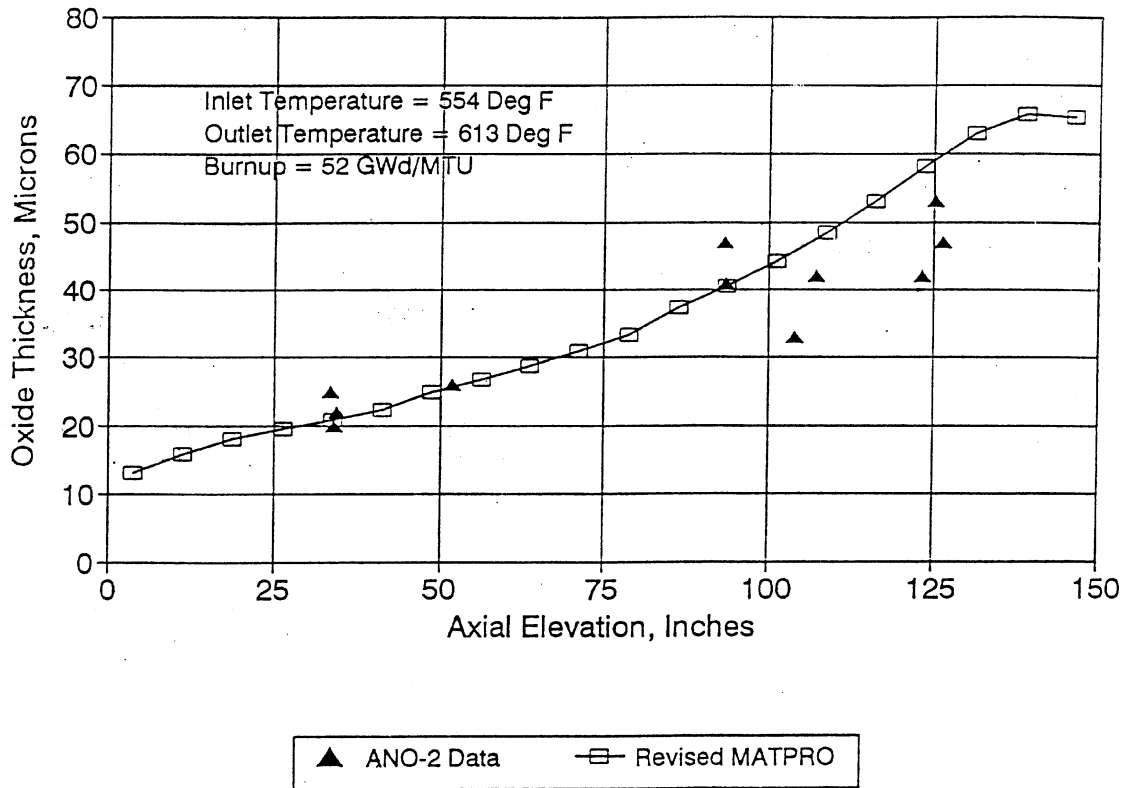
Figure 8.5. Revised MATPRO Oxidation Model vs. ANO-2 Data

$A = 6.3 \times 10^9 \ \mu m^3/day$

$Q_1 = 32,289 \ cals/mol$

$C_0 = 8.04 \times 10^7 \ \mu m/day$

$M = 1.91 \times 10^{-15} \ cm^2\text{-}sec/n$

$P = 0.24$

$Q_2 = 27,354 \ cals/mol$

$U = 2.38 \times 10^8 \ \mu m/day$

$R = 1.98 \ cals/mol/°K$

$T_I = $ temperature of oxide-to-metal interface, K

In the FRAPCON-3 code, the oxidation model is contained in Subroutine CORROS. In CORROS, time-integrated forms of the above expressions are used where the limits of integration are zero and the size of the current time step. The oxidation-layer thickness increments thus calculated are added to the previous total thickness to find the end-of-step total thickness.
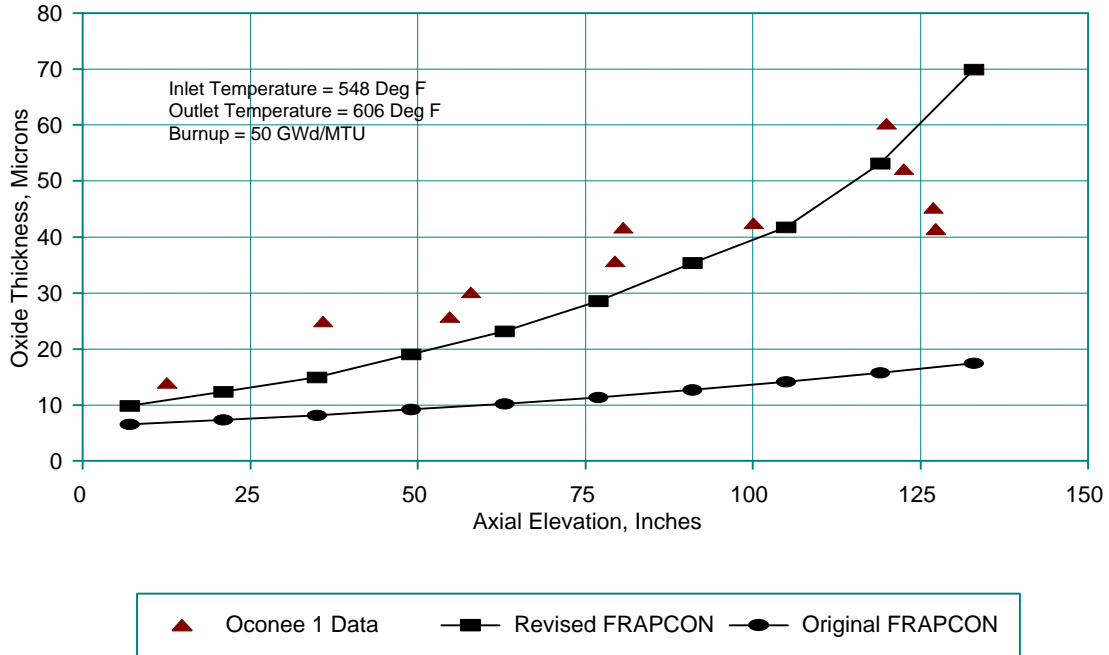
Figure 8.6. Comparison of Original and Revised FRAPCON Oxidation to Oconee-1 Data

The integration of the pre-transition equation is done without regard to the feedback between oxide-layer thickness and oxide-metal interface temperature. This is because the maximum value of the pre-transition layer thickness ($< 2 \, \mu$m) is so small that significant feedback does not occur. That is not true, however, for the post transition linear rate law, and in that case, the oxide-layer thickness is converted to weight gain, and Garzarolli et al.'s (1980) approximate integral solution is used, again applied over the current time step. This solution has the form

$$\Delta w_{i+1} = \Delta w_i + \frac{RT_o^2 \, \lambda}{\gamma \, Q \, q''} \, \ell n \left[1 - \frac{\gamma \, Q \, q''}{RT_0^2 \lambda} k_0 \, \exp\left[\frac{-Q}{RT_0}\right] \exp\left[\frac{\gamma \, Q \, q'' \, \Delta w_i}{RT_0^2 \, \lambda}\right] (t_{i+1} - t_i) \right]^{-1} \qquad (8.3)$$

where   i, i + 1 = refer to (ends of) previous and current time step
$\quad k_0$ = rate constant, g/(cm^2-d)
$\quad T_o$ = oxide-to-water interface temperature, K
$\quad \Delta w$ = weight gain, g/cm^2
$\quad \lambda$ = oxide thermal conductivity, W/cm $\cdot$ K
$\quad q''$ = heat flux, W/cm^2
$\quad Q$ = activation energy, cal/mol
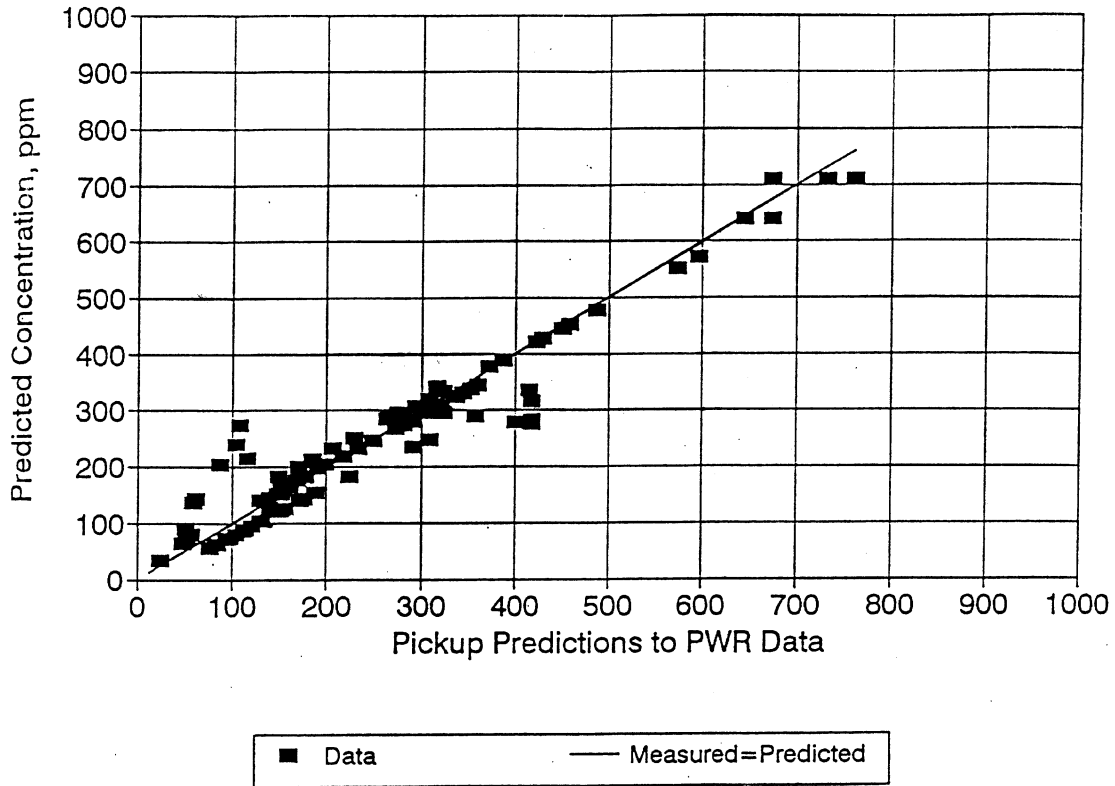
Figure 8.7. Comparison of Revised FRAPCON Hydrogen Predictions to PWR Data with Burnups Greater than 30 GWd/MTU

$$\gamma = \frac{1.56[Zr],}{2\ [0]\ \rho_{Zr}}\ cm^3/g$$

where   [Zr] and [0] = the atomic weights of Zr and 0 in consistent units and
ρ_{Zr} = the density of Zircaloy-4

8.3.2 The BWR Corrosion Model

The BWR corrosion model proceeds on a linear rate from the beginning. It has the form

$$ds/dt\ =\ corrosion\ rate\ (\mu m/day)$$

(8.4)

where $ds/dt = K\ [\exp(-Q/RT_I)]\ [1 + Cq\ "\ \exp(Q/RT_I)]$
Q = 27,350 cals/mol
R = 1.987 cals/mol/°K
C = 2.5×10^{-16} M²/W

$K = 8.04 \times 10^{-7}$ µm/day

T_I = temperature of the oxide-to-metal interface, K

q" = surface heat flux, W/m^2

As with the PWR model, this equation is time-integrated over the current time step, using the Garzarolli approximation on the first term and simply integrating the constant-rate second term, which is independent of temperature. Then the calculated thickness increment is added to the previous cumulative thickness.

8.3.3 The Hydrogen Pickup Model

The pickup fraction for PWRs is set at 15%, based on the data presented in Figure 8.7. For BWRs, the current pickup logic in subroutine CHUPTK is retained (except for the reduction logic), which results in somewhat lower pickup fractions than for PWRs.

8.4 Changes to the MATPRO Models (Subroutines CORROS and CHUPTK)

A FORTRAN version of the integrated EPRI corrosion models for BWR and PWR conditions has been created to replace the existing subroutine CORROS. The call list for the new subroutine is identical to that for the previous subroutine, with the exception that the new subroutine requires the current local value of the fast neutron flux. This flux array is already being calculated in FRAPCON-3 because it is needed by other subroutines. The new subroutine CORROS still provides separate calculations for BWR vs PWR reactor types (with the model selection criterion based on coolant temperature relative to the saturation value of the coolant) and returns the oxide layer thickness in meters.

The revised hydrogen pickup fractions have been introduced into the MATPRO subroutine CHUPTK, and the logic that originally reduced these fractions by approximately a factor of 2.0 has been eliminated.

8.5 Range of Application and Uncertainty

The revised fuel cladding oxidation and hydrogen pickup models have the following ranges of application:

Burnup:	0 to 70 GWd/MTU (pellet burnup)
Cladding/Oxide Interface Temperature:	525 to 595 K
Cladding Types:	ASTM Standard-Range Zircaloy-2 and Zircaloy-4
Coolant Chemistry:	Lithium and pH effects are not included in model

This range of application is based on the data from which the model was developed and the corrosion data used for verification in this report. The uncertainty on the oxide-layer thickness (one standard deviation) for predicted thicknesses greater than 30 µm is ± 15 µm, based on the least-squares fit to the recent data sets (Figure 8.3).

The uncertainty on the hydrogen content as a function of oxide layer thickness is ± 45 ppm for oxide thicknesses greater than 30 µm, based on similar least-squares fitting (Figure 8.7). This corresponds to an uncertainty of approximately 10 to 20% relative to the pickup fraction.

8.6 Bibliography

(Note: Bibliographical entries are not called out in the text. For called-out references, see Section 11.0.)

Garzarolli, F. 1985. "Progress in Understanding PWR Fuel Rod Waterside Corrosion." In*ANS/ENS International Topical Meeting on Light Water Reactor Fuel Performance*, Orlando, Florida, April 1985, p. 3-55.

Mardon, Jean-Paul, et al. 1997. "Update on the Development of Advanced Zirconium Alloys for PWR Fuel Rod Cladding," *Proceedings of the ANS Internatonal Topical Meeting on Light Water Reactor Fuel Performance*, Portland, Oregon, March 2-6, 1997.

Marino, G. P. and R. L. Fischer. 1978. *Corrosion of Zircaloy-4 Tubing in 68 °F Water*, WAPD-TM-1332.

Ogata, K. 1989. "A Systemic Survey of the Factors Affecting Zircaloy Nodular Corrosion," *Proceedings of the Eighth International Symposium on Zirconium in the Nuclear Industry*, (June 19-23, 1988, San Diego, California), ASTM STP 1023 pp. 291-314, American Society for Testing and Materials, Philadelphia, Pennsylvania.

Pati, S. R. et al. 1997. "Performance of Standard and Advanced Fuel Rod Cladding for High Burnup Applications in PWRs," *Proceedings of the ANS International Topical Meeting on Light Water Reactor Fuel Performance*, Portland, Oregon, March 2-6, 1997.

Rudling, P. 1989. "Corrosion Performance of Zircaloy-4 PWR Fuel Cladding," *Proceedings of the Eighth International Symposium on Zirconium in the Nuclear Industry*, (June 19-23, 1988, San Diego, California), ASTM STP 1023 pp. 213-226, American Society for Testing and Materials, Philadelphia, Pennsylvania.

Rudling, P. 1989. "Corrosion Performance Ranking of Zircaloy-2 for BWR Applications," *Proceedings of the Eighth International Symposium on Zirconium in the Nuclear Industry*, (June 19-23, 1988, San Diego, California), ASTM STP 1023 pp. 315-333, American Society for Testing and Materials, Philadelphia, Pennsylvania.

Sabol, G. P. et al., "In-Reactor Fuel Cladding Corrosion Performance at Higher Burnups and Higher Coolant Temperatures," *Proceedings of the ANS International Topical Meeting on Light Water Reactor Fuel Performance*, Portland, Oregon, March 2-6, 1997.

Urbanic, V. F. 1991. "Investigation of Variables that Influence Corrosion of Zirconium Alloys during Irradiation," *Proceedings of the Ninth International Symposium on Zirconium in the Nuclear Industry* (November 5 to 8, 1990, Kobe, Japan), ASTM/STP 1132, pp. 665-679, American Society for Testing and Materials, Philadelphia, Pennsylvania.

Van Swam, L.F.P. 1991. "The Corrosion of Zircaloy-4 Fuel Cladding in Pressurized Water Reactors," *Proceedings of the Ninth International Symposium on Zirconium in the Nuclear Industry* (November 5 to 8, 1990, Kobe, Japan), ASTM/STP 1132. pp. 758-779, American Society for Testing and Materials, Philadelphia, Pennsylvania.

Van Swam, L.F.P. et al. 1997. "Behavior of Zircaloy-4 and Zirconium Liner Zircaloy-4 Cladding at High Burnup," *Proceedings of the ANS International Topical Meeting on Light Water Reactor Fuel Performance,* Portland, Oregon, March 2-6, 1997.

Videni, K. 1972. "Property of Zirconium Base Cladding Materials—Corrosion and Hydrogen Pickup," *Nuclear Engineering and Design*, Vol. 20, pp. 167-199.

Warr, B. D. 1991. "Oxide Characteristics and Their Relationship to Hydrogen Uptake in Zirconium," *Ninth International Symposium on Zirconium in the Nuclear Industry* (November 5 to 8, 1990, Kobe, Japan), ASTM STP 1132 pp. 740-755, American Society for Testing and Materials, Philadelphia, Pennsylvania.

9.0 Modifications to Mechanical Models

9.1 Background

The mechanical properties of fuel rod Zircaloy cladding have been known to change with irradiation because of damage induced from the fast neutron fluence. The changes are similar to cold-working the material because dislocation tangles are created that tend to both strengthen and harden and decrease the ductility.

Recent mechanical testing of high-burnup PWR cladding, e.g., Balfour (1982b), Dideon (1983), Garde (1986), Newman (1986), Newman (1990), and Smith et al. (1994), demonstrates that ductilities are dropping below the 1% uniform strain criterion suggested for LWR fuel rods in the NRC Standard Review Plan, Section 4.2. The decrease in cladding ductility is believed to be due to the increase in hydrides resulting from increased waterside corrosion at high burnups. The presence of hydrides in Zircaloy and irradiation damage are thought to decrease ductility because the hydrides pin the irradiation-induced dislocations (Garde 1989). Further, ductility decreases can occur when the hydrides become radially orientated with respect to the axial direction. This is because the hydrides become crack initiation points perpendicular to the stresses and can penetrate the cladding in the radial direction. The latter phenomenon can lead to cladding ductilities near zero.

The hydrides have been shown to preferentially precipitate in the perpendicular direction when the stresses are tensile and precipitate parallel to the stresses when they are compressive. Therefore, hydrides precipitate out in the circumferential direction in fuel cladding when the radial hoop stress remains compressive.

Typical low burnup fuel rods have compressive hoop stresses in their cladding (due to the high system pressures) until the fuel-to-cladding gap closes to hard contact at a burnup level between 40 to 45 GWd/ MTU. When the fuel-to-cladding gap closes, the cladding is subjected to tensile hoop stresses, and for some fuel rods, accelerated corrosion begins at these high-burnup levels.

The combination of both tensile hoop stresses and accelerated corrosion can lead to some hydrides precipitating in the radial direction, increasing the likelihood of brittle failure. A fuel rod even at 50-GWd/MTU burnup does not have fuel-cladding gap closure along its entire length, and neither is there accelerated corrosion along the entire rod length. For PWR fuel rods, corrosion is typically greatest in the upper half of the rod (see Figures 8.4, 8.5, and 8.6). The gap between fuel and cladding generally closes first in the highest fuel burnup region near the center of PWR fuel rods. Therefore, it is proposed that lower cladding ductilities will only occur in locations where both of these phenomena are prevalent. This is a likely hypothesis to explain why not all cladding axial locations with high-burnup levels or high corrosion levels have low cladding ductilities and the large scatter in strain data at similar hydride levels.

9.2 Recent Experimental Evidence for Mechanical Model Changes

Recent mechanical-properties data associated with high-burnup Zircaloy 4 cladding discharge from PWRs are reported in Balfour (1982b), Dideon (1983), Garde (1986), Newman (1986), Newman (1990), and Smith et al. (1994). The data include measured values of yield strength, tensile strength, and uniform strain spanning fast fluence levels up to 12×10^{25} n/m^2, oxide thicknesses between 4 and greater than 100 μm, and total hydrogen cladding content between 10 and 720 ppm. The mechanical properties tests were typically performed at a strain rate of 8×10^5/sec and at temperatures between 295 and 673K (i.e., up to the temperature range of cladding during normal reactor operations).

Figures 9.1, 9.2, and 9.3 compare the original MATPRO predictions for uniform strain, yield strength, and tensile strength to data. The data sources are from Balfour (1982b), Dideon (1983), Garde (1986), Newman (1986), Newman (1990), and Smith et al. (1994). As shown, MATPRO underpredicts uniform strain and overpredicts both yield strength and tensile strength.

Analysis of recent mechanical properties data has shown that cladding hydrides degrade cladding tensile strength and ductility (Figures 9.4 and 9.5, respectively). The accumulation of hydrogen in Zircaloy cladding results from the oxidation process occurring at the cladding surface, which tends to increase with increasing burnup. Hydrogen is produced as a result of cladding oxidation and a fraction
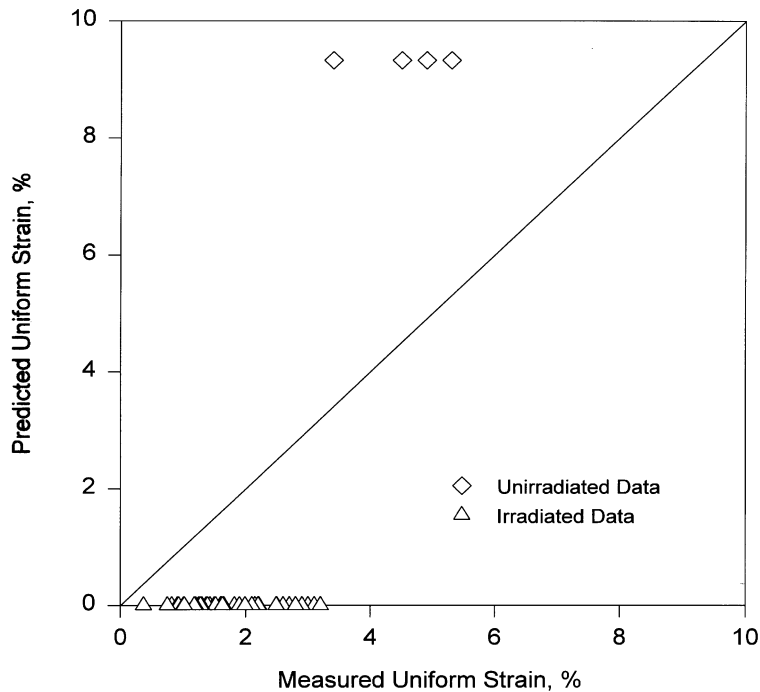

Figure 9.1. MATPRO Uniform Strain Model
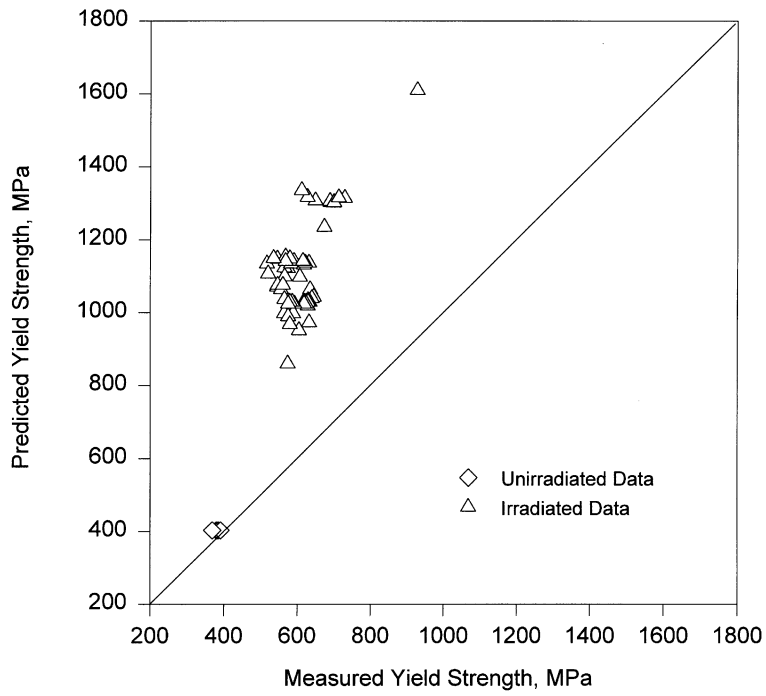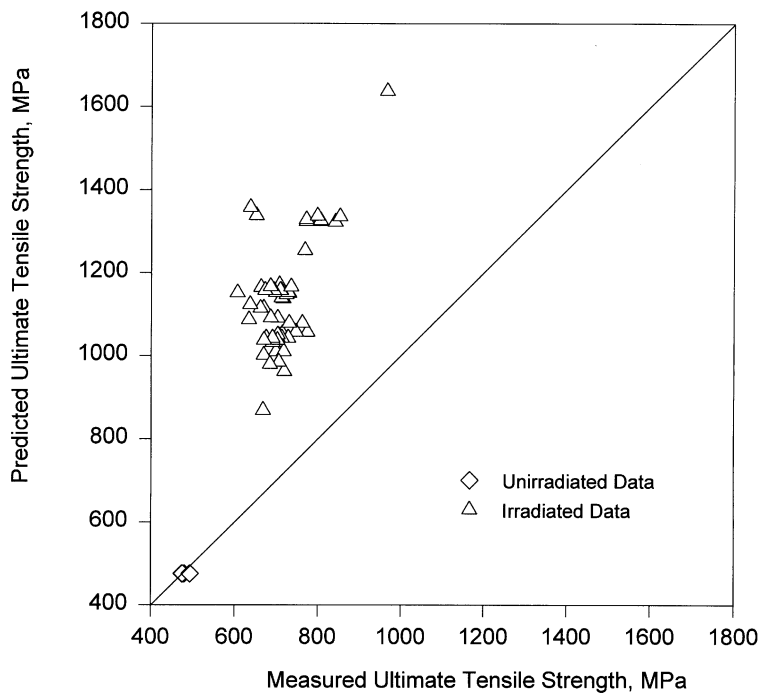
Figure 9.2. MATPRO Yield Strength Model

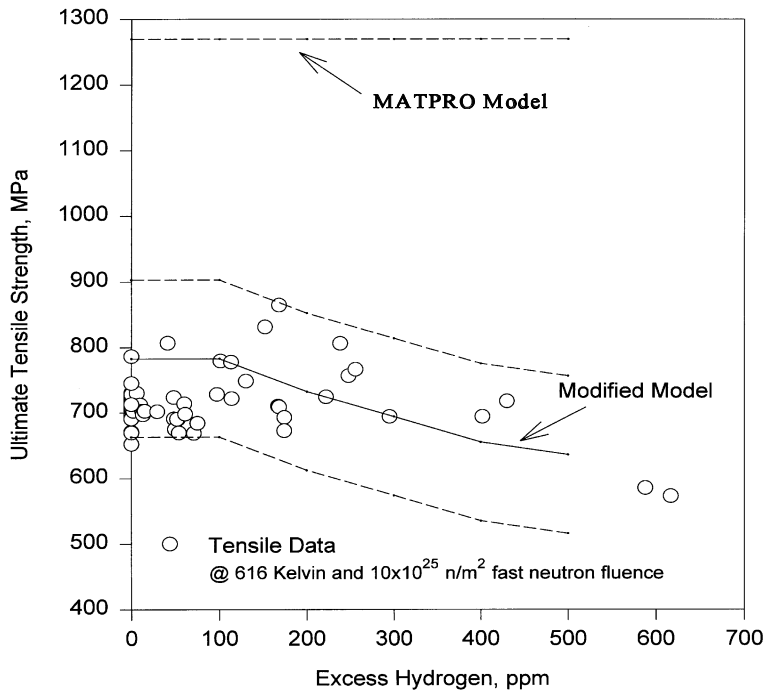**Figure 9.3**. MATPRO Ultimate Tensile Strength Model

Figure 9.4. Tensile Strength of Zircaloy-4 Cladding with Models
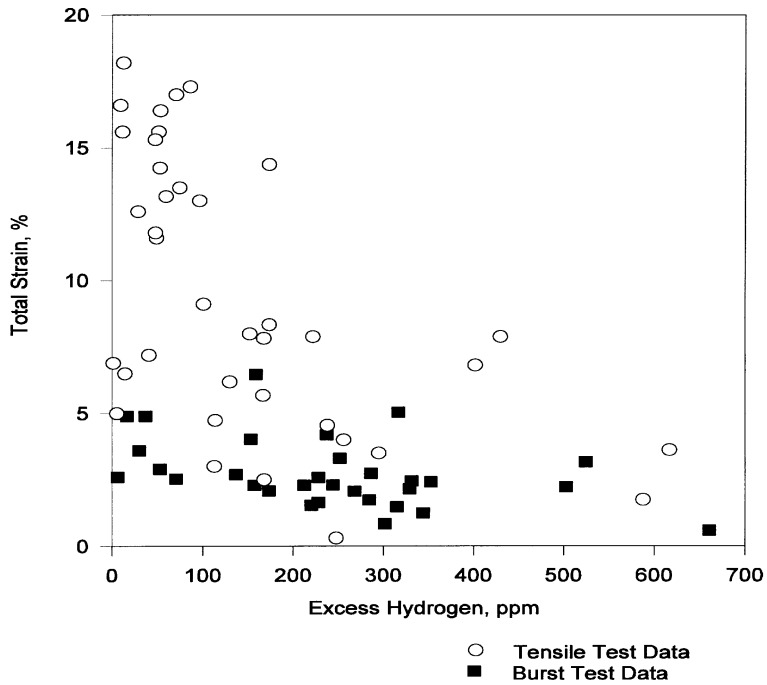

Figure 9.5. Total Tensile and Burst Strain vs. Excess Hydrogen

of the produced hydrogen is absorbed in the Zircaloy metal. The hydrogen will migrate to the cooler regions of the cladding and precipitate as zirconium hydrides when the concentration exceeds the solubility limits (Sawatzksy and Wilkins 1967) for a given temperature. The axial distribution of hydrogen in cladding generally follows the axial distribution of oxide thickness along a fuel rod. The radial distribution of hydrides across a section of cladding is characterized by a relatively high density of hydrides near the outer surface and a much lower density throughout the bulk of the wall (see also Section 8 for a discussion of corrosion and hydriding).

In general, hydrides form in a circumferential direction as a result of the stress exhibited by the cladding. In low concentrations (<200 ppm), it is believed that hydrides pin dislocations during the deformation process, thus strengthening the cladding, and this results in a decrease in ductility on the order of 1 to 2% uniform strain. Unirradiated cold-worked and stress-relieved cladding has measured uniform strains on the order of 4% to 6%. However, as the concentration of hydrides in the cladding exceed 300 to 400 ppm, and the hoop tensile stresses develop in the fuel rod cladding at high burnups (>45 GWd/MTU), significant radial hydrides densities can be orientated in the radial direction resulting in crack initiation sites in the metal. The crack initiation sites decrease the ductility to the point where the cladding tensile strength approaches the yield strength.

The strain capability decreases as radial hydrides form. As long as the concentration of hydrogen remains below its solubility limit, there is no effect on uniform strain. However, hydrogen in excess of the solubility limit will produce a noticeable reduction in uniform strain and ductility.

Therefore, the mechanical models have been modified to predict the current high-burnup data and to account for the effects of hydrogen in these models.

9.3 Recommended Changes to MATPRO Mechanical Models

The following MATPRO models have been modified to account for the effects of hydriding due to waterside corrosion:

- Strength Coefficient (Subroutine CKMN)

- Strain Hardening Exponent (Subroutine CKMN)

- Uniform Strain (Subroutine CMLINMIT)

In addition, the strain-hardening dependence on fast fluence appears to be inadequate for fast fluences above 3×10^{25} n/m^2. Therefore, a revised strain-hardening term as a function of fast fluence has been adopted. A new uniform strain model has been adopted (the strain-hardening exponent equals plastic strain at maximum load) over the original ideal relationship in MATPRO. Review of actual data suggests that this ideal relationship is inadequate for predicting uniform strain.

9.3.1 Data Reduction

High-burnup Zircaloy-4 mechanical properties data from Balfour (1982b), Dideon (1983), Garde (1986), Newman (1986), and Smith et al. (1994) were compiled for model fitting. The data include yield strength, tensile strength, and uniform strain for the various values of temperature, fast fluence, and hydrogen content.[a] Values for the strength coefficient and strain hardening exponent were determined by fitting each data set, assuming the following relationship:

$$\sigma = K \cdot \epsilon^n \tag{9.1}$$

where σ = true stress (MPa)
ϵ = true strain (unitless)
K = strength coefficient (MPa)
n = strain hardening exponent (unitless)

The parameters K and n describe the metallurgical state of the cladding and vary as a function of temperature, cold work, fast fluence, and hydrogen content. Samples of unirradiated cladding were also included to verify the model. The n and K values associated with the unirradiated data compare well with MATPRO's models (i.e., they were within the expected error for the model).

The parameters that require modification for irradiated cladding are described below.

9.3.2 Strength Coefficient, K

To develop a hydrogen-dependent term for inclusion in MATPRO's strength coefficient model, MATPRO's dependence on temperature, cold work, and fast fluence were assumed to be correct. The cold-work value used for cladding test samples was assumed to be equal to 0.5, based on discussions with individuals at ABB Combustion Engineering, Babcock & Wilcox, Westinghouse, and Sanvik Special Metals Corporation. This value was based on an initial cold work of 75% after the last reduction in tubing wall thickness followed by a stress relief anneal.

Test specimens having average hydrogen contents less than the solubility limit were first considered. Figures 9.6 and 9.7 present strength-coefficient values versus temperature and fast fluence. The strength-coefficient data are determined from the stress-strain data and the simultaneous solution to Equations 9.1 and 9.9. The MATPRO models are superimposed for comparison. In general, MATPRO's predictions of the strength coefficient are good. After subtracting the terms that depend on temperature, cold work, and fast fluence from the measured strength coefficient values for all data (i.e., test samples with hydrogen less than and greater than the solubility limit), Figure 9.8 plots the data as a

---

(a) A hot-vacuum technique was used to measure the hydrogen in the cladding, and, therefore, the results provide an average value of hydrogen per cladding sample.
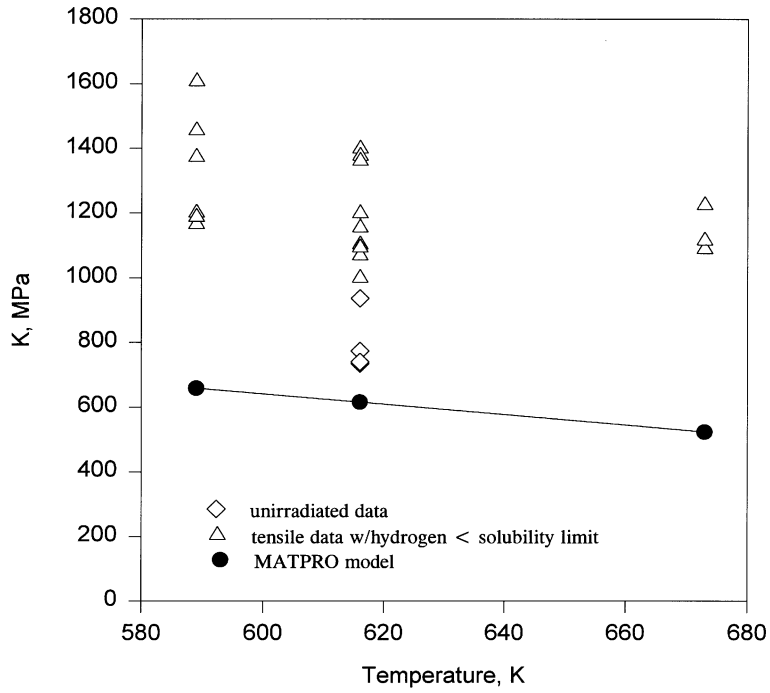
Figure 9.6. Strength Coefficient vs. Temperature
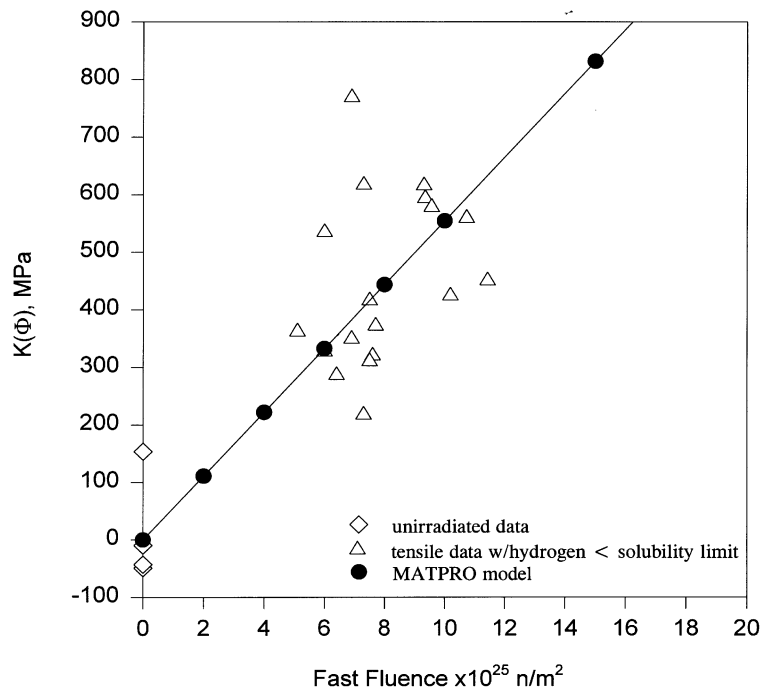
Figure 9.7. Strength-Coefficient Dependency on Fast Fluence
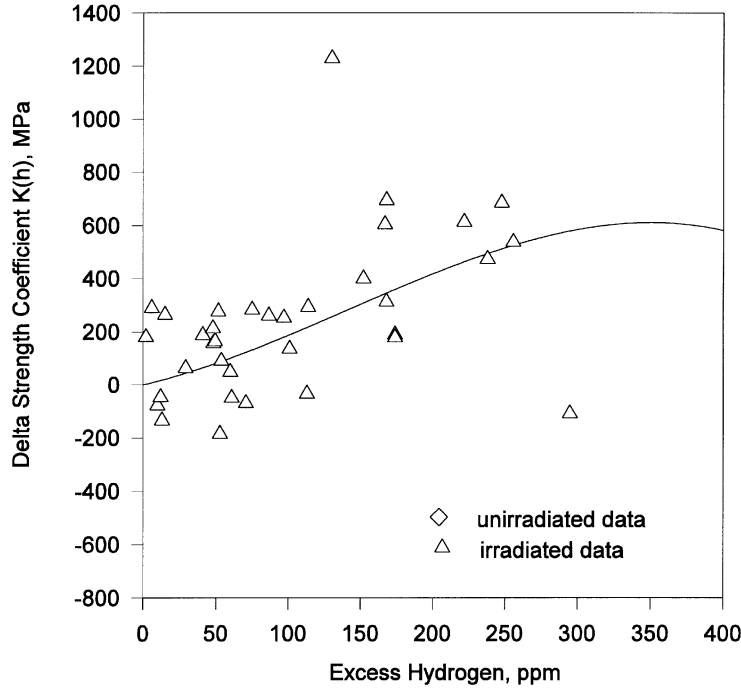
Figure 9.8. Strength-Coefficient Dependency on Hydrogen

function of hydrogen in excess of the solubility limit. This figure shows a strong dependence on hydrogen. A regression of the strength coefficient as a function of excess hydrogen was performed on the data using a third order polynomial fit, which is shown below as the K(h) term.

$$K(h) \ = \ h \bullet [1.288E6 \ + \ h \bullet (7.546E3 - h \bullet 17.84)] \tag{9.2}$$

where   K(h) = hydrogen contribution to strength coefficient
            h = 400 ppm for excess hydrogen > 400 ppm

The complete expression for the strength coefficient is

$$K \ = \ K(T) \ + \ K(CW, \ \Phi) \ + \ K(h) \tag{9.3}$$

where   K(T)   =   1.17628E9 + T•(4.54859E5 + T•(-3.28185E3 + T•1.72752))
            K(T)   =   Temperature dependence from MATPRO
       K(CW,Φ)   =   0.546 COLDW• K(T) + 5.54E-18•Φ
       K(CW,Φ)   =   Cold work and fast fluence dependence from MATPRO
            k   =   Strength coefficient
            T   =   Temperature, °K
          CW   =   Cold work, fraction
            Φ =   Fast neutron flux, n/m^2> 1 mev

Figure 9.9 presents the strength-coefficient model prediction versus the strength coefficients from the data along with the 95% confidence bounds of the model predictions.

9.3.3 Strain-Hardening Exponent, n

The MATPRO temperature dependence on the strain-hardening exponent was retained. The approach used to develop a hydrogen-dependent term for the strain-hardening exponent was similar to that used for the strength coefficient, i.e., used the stress-strain data and Equations 9.1, 9.3, and 9.9 to determine the strain exponents; however, the fast-fluence term used in MATPRO did not agree with the data. The temperature dependence was removed from those data with very low hydrogen levels (below hydrogen solubility limit) using MATPRO's strain-hardening exponent temperature-dependent term. The data plotted were a function of fast fluence (see Figure 9.10) and indicated a slight linear dependence on fast fluence.

Strain hardening as a function of hydrogen was developed by removing the temperature and fluence dependencies from the data using MATPRO's temperature dependence and the linear fluence term.
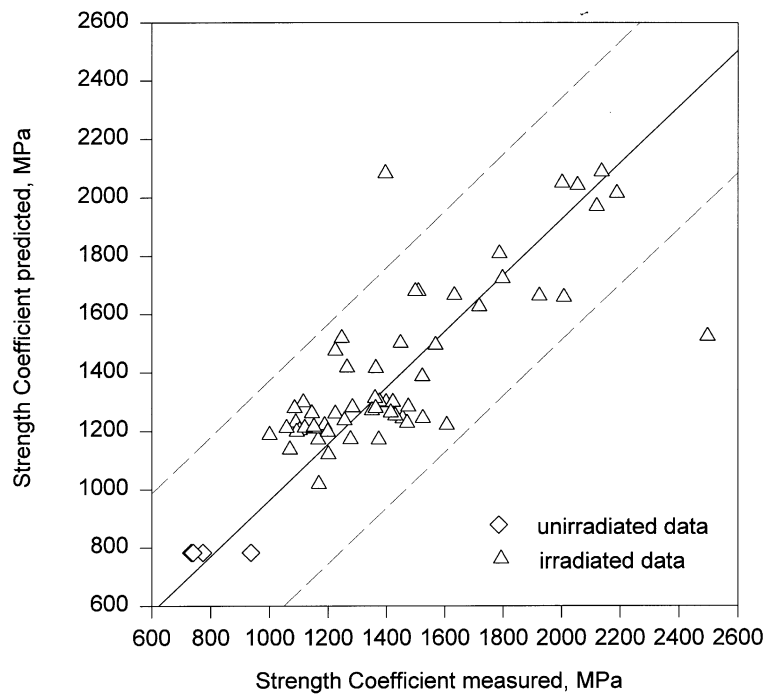
Figure 9.9. Strength Coefficient Model
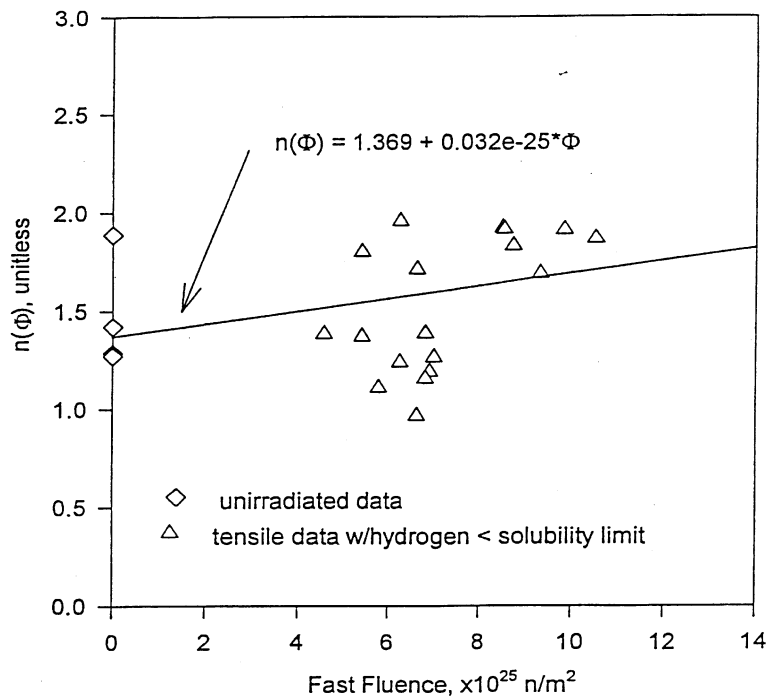
Figure 9.10. Strain-Hardening Exponent Dependency on Fast Fluence

Figure 9.11 plots the corrected data plotted versus hydrogen. The fit of strain hardening is a third order polynomial and results in the following hydrogen dependence:

$$n(h) = 1 + 2.298E\text{--}3 \cdot h_{ex} + 4.138E\text{--}6 \cdot h_{ex}^2 - 1.5E - 8h_{ex}^3 \tag{9.4}$$

where $n(h)$ = hydrogen dependence on the strain hardening exponent, unitless
$\quad\quad h_{ex}$ = 400 for excess hydrogen > 400 ppm

The complete strain hardening relationship is

$$n = n(T) \cdot n(\Phi) \cdot n(h_{ex}) \tag{9.5}$$

where $n(T)$ = $9.490E\text{-}2 + T\cdot(1.165E\text{-}3 + T\cdot(\text{-}1.992E\text{-}6 + T\cdot9.588E\text{-}10))$
$\quad\quad n(T)$ = Temperature dependence of strain hardening exponent from MATPRO
$\quad\quad n(\Phi)$ = $1.369 + 0.032E\text{-}25 \cdot \Phi$, and
$\quad\quad n(\Phi)$ = Fast fluence dependence of strain hardening exponent
$\quad\quad\quad T$ = Temperature K
$\quad\quad\quad \Phi$ = Fast fluence, $n/m^2 > 1.0$ Mev
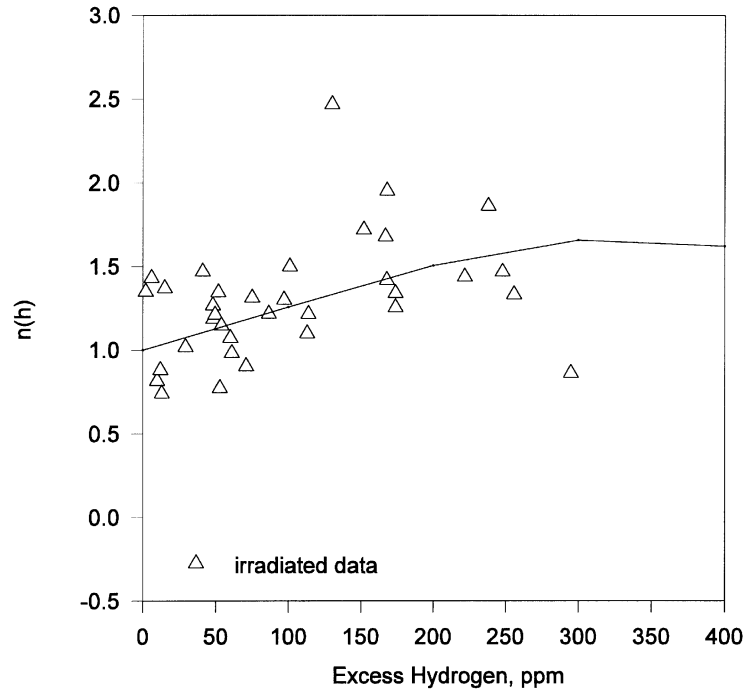
Figure 9.11. Strain-Hardening Exponent Dependency on Hydrogen

Figure 9.12 compares the strain-hardening exponent versus the estimated strain-hardening exponent from Equations 9.4 and 9.5 along with the 95% confidence bounds.
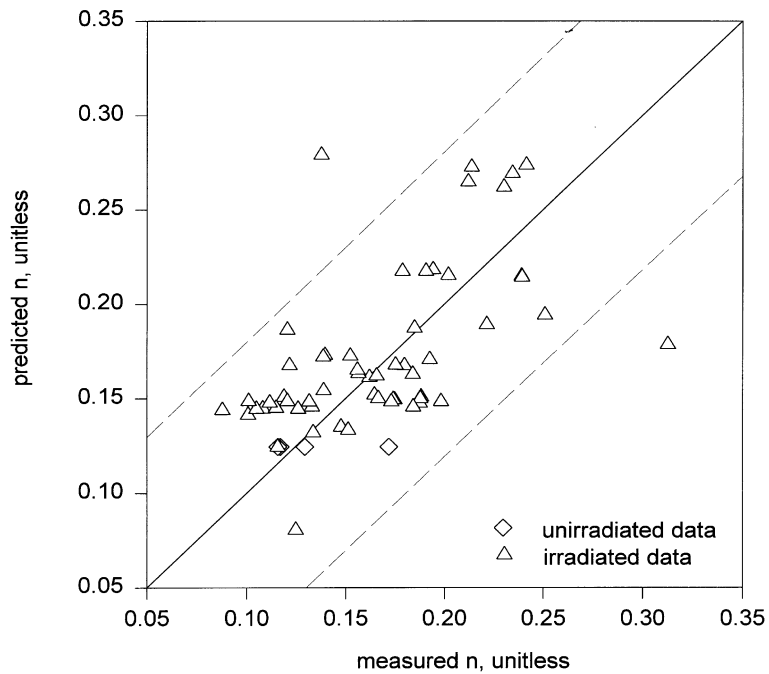
Figure 9.12. Strain-Hardening Exponent Model

9.3.4 Uniform Strain, ϵ

Figure 9.13 shows uniform strain data with low hydrogen levels (i.e., specimens below solubility limit) as a function of test temperature between 580K and 680K. A linear fit to these data provided the following relationship.

$$\epsilon(T) = 0.096 - 1.142E{-}4 \bullet T \qquad (9.6)$$

where $\epsilon(T) =$ Temperature-dependence of uniform strain
    $T =$ Temperature, K

This temperature dependence was then removed from the data with low hydrogen levels (i.e., specimens having hydrogen below the solubility limit), and the data were plotted as a function of fast fluence in Figure 9.14 to determine its fast-fluence dependence. Figure 9.14 shows uniform strain exponentially decreasing with increasing values of fast fluence and reaching an asymptotic value at 4×10^{5}n/m^2. A linear fit of the natural log of the corrected uniform strain data as a function of fast fluence has provided the following exponential relationship:

$$\epsilon(\Phi) = 0.01856\exp(-\Phi/10^{25}) \qquad (9.7)$$

where $\epsilon(\Phi) =$ fast fluence dependence on uniform strain
    $\Phi =$ fast fluence, n/m^2, $>$/mev
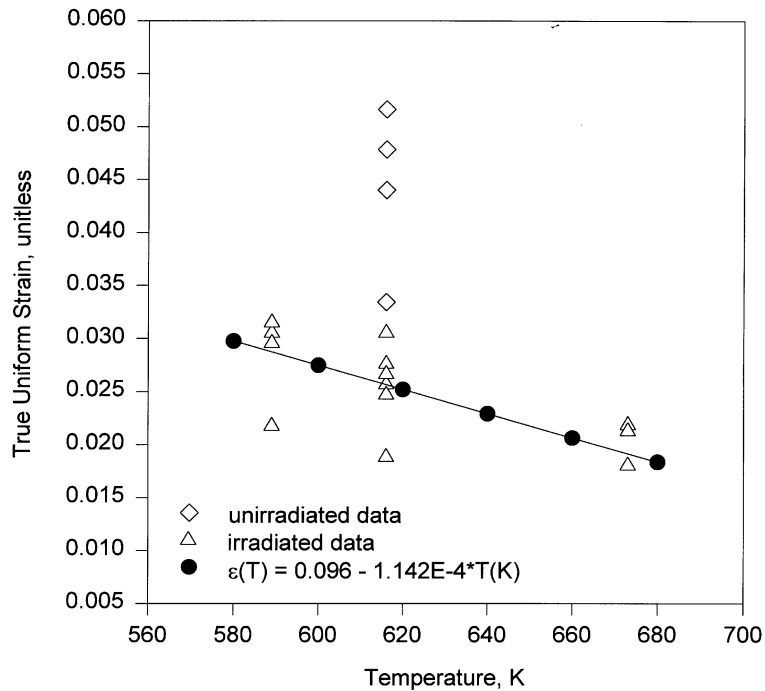
Figure 9.13. Uniform Strain vs. Temperature
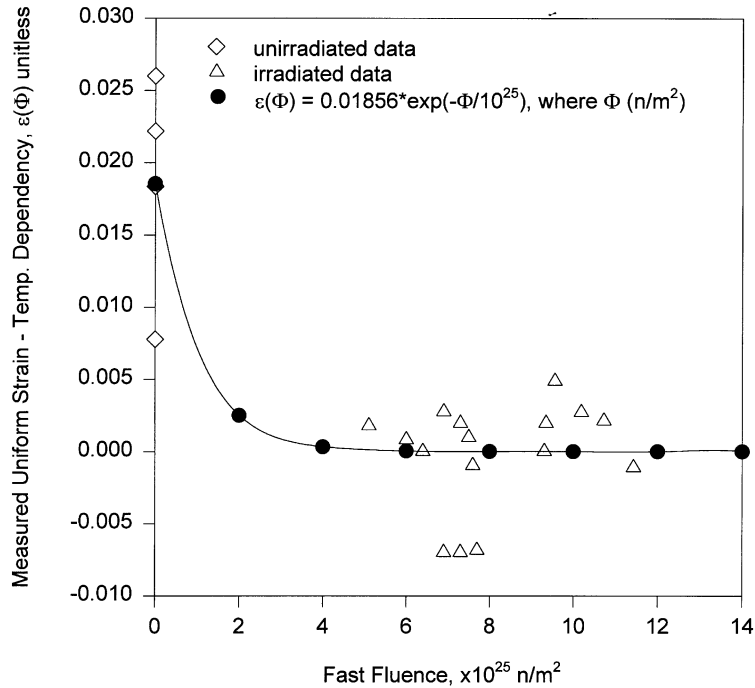
Figure 9.14. Uniform Strain Dependency on Fast Fluence

The entire set of uniform strain data were corrected for temperature and fast fluence using Equations 9.6 and 9.7 and plotted as a function of excess hydrogen level in Figure 9.15. A linear fit of the $\log_{10}$ corrected uniform strain data as a function of excess hydrogen has provided the following relationship:

$$\epsilon(h) = -[h_{ex}/(8.05 \times 10^5)]^{0.5} \tag{9.8}$$

where $\epsilon(h)$ = hydrogen dependence on uniform strain
         h_{ex} = excess hydrogen, ppm

The uniform strain model is simply $\epsilon = \epsilon(T) + \epsilon(\Phi) + \epsilon(h)$ and is plotted versus the measured uniform strain data in Figure 9.16. If the model calculates a negative strain, the code warns the user that the cladding temperature and excess hydrogen levels are outside of the range of data used to develop the mechanical models and sets the uniform strain capability at zero. Figure 9.16 also shows the 95% confidence bounds on the model.

9.3.5 Assembled Model: Tensile and Yield Strength and Uniform Strain

Tensile strength, yield strength, and strain are calculated using the same relationships in MATPRO's CMLIMT subroutine with slight modifications. The true ultimate strength is calculated using the following equation:
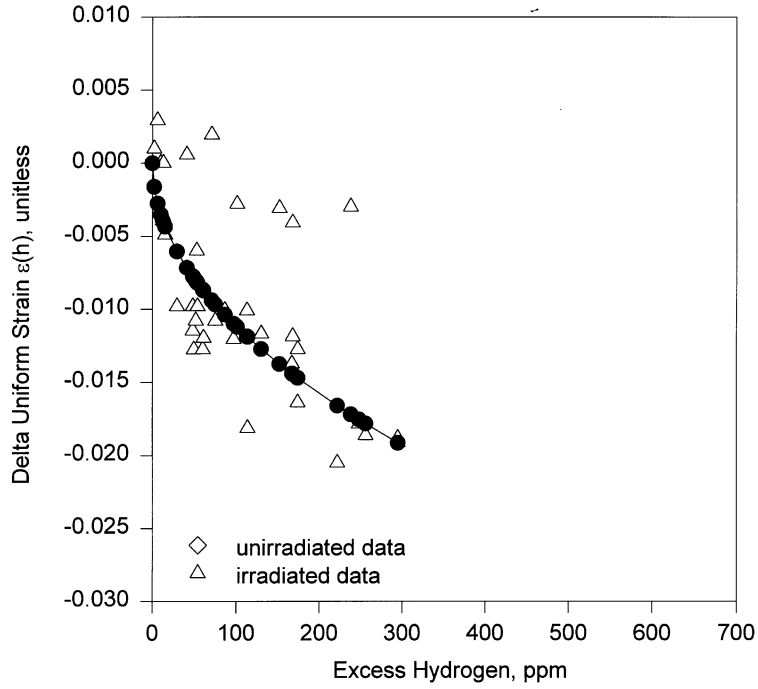
Figure 9.15. Uniform Strain Dependency on Hydrogen
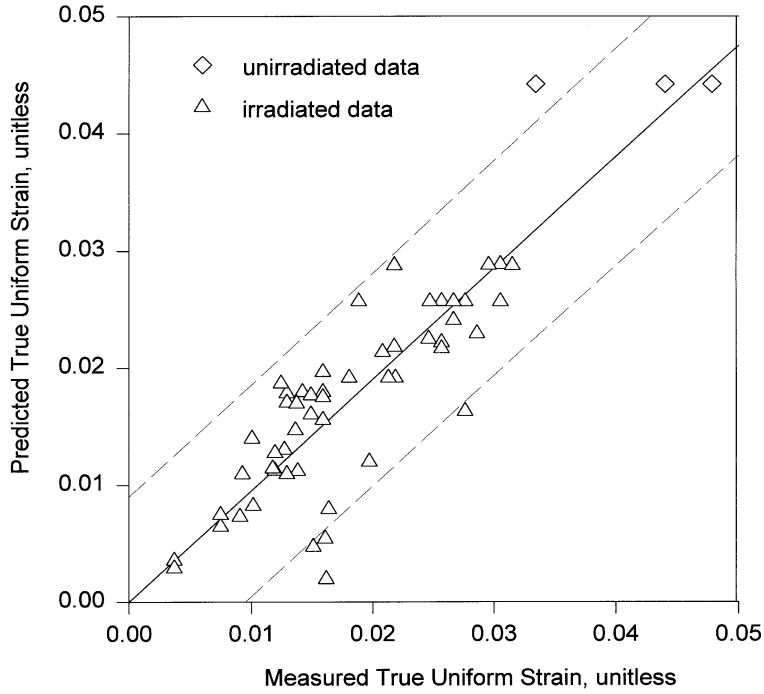
Figure 9.16. New Uniform Strain Model

$$\sigma = K * (\acute{\varepsilon}/10^{-3})^m * \epsilon_{p+e}{}^n \tag{9.9}$$

where
σ = true ultimate strength (Mpa)
K = strength coefficient (Mpa)
$\acute{\varepsilon}$ = strain rate (unitless)
m = strain rate sensitivity constant from MATPRO (unitless)
ϵ_{p+e} = true strain at maximum load (unitless)
n = strain hardening exponent (unitless)

This is a change in the original model in that the true strain at maximum load in the original equation was set equal to the strain hardening exponent.

The CMLIMT subroutine equations predicting true yield strength and true strain at yield remain unchanged. True uniform strain is calculated using the proposed uniform strain model.

As a check on the goodness-of-fit to the data, zero-intercept linear-regression analyses of measured versus predicted values for uniform strain, yield strength, and tensile strength were performed. Figures 9.17 and 9.18 show the results. Ninety-five percent prediction intervals are included to provide a measure of the accuracy of the models. This means that 95% of the measured data will fall within the calculated interval. For tensile strength, the error is approximately 17%, which is consistent with the standard error currently provided in the CMLIMT subroutine in MATPRO.
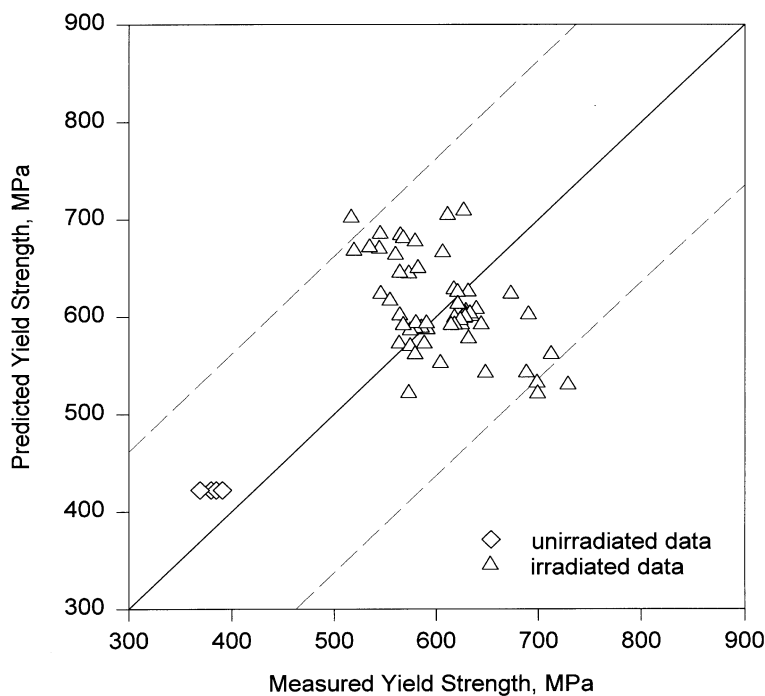
Figure 9.17. Yield Strength Model Using Modified Parameters
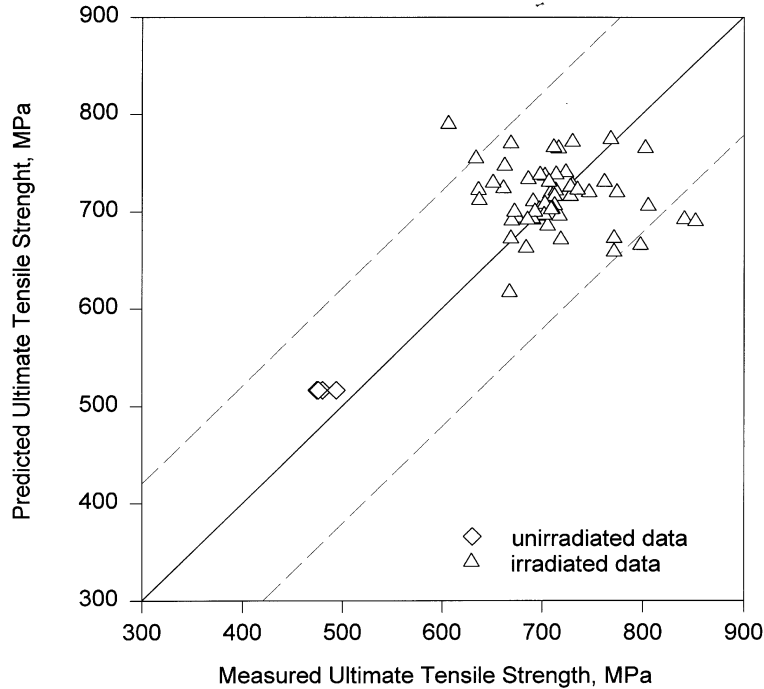
Figure 9.18. Ultimate Tensile Strength Model Using Modified Parameters

9.4 Range of Application and Uncertainty

The ranges of application for the cladding mechanical models are

Cladding temperatures:	560 to 700K
Oxide corrosion thickness:	0 to 100 µm
Excess/hydrogen level:	0 to 650 ppm
Strain rates:	10^{-4} to 10^{-5}/sec
Zircaloy:	Cold work and stress relieved
Fast fluences:	0-12 $\times$ 10^{25} n/m^2

Uncertainty (standard deviation) on yield and tensile strength are approximately 17% relative.

9.5 Bibliography

(Note: Bibliographical entries are not called out in the text. For called-out references, see Section 11.0.)

Hindle, E. D. And G. F. Slattery. 1971. "Stress Orientation of Hydride Platelets in Zirconium Alloy Tubing and Its Effect on Mechanical Properties." In *Proceedings of the International Conference on Corrosion*, British Nuclear Society, London, United Kingdom.

Louthan, M. R., and R. P. Marshall. 1962. "Control of Hydride Orientation in Zircaloy." *J. Nucl. Mater.* 9(2):170.

10.0 Modifications to the MATPRO Model for Fuel Rod Axial Growth

10.1 Background

Fuel rod Zircaloy cladding for commercial reactor fuel rods "grows" (i.e., develops permanent strain) in the axial direction during irradiation because of the combined effects of the cladding texture and the irradiation damage caused by fast neutron fluence. Fuel-cladding mechanical interaction can also contribute to the rod elongation by promoting plastic strain and enhanced creep. The fuel assembly support and constraint designs must also take into account axial growth to avoid mechanical interaction between the rods and the assembly support plates, which would cause rods to bow and reduce localized coolant channels or increase contact between rods. As a consequence, cladding would dry out, overheat, and fail. Cladding growth also changes the plenum volume and hence impacts rod internal pressure calculations; this is accounted for in FRAPCON-3.

These effects have long been recognized (see, for example Harbottle 1970) and are accounted for in fuel rod and assembly design. FRAPCON-3 will be used as an audit code for evaluating fuel vendors' design codes, and thus must accurately estimate the degree of rod axial growth.

10.2 Data Supporting Model Changes

The MATPRO subroutine CAGROW contains the FRAPCON-2 growth model, which is based on low-burnup, low-fluence data found in Harbottle (1970), Kreyns (1966), and Daniel (1971). The CAGROW model, in which growth is proportional to the 0.5 power of the fast neutron fluence, significantly underpredicts cumulative growth strains as a function of fast neutron fluence at fluences greater than 1×10^{25} n/m^2 (see Figure 10.1). This is probably because the database used samples with fluences less than 1×10^{25} n/m^2 for model development.

D. G. Franklin (1982) proposed a model, based on high-fluence PWR data, in which axial growth is proportional to the fluence raised to the 0.845 power. The MATPRO model and the Franklin model have been compared to the axial growth data, and the Franklin model was found to be acceptable for application to PWR rods and (with modification) to BWR rods, as discussed in the following section.

10.3 The Franklin Model Compared to Rod-Growth Data

The Franklin model was compared to high-burnup, high-fluence rod-growth data on commercial and test fuel rods taken from Balfour (1982a) [BR-3], Dideon (1983) [ANO-1], Newman (1986) [Oconee-1], Smalley (1974) [Saxton Core III], Smith (1983) [Fort Calhoun], Smith (1986) [ANO-2], Smith et al. (1994), West et al.
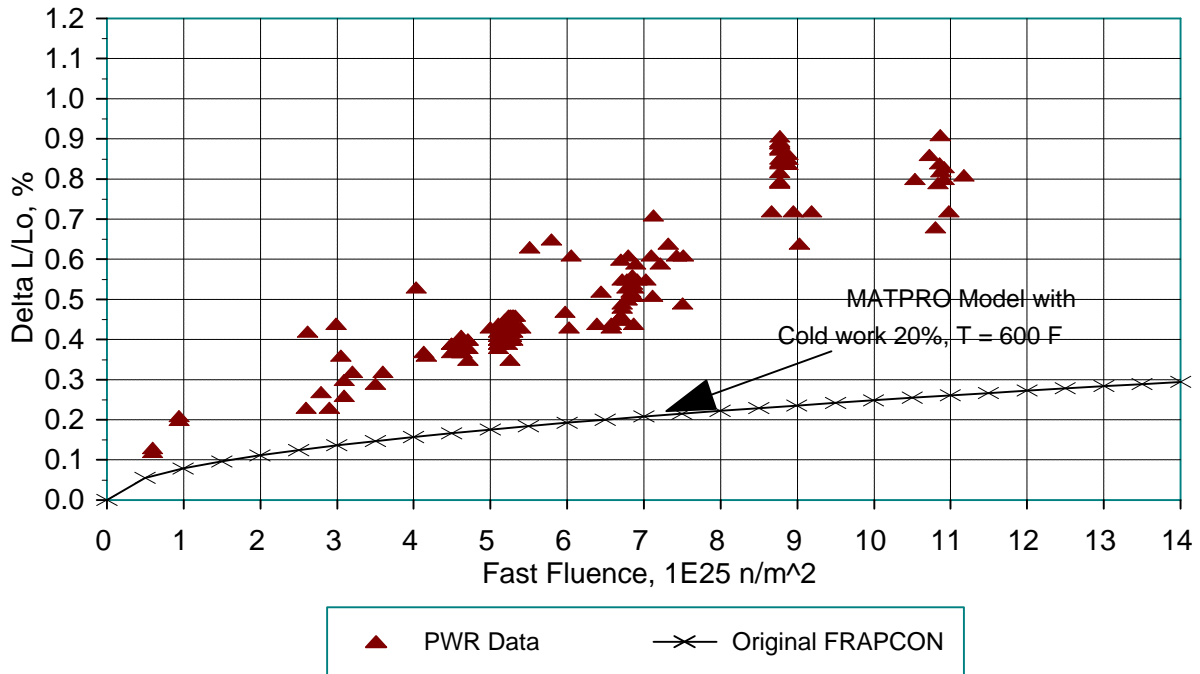
Figure 10.1. Original FRAPCON Model Compared to PWR Rod Axial Growth Data

(1983) [G-E Monticello], and Barner et al. (1990) [HBEP TVO-1] (see Figure 10.2). The Franklin model clearly provides a best-estimate fit to the data, with the exception of the fully-annealed Zry-2 data from BWR rods found in West et al. (1983) and Barner et al. (1990).

As a check on the goodness-of-fit to the PWR data, a zero-intercept linear regression analysis was performed on measured vs. predicted values. The slope of the regression line was 1.0014 (very close to 1.0), and the standard deviation was 0.070% ΔL/L (see Figure 10.3). This provides the uncertainty of the model based on these data.

Franklin (1982) addressed the issue of whether elongation due to pellet-cladding interaction (PCI) was included in his fuel rod growth data. Franklin did this by comparing the fuel rod growth data as a function of fast neutron fluence to that of cladding tubes irradiated without fuel (nonfueled rods). If PCI were a contributor to the growth data, the fueled rods would be expected to have significantly greater growth at a given fluence than the nonfueled rods. Franklin's original comparison is expanded in Figure 10.4 by including the PWR high-fluence growth data (from Figure 10.3). As can be seen, the non-fueled cladding data lie within the scatter band of the fueled cladding data, at fluences greater than 3×10^5 n/m^2. On the basis of this comparison, the Franklin model is used in FRAPCON-3 for PWR cladding without adjustment for inherent PCI effects.

Delta L/L % = 9.09E-23 x (phi*t)^0.845
for phi*t in n/m^2
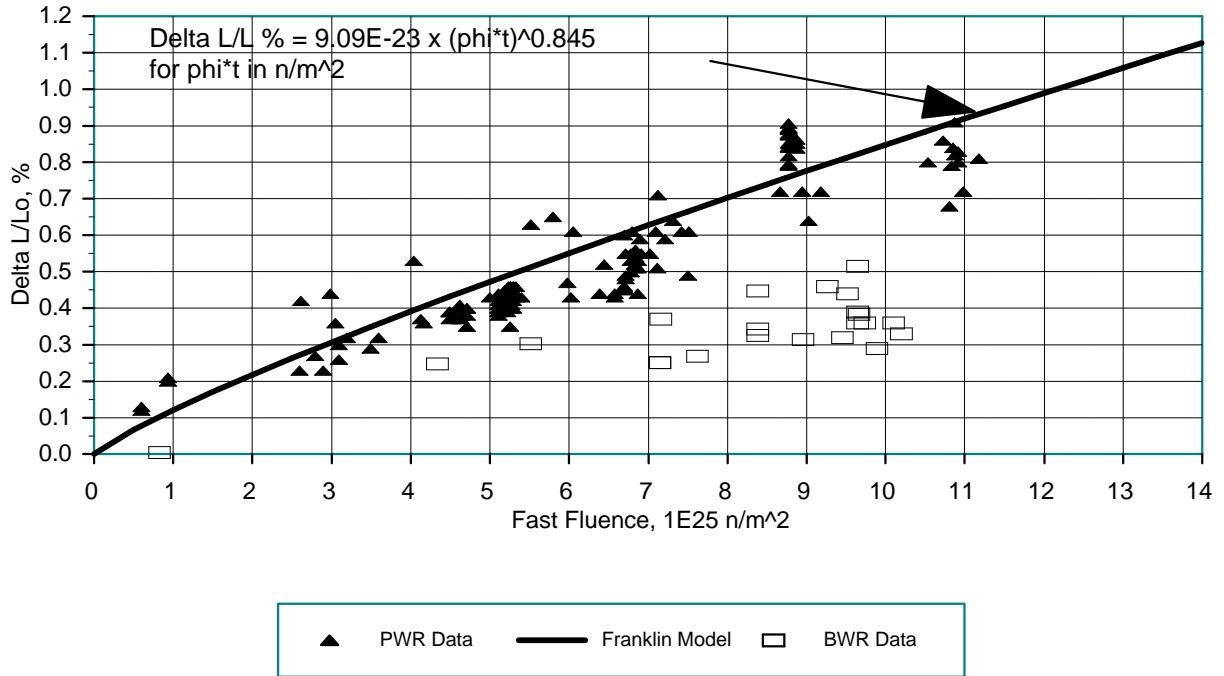
Figure 10.2. Franklin/Revised FRAPCON Model Compared to PWR Rod Growth Data

Standard deviation = 0.075 %

| ⋈ | Oconee-1 | ▲ | BR-3 | + | ANO-1 |
| ▭ | ANO-2 | ✕ | Saxton Core III | ▽ | Fort Calhoun |
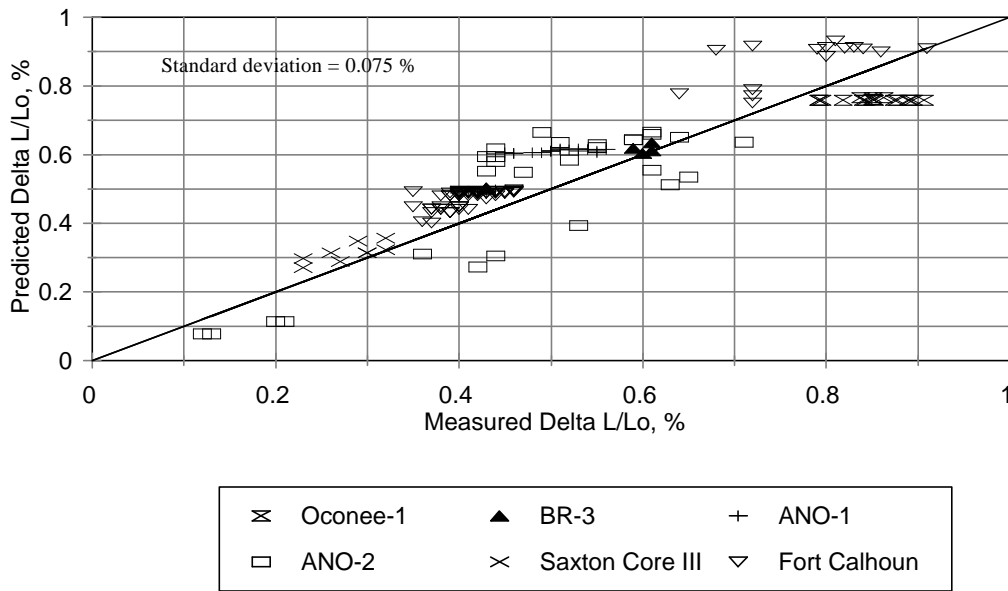
Figure 10.3. Comparison of Franklin Growth Model to PWR Rod Axial Growth Data
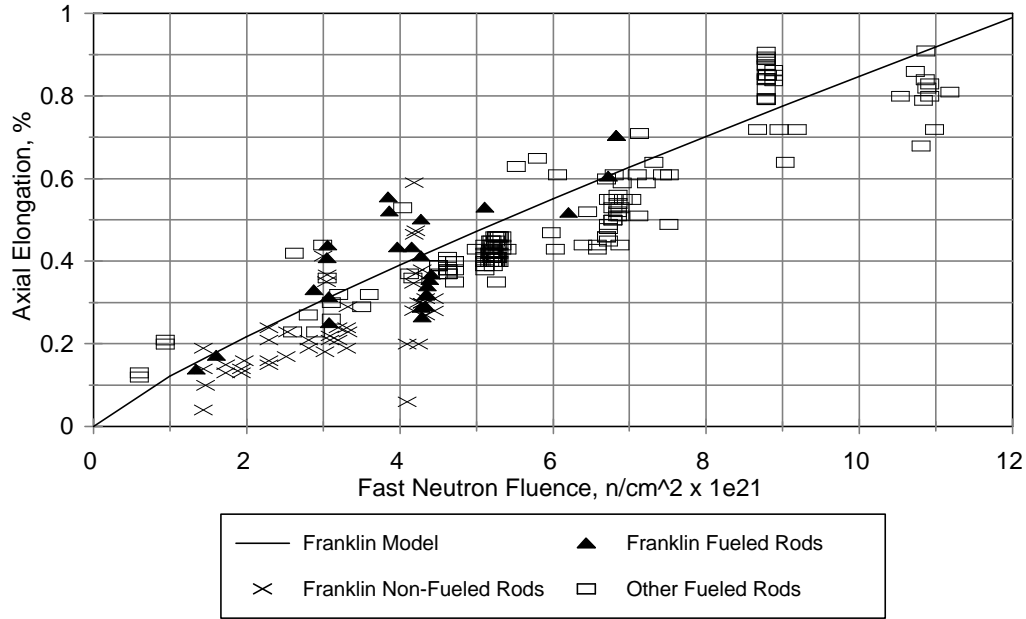
Figure 10.4. Franklin Rod Axial Growth Model Compared to Fueled and Non-Fueled PWR Rods

The Franklin model overpredicts the BWR Zircaloy-2 data by a factor of approximately 2.0, as shown in Figure 10.2. The Franklin model in CAGROW is therefore reduced by the factor 0.5 for fully annealed Zircaloy-2 cladding. Figure 10.5 compares this revised model to BWR rod-growth data. Note that the standard error in this comparison is even less than in the comparison to the PWR rod data.

These proposals are reflected in the revised subroutine.

10.4 Description of the Model

The Franklin correlation for PWR rod axial growth is simply

$$\text{growth strain } (\Delta L/L) \text{ increment} = C\ \{\ (\phi t_{i+1})^{0.845} - (\phi t_i)^{0.845}\} \tag{10.1}$$

where $C = 2.8 \times 10^{-25}$ per n/m^2
$\qquad \phi t = $ fast neutron cumulative fluence, n/m^2, E > 1 mev
i,i+1 refers to the end of the previous and current time step, respectively.

The strain increments at each axial node are accumulated through time, and the nodal strains are added together each time step to obtain the current cumulative axial rod growth. It is noted that the model is based on rod average fluences, but it is applied using localized nodal fluences and summed to give a total growth strain. The error introduced in the growth strains between applying the model using a rod average fluence and local fluence is insignificant (<3% relative) because the growth model is nearly linear with fluence.
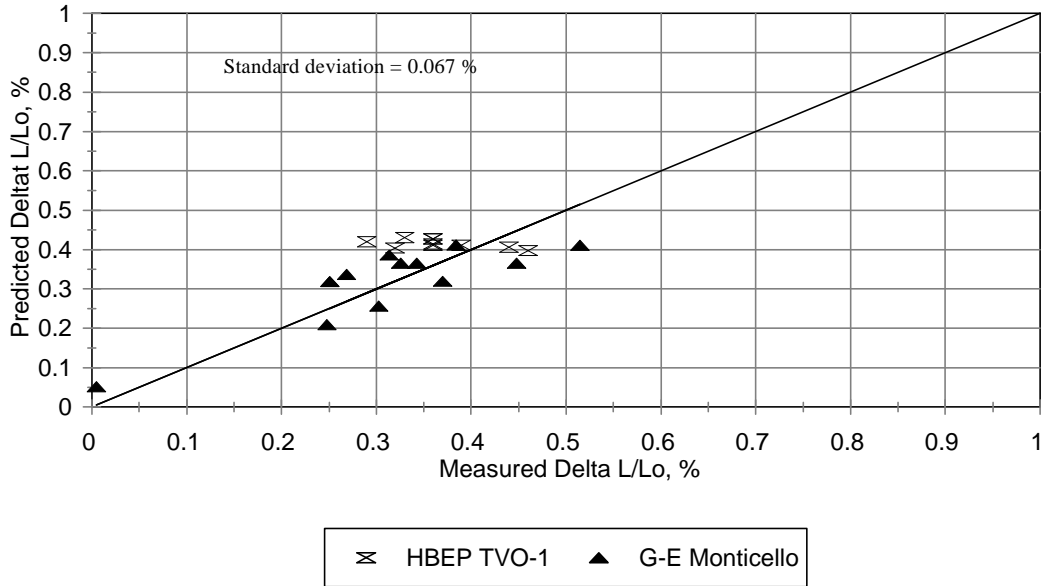
Figure 10.5. Revised FRAPCON Growth Model Compared to BWR Rod Growth Data

For BWR cases, the growth strains are reduced by the factor 0.5, based on the comparisons shown in Section 10.3.

10.5 Modification to FRAPCON

The equation listed in Section 10.4 replaces the current equation in Subroutine CAGROW. That subroutine has been modified to bring in fast neutron fluence, and the logic for handling the growth strains has been changed to the accumulation of incremental strains. As noted earlier, the growth strains are primarily used to calculate the rod volume and rod pressure in FRAPCON-3.

10.6 Range of Application and Uncertainty Bounds

The ranges of application for the axial growth model are based on the range of the data and, therefore, are

> Cladding temperature: 700 to 900K
> Local burnup: 0 to 65 GWd/MTU (0 to 12×10^{25} n/m^2 fluence, E > 1 mev)

The uncertainty (one standard deviation) on the growth strain is ± 0.070% absoluteΔL/L, based on statistical analysis of the PWR data sets listed herein. The BWR growth model is assumed to have the same uncertainty as the PWR model, even though the comparison to BWR data shows an even lower standard error (0.067% swelling, compared to 0.070% for the PWR model). The higher uncertainty was retained because the data set for BWR rods includes only two data sources.

11.0 References

Anselin, F. 1969. *The Role of Fission Products in the Swelling of Irradiated UO$_2$ and (U,Pu)O$_2$ Fuel*, GEAP-5583. General Electric Company, San Jose, California.

American Nuclear Society (ANS). 1982. "Method for Calculating the Fractional Release of Volatile Fission Products from Oxide Fuel," ANSI/ANS-5.4-1982. ANS5.4 of the Standards Committee of the American Nuclear Society.

Balfour, M. G. 1982a. *BR-3 High Burnup Fuel Rod Hot Cell Program, Final Report, Vol. 1*. D0E/ET/34073-1, Westinghouse Electric Corporation, Pittsburgh, Pennsylvania.

Balfour, M. G. 1982b. *Zorita Research and Development Program*, *Vol. 1*. Final Report, WCAP-10180, Westinghouse Electric Company, Pittsburgh, Pennsylvania.

Barner, J. O., M. E. Cunningham, M. D. Freshley, and D. D. Lanning. 1990. *High Burn up Effects Program Summary Report*, DOE/NE/3406-1, Battelle, Pacific Northwest Laboratories, Richland, Washington.

Baroch, C. J. and M. A. Rigdon. 1973. "Irradiation Behavior of UO$_2$ at Burnups from 10 to 80 GWd/tonne U," Paper No. 58 in *Proceedings of the BNES International Conference on Nuclear Fuel Performance,* October 15-19, 1973, London (CONF-731004).

Berna, G. A., M. P. Bohn, W. N. Rausch, R. W. Williford, and D. D. Lanning. 1981. *FRAPCON-2: A Computer Code for the Calculation of Steady State Thermal-Mechanical Behavior of Oxide Fuel Rods*, NUREG/CR-1845, prepared for the U.S. Nuclear Regulatory Commission by Pacific Northwest Laboratory, Richland, Washington.

Berna, G. A., C. E. Beyer, M. M. Bohn, K. L. Davis, and D. D. Lanning. 1997. *FRAPCON-3: A Computer Code for the Calculation of Steady-State, Thermal-Mechanical Behavior of Oxide Fuel Rods for High Burnup,* NUREG/CR-6534, PNNL-11513, Vol. 2, prepared for the U.S. Nuclear Regulatory Commission by Pacific Northwest Laboratory, Richland, Washington.

Beyer, C. E., and C. R. Hann. 1974. *Prediction of Fission Gas Release from UO$_2$ Fuel*, BNWL-1875, Pacific Northwest Laboratory, Richland, Washington.

Beyer, C. E., C. R. Hann, D. D. Lanning, F. E. Panisko, and L. J. Parchen. 1975. *GAPCON-THERMAL-2: A Computer Code for Calculating the Thermal Behavior of an Oxide Fuel Rod*, BNWL-1898, Battelle Pacific Northwest Laboratory, Richland, Washington.

Beyer, C. E., D. D. Lanning, G. A. Berma, and K. J. Geelhood. 1997. *FRAPCON-3: Integral Assessment,* NUREG/CR-6534, PNNL-11513, Vol. 3, prepared for the U.S. Nuclear Regulatory Commission by Pacific Northwest Laboratory, Richland, Washington.

Booth, A. H. 1957. *A Method of Calculating Fission Gas Diffusion from UO_2 Fuel and its Application to the Y-2-f Loop Test*, AECL 496, and CRDC-721, Atomic Energy of Canada Ltd.

Chantoin, P. M., E. Sartori, and J. A. Turnbull. 1997. "The Compilation of a Public Domain Database on Nuclear Fuel Performance for the Purpose of Code Development and Validation," presented in *Proceedings of the ANS/ENS International Topical Meeting on Light Water Reactor Fuel Performance*, Portland, Oregon, March 2-6, 1997, pp. 515:522.

Cheng, B., P. M. Gilmore, and H. H. Klepfer. 1996. "PWR Zircaloy Fuel Cladding Corrosion Performance, Mechanisms, and Modeling," presented in the *Proceedings of the 11th International Symposium on Zirconium in the Nuclear Industry*, Garmish-Parenkirchen, Germany, September 11-14, 1995, American Society for Testing and Materials, Philadelphia, Pennsylvania.

Chubb, W., V. W. Storhok, and D. L. Keller. 1972. "Observations Relating to the Mechanisms of Swelling and Gas Release in Uranium Dioxide of High Temperature," *J. of Nucl. Mater.,* Vol. 44, pp. 136-152.

Coleman, D. R. 1985. *Evaluation of Power Reactor Fuel Rod Analysis Capabilities Phase 2 Topical Report,* Vol. 2: Code Evaluation, NUREG/CR-3741. Prepared for Division of Accident Evaluation, Office of Nuclear Regulatory Research, U.S. Nuclear Regulatory Commission, Washington, D.C.

Cunningham, M. E. 1992. "Development and Characteristics of the Rim Region in High Burnup UO_2 Fuel Pellets." *J. of Nucl. Mater.*, Vol. 188, pp. 19-27.

Cunningham, M. E., and C. E. Beyer. 1984. *GT2R2: An Updated Version of GAPCON-THERMAL-2*, NUREG/CR-3907, PNL-5178, Pacific Northwest Laboratory, Richland, Washington.

Daniel, R. 1971. *In-Pile Dimensional Changes of Zircaloy-4 Tubing having Low Hoop Stresses*. WAPD-TM-973, Westinghouse Advanced Products Divisions, Pittsburgh, Pennsylvania.

Daniel, R. C. and I. Cohen. 1964. *In-Pile Effective Thermal Conductivity of Oxide Fuel Elements to High Fission Depletion*. BAPL Report WAPD-246. Bettis Atomic Power Laboratory/Westinghouse Advanced Products Division, U.S. Department of Energy, Washington, D.C.

Dean, R. A. 1962. *Thermal Contact Conductance Between UO_2 and Zircaloy 2*. CVNA-127, Carolina Virginia Nuclear Station, Virginia.

Dideon, C. G. 1983. *Fuel Performance under Extended Burn up for the B&W 15x15 Design*. DOE/ET/34212, Babcock and Wilcox, Lynchburg, Virginia.

Fenech, H. and W. M. Rohsenow. 1959. *Thermal Conductance of Metallic Surfaces in Contact*. NYO 2136, DOE New York Operations Office.

Fiero, I. B., M. A. Krammen, and H. R. Freeburn. 1987. *ESCORE - the Steady-State Core Reload Evaluator Code: General Description*, EPRI-NP-5100, Projects 2061-6, -13 Final Report. Prepared for Electric Power Research Institute, Palo Alto, California.

Forsberg, K. and A. R. Massih. 1985. "Diffusion Theory of Fission Gas Migration in Irradiated Nuclear Fuel UO_2," *J. of Nucl. Mater.,* Vol.135, pp.140-148.

Forsberg, K., F. Lindstrom, and A. R. Massih. 1994. "Modeling of Some High Burnup Phenomena in Nuclear Fuel" paper 2.5 in the *Technical Committee Meeting on Water Reactor Fuel Element Modeling at High Burnup, and Experimental Support,* 19-23 September 1994 in Windermere, England, IWGFPT/41, International Atomic Energy Agency, Vienna, Austria.

Franklin, D. G. 1982. "Zircaloy Cladding Deformation during Power Reactor Irradiation." In *Proceedings of the Fifth International Symposium on Zirconium in the Nuclear Industry*, ASTM-STP-754, pp. 235-267.

Franklin, D. G., J. A. Roberts, and Che-Yu Li. 1984. "Low Temperature Swelling and Densification Properties of LWR Fuels," *J. of Nucl. Mater.* Vol. 125, pp. 96-103.

Freshley, M. D., D. W. Brite, J. L. Daniel, and P. E. Hart. 1976. "Irradiation Induced Densification of UO_2 Pellet Fuel," *J. of Nucl. Mater.* Vol. 62, p.183.

Fukushima, S., T. Ohmichi, A. Maeda, and H. Watanabe. 1982. "The Effect of Gadolinium Content on the Thermal Conductivity of Near-Stoichiometric $(U,Gd)O_2$ Solid Solutions," *J. Nucl. Mater.* Vol. 105, pp. 201-210.

Galbraith, K. P. 1973. *Pellet-Cladding Gap Closure from Pellet Cracking Data and Analysis*, XN-73-17, Seimens Power Corporation (Formerly Exxon Nuclear), Richland, Washington.

Garde, A. M. 1986. *Hot Cell Examination of Extended Burnup Fuel from Fort Calhoun*. DOE/ET/34030-11, CEND-427, Combustion Engineering Co., Windsor, Connecticut.

Garde, A. M. 1989. "Effects of Irradiation and Hydriding on the Mechanical Properties of Zircaloy-4 at High Fluence." In *Zirconium in the Nuclear Industry: Eighth International Symposium*, ASTM STP-1023, pp. 548, L.F.P. Van Swam and C. M. Eucken, Eds., American Society for Testing Materials, Philadelphia.

Garner, R. W., D. T. Sparks, R. H. Smith, P. H. Klink, D. H. Schneider, D. X. Chick and P. E. MacDonald. 1978. *Gap Conductance Test Series 2, Test Results Report for Tests GC2-1,2-2 and 2-3*. NUREG/CR-0300, TREE-1268, EG&G Idaho, Inc., Idaho Falls, Idaho.

Garnier, J. E., and S. Begej. 1979. *Ex-Reactor Determination of Thermal Gap and Contact Conductance between Uranium Dioxide: Zircaloy-4 Interfaces; Stage I: Low Gas Pressure.* NUREG/CR-0330, PNL-2696, prepared for the U.S. Nuclear Regulatory Commission by Pacific Northwest Laboratory, Richland, Washington.

Garzarolli, F., D Jorde, R. Manzel, G. W. Parry, and P. G. Smerd. 1980. *Review of PWR Fuel Rod Waterside Corrosion Behavior,* EPRI NP-1472, Interim Report, Electric Power Research Institute, Palo Alto, California.

Garzarolli, F., W. Jung, H. Shoenfeld, A. M. Garde, G. W. Parry, and P. G. Smerd. 1982. *Review of PWR Fuel Rod Waterside Corrosion Behavior*, EPRI NP-2789, Project 1250 Final Report, Electric Power Research Institute, Palo Alto, California.

Hagrman, D. L., G. A. Reymann, and G. E. Mason. 1981. *A Handbook of Materials Properties for Use in the Analysis of Light Water Reactor Fuel Rod Behavior.* MATPRO Version 11 (Revision 2). NUREG/CR-0479 (TREE-1280), prepared by EG&G Idaho, Inc., Idaho Falls, Idaho for the U.S. Nuclear Regulatory Commission, Washington, D.C.

Harbottle, J. E. 1970. "The Temperature and Neutron Dose Dependence of Irradiation Growth in Zircaloy-2." In *Irradiation Effect on Structural Alloys for Nuclear Reactor Applications*, ASTM-STP-485, pp. 287-299.

Harding, J. H. and D. G. Martin. 1989. "Recommendation for the Thermal Conductivity of UO_2," *J. of Nucl. Mater.*, Vol. 166, pp. 223-226.

Hargreaves, R. and D. A. Collins. 1976. "A Quantitative Model for Fission Gas Release and Swelling in Irradiated Uranium Dioxide," *J. Brit. Nucl. Ener.*, Vol. 15, p.311.

Hirai, M. and S. Ishimoto. 1991. "Thermal Diffusivities and Thermal Conductivities of UO_2-Gd_2O_3," *Mater.*, Vol 28, pp. 995-1000.

Inaba, H. et al. 1987. "Heat Capacity Measurement of $(U_{1-y},Gd_y)O_2$ from 310 to 1500 K." In *J. of Nucl. Mater.*, Vol. 149, pp. 341-348.

International Atomic Energy Agency (IAEA). 1993. *Corrosion of Zirconium Alloys in Nuclear Power Plants*. IAEA-TECDOC-684, International Atomic Energy Agency, Vienna, Austria.

Johnson, A. B. Jr. 1987. *Zirconium Alloy Oxidation and Hydriding Under Irradiation: Review of Pacific Northwest Laboratory Test Program Results.* EPRI-NP-5132, Electric Power Research Institute, Palo Alto, California.

Knudsen, P. et al. 1993. "Fission Gas Release and Fuel Temperature During Power Transients in Water Reactor Fuel at Extended Burnup." *Proceedings of a Technical Committee Meeting held in Pembroke, Ontario, Canada. 28 April - 1 May 1992.* IAEA-TECDOC-697. International Atomic Energy Agency, Vienna, Austria.

Kolstad, E. 1992. "Fuel Rod and Core Materials Investigations Related to LWR Extended Burn up Operation," *J. of Nucl. Mater.*, Vol. 188, pp. 104-113.

Kolstad, E. H. Devold, and V. Tossi. 1991. "High Burn up Fuel Behavior Studies by In-Pile Measurements," *ANS/ENS International Topical Meeting on LWR Fuel Performance*, Avignon, France, pp. 838-849.

Kreyns, P. H., quoted by E. Duncombe et al. 1966. *Comparisons with Experiment of Calculated Changes and Failure Analysis of Irradiated Bulk Oxide Fuel Test Rods using the CYGRO1 Computer Program.* WAPD-TM-583, Westinghouse Advanced Products Division, Pittsburgh, Pennsylvania.

Lanning, D. D. and C. R. Hann. 1975. *Review of Methods Applicable to the Calculation of Gap Conductance in Zircaloy-Clad UO_2 Fuel Rod*. BNWL-1984, Battelle Northwest Laboratory, Richland, Washington.

Lanning, D. D. 1982. "The Possible Impact of Fuel Pellet Cracking on Inferred Gap Conductance and Stored Energy," *Nuclear Technology*, Vol. 56, pp. 565-574.

Lanning, D. D., and M. E. Cunningham. 1981. "Trends in Thermal Calculations for Light Water Reactor Fuel (1971-1981)," in *Proceedings of the Ninth Water Reactor Safety Research Information Meeting,* Gaithersburg, Maryland, Oct. 26-30, 1981.

Lanning, D. D., and E. R. Bradley. 1984. *Irradiation History and Interim Postirradiation Data for IFA-432,* NUREG/CR-3071. Pacific Northwest Laboratory for the U.S. Nuclear Regulatory Commission, Washington, D.C.

Lassmann, K., C. O'Carrol, J. VanderLaar, and C. T. Walker. 1994. "The Radial Distribution of Plutonium in High Burnup UO_2 Fuels," *J. Nucl. Mater.*, Vol. 208, pp. 223-231.

Lassmann, K., C. T. Walker, J. VanderLaar, and F. Lindstrom. 1995. "Modeling the High Burn up Structure in LWR Fuel," *J. of Nucl. Mater.*, Vol. 225, pp. 1 to 8.

Limback, M. 1994. "Corrosion and Hydriding Performance of Zircaloy-2 and Zircaloy-4 Cladding Materials in PWRs." In *ANS/ENS International Topical Meeting on Light Water Reactor Fuel Performance*, West Palm Beach, Fla., April 1994, p. 286.

Lokken, R. O., and E. L. Courtwright. 1977. *A Review of the Effects of Burnup on the Thermal Conductivity of UO_2*, BNWL-2270, Pacific Northwest Laboratory, Richland, Washington.

Lucuta, P.G., R. A. Verrall, H. J. Matzke, and H. A. Tasman. 1991. "Microstructural Features of SIMFUEL - Simulated High-Burnup UO$_2$-Based Nuclear Fuel," *J. of Nucl. Mater.,* vol 178, p. 48-60.

Lucuta, P. G., H. J. Matzke, R. A. Verrall, and H. A. Tasman. 1992. "Thermal Conductivity of SIMFUEL," *J. of Nucl. Mater.*, Vol. 188, pp. 198-204.

Lucuta, P. G., H. J. Matzke, and R. A. Verrall. 1995. "Thermal Conductivity of Hyperstoichiometric SIMFUEL," *J. of Nucl Mater.*, Vol. 223, pp. 51-60.

Lucuta, P. G., H. S. Matzke, and I. J. Hastings. 1996. "A Pragmatic Approach to Modeling Thermal Conductivity of Irradiated UO$_2$ Fuel: Review and Recommendations," *J. of Nucl. Mater.,* Vol. 232, pp. 166-180.

Massih, A. R., S. Persson, and Z. Weiss. 1992. "Modeling of (U,Gd)O$_2$ Fuel Behavior in Boiling Water Reactors," in *proceedings of Symposium E on Nuclear Materials for Fission Reactors of the 1991 E-MRS Fall Conference; J. of Nucl. Mater.,* Vol. 188, pp. 319-330.

Manzel, R. 1993. "Fission Gas Release of High Burn up Fuel," in TECDOC-697. p. 63 in Proceedings of a Technical Committee Meeting, Pembroke, Ontario, Canada, International Atomic Energy Agency.

Matsamura, T., and T. Kameyama. 1988 "Burn up and Plutonium Distribution Near the Surface of High Burn up Fuel," *Proceedings of IAEA Technical Committee Meeting on Water Reactor Fuel Element Computer Modeling in Steady State, Transient, and Accident Conditions,* Preston, United Kingdom.

Nelson, R. C., J. A. Baumgartner, K. J. Perry, and E. L. Zebroski. 1971. *Irradiation Induced Swelling Rates of PuO$_2$ - UO$_2$ Fuel with Strong Radial Restraint,* GEAP-13686, General Electric Company, San Jose, California.

Newman, L. W. 1986. *The Hot Cell Examination of Oconee 1 Fuel Rods After Five Cycles of Irradiation,* DOE/ET/34212-50, Babcock and Wilcox Company, Lynchburg, Virginia.

Newman, L. W. 1990. *Development of an Extended Burn up Mark B Design-Thirteen Progress Report, July 1987 to December 1989 and Project Summary.* DOE/ET/34213-16, BAW-1532-13, Babcock and Wilcox, Lynchburg, Virginia.

Newman, L. W., T. A. Thornton, and B. J. Wrona. 1984. *Thermal and Physical Properties of Urania-Gadolinia Fuel,* DOE/ET/34212-43. Babcock & Wilcox, Lynchburg, Virginia.

Oguma, M. 1983. "Cracking and Relocation Behavior of Nuclear Fuel Pellets During Rise to Power," *Nucl. Eng. Design,* Vol. 76, pp. 35-45.

Palmer, I. D., et al. 1982. "A Model for Predicting the Radial Power Profile in a Fuel Pin," presented at the *IAEA Specialist's Meeting on Water Reactor Fuel Element Performance Computer Modeling,* Preston United Kingdom, *Applied Science 1983,* p. 321.

Pyecha, T. D. 1985. "Waterside Corrosion of PWR Fuel Rods Through Burnups of 50,000 MWD/MTU." In *ANS/ENS International Topical Meeting on Light Water Reactor Fuel Performance*, Orlando, Florida, April 1985, pp. 3-17 to 3-55.

Rest, J. 1980. "The Mechanistic Prediction of Transient Fission-Gas Release from LWR Fuel," *Nucl. Eng. Design,* Vol. 56, pp. 233-256.

Ross, A. M. and R. L. Stoute. 1962. *Heat Transfer Coefficient between UO_2 and Zircaloy-2.* AECL-1552, Atomic Energy of Canada, Ltd. Toronto, Canada.

Sawatzky, A. and B. J. Wilkins. 1967. "Hydrogen Solubility in Zirconium Alloys Determined by Thermal Diffusion," *J. of Nucl. Mater.*, Vol. 22, pp. 304-310.

Seifken, K. J., C. M. Allison, M. P. Bohn, and S. O. Peck. 1981. *FRAP-T6: A Computer Code for the Transient Analysis of Oxide Fuel Rods*, NUREG/CR-2148, Idaho National Engineering Laboratory, Idaho Falls, Idaho.

Shann, S. H. 1991. "A Two-Group Radial Power Distribution Prediction Model," *ANS/ENS International Topical Meeting on Light Water Reactor Fuel Performance,* Avignon, France, p. 578.

Smalley, W. R. 1974. *Evaluation of Saxton Core III Fuel Material Performance*. WCAP-3385-57, Westinghouse Electric Corporation, Pittsburgh, Pennsylvania.

Smith, G. P. 1983. *The Evaluation and Deomonstration of Methods for Improved Fuel Utilization*. DOE/ET/34010-10, Combustion Engineering, Windsor, Connecticut.

Smith, G. P. 1986. *The Nondestructive Examination of Fuel Assemblies with Standard and Advanced Design after Three Cycles of Irradiation*. DOE/ET/34013-12, Combustion Engineering, Windsor, Connecticut.

Smith, G. P., R. C. Pirek, H. R. Freeburn, and D. Schrire. 1994. *The Evaluation and Demonstration of Methods for Improved Nuclear Fuel Utilization*, DOE/ET/34013-15, Combustion Engineering, Windsor, Connecticut.

Speight, M. V. 1969. "A Calculation on the Migration of Fission Gas in Material Exhibiting Precipitation and Re-solution of Gas Atoms under Irradiation," *Nucl. Sci. Eng.* Vol .37, pp. 180-185.

Stehle, H., and H. Lassmann. 1974. "The Dependence of In-Reactor UO_2 Densification on Temperature and Microstructure," *J. of Nucl. Mater.*, Vol. 52, p. 303-308.

Susuki, S., K. Murakami, and T. Takahashi. 1994. "Burn up Extension and Improved Reliability." In *ANS/IAEA International Topical Meeting on LWR Fuel Performance*, West Palm Beach, Florida, April 1994, pp. 352-359.

Todreas, N. and G. Jacobs. 1973. "Thermal Contact Conductance of Reactor Fuel Elements." *Nucl. Sci. Eng.* 50:283.

Turnbull, J. A. 1974. "The Effect of Grain Size on the Swelling and Gas Release Properties of UO_2 During Irradiation," *J. of Nucl. Mater.*, Vol. 50, pp. 62-68.

Turnbull, J. A. and M. O. Tucker. 1974. "Swelling in UO_2 under Conditions of Gas Release," *Philosoph. Mag.*, Vol. 30, pp. 47-64.

Vesterlund, G., and L. V. Corsetti. 1994. "Recent ABB Fuel Design and Performance Experience," *ANS/ENS International Topical Meeting on Light Water Reactor Fuel Performance*, West Palm Beach, Florida, April 1994, pp. 62-70.

Weisman, J., and P. E. MacDonald. 1969. "Fission Gas Release from UO_2 Fuel Rod with Time Varying Power Histories," *ANS Transactions,* Vol. 12, pp. 900-901.

West, J. S., S. E. Kasib, and S. Y. Ogawa. 1983. *EOC9-Final Fuel Bundle Examination at Monticello Nuclear Generating Station*. DOE/ET/34031-16, General Electric Company, San Jose, California.

White, R. J. and M. O. Tucker. 1983. "A New Fission-Gas Model,"*J. of Nucl. Mater.*, Vol. 118, pp. 1-38.

Wiesenack, W. 1995. "High Burn up Phenomena - Results from Experiments in the Halden Reactor," presented at the *CSNI Specialists' Meeting on Transient Behavior of High Burn up Fuel,* September 12 to 14, 1995 at Cadarache, France, OCDE/GD(96) 197, NEA/CSNI/R(95)22, pp. 405-416.

Wiesenack, W. 1997. "Assessment of UO_2 Conductivity Degradation Based on In-Pile Temperature Data," in *Proceedings of the ANS/ENS International Topical Meeting on Light Water Reactor Fuel Performance,* Portland, Oregon, March 2-6, 1997, pp. 507-511.

Williford, R. E., C. L.Mohr, D. D. Lanning, M. E. Cunningham, W. N. Rausch, and E. R. Bradley. 1980. Interim Report, *The Analysis of Fuel Relocation for the NRC/PNL Halden Assemblies IFA-431, IFA-432 and IFA-513,* NUREG/CR-0588, PNL-2709, Pacific Northwest Laboratory, Richland, Washington.

Zimmermann, H. 1978. "Investigations on Swelling and Fission Gas Behavior in Uranium Oxide," *J. Nucl. Mater.,* Vol. 75, pp. 154-161.

Appendix A

Supplement for Section 2.0

A.1 The ANS5.4 Subroutine in FRAPCON

Two separate sets of equations for the fission gas diffusion constant and its burnup enhancement factor appear in the GT2R2 ANS-5.4 gas release subroutine (Cunningham and Beyer 1984). The "original" version corresponds to the documented product of the ANS-5.4 Working Group, and the "modified" version includes changes that Pacific Northwest Laboratory made in 1984 to the model diffusion coefficients to improve GT2R2 predictions with ANS-5.4 to benchmark cases. These comparisons showed that the "original" coefficients provided a slightly better comparison to the steady-state FGR data. Both sets of equations have been used in FRAPCON-3 to predict FGR for its benchmark data cases (listed in Section 2), including both the steady-state and power-ramp cases. Based on these comparisons, the "original" set of equations is retained in the ANS-5.4 subroutine in FRAPCON-3.

Thus, diffusion constant, D, as a function of Kelvin temperature, T, is given by

$$D = 0.61 \exp(-36386/T) \tag{A.1}$$

(Note that this diffusion constant corresponds to D/a^2 in the MASSIH system of equations, where a is the grain radius.)

The above diffusion constant is multiplied by the burnup enhancement factor, F, which is multiplied again, and the above diffusion constant is given by

$$F = 100^{Bu/28} \tag{A.2}$$

where Bu = the pellet-average burnup in GWd/MTU.

A.1.1 Reference

Cunningham, M. E., and C. E. Beyer. 1984. *GT2R2: An Updated Version of GAPCON-THERMAL-2, NUREG/CR-3907,* PNL-5178, Pacific Northwest Laboratory, Richland, Washington.

A.2 Detailed Description of the Modified MASSIH Model

The original MASSIH model begins by solving the gas-diffusion equation for constant production and properties in a spherical grain:

$$dC/dt = D(t)\Delta_r C(r,t) + \beta(t) \tag{A.3}$$

with boundary conditions

$$C(r,0) = 0$$
$$C(a,t) = 0$$

where C = gas concentration
          β = gas production
          $\Delta_r = d^2/dr^2 + 2/r \cdot d/dr$
          D = diffusion constant
          a = outside radius

Forsberg and Massih attempt to solve the equation for the case where there is resolution of gas on the grain surface, which changes the outer boundary condition to

$$C(a,t) = b(t)\lambda N(t)/2D \tag{A.4}$$

where N = surface gas concentration
       λ = resolution layer depth
       b = resolution rate.

They make use of a three-term approximation to the integration kernal K, where

$$\int_0^t 4\pi r^2 C(r,t)dr = \int_0^t K(\tau-\tau_0)\beta_e(\tau_0)d\tau_0$$

$$\text{and } \beta_e = \beta/D$$

$$\text{and } K = 8a^3/\pi \sum_{n=1}^{\infty} \exp(-n^2\pi^2\tau/a^2)/n^2$$

A.2.1 Grain-Boundary Accumulation and Resolution

The final solution for a given time step, *without resolution* and with constant production rate during the step, can be written as

$$\Delta G = \sum_{n=1}^{3} \Delta G_n$$

$$\Delta G_B = -\Sigma f_n G_n(\tau_1) + \int_{\tau1}^{\tau2} \text{funct}(\tau_2 - \tau_0) q(\tau_0) d\tau_0 \qquad (A.5)$$

where q is determined from

$$a^2 q[-\sum_{n=1}^{3}(f_n A_n/B_n) + \text{Funct}(\Delta\tau)] = \beta\Delta t$$

and where

ΔG = change in gas concentration in fuel grain

ΔG_B = change in gas concentration on grain boundaries

and where

$$\text{funct} = 6/\sqrt{\pi} \ ([\tau_2 - \tau_0]/a^2)^{1/2} - 3([\tau_2 - \tau_0]/a^2) \ \text{if} \ \tau < 0.1$$

$$\text{funct} = 1 - (6/\pi^2)\exp(-\pi^2[(\tau_2-\tau_0)/a^2]) \ \text{if} \ \tau > 0.1$$

$$\text{Funct} = \int_{\tau1}^{\tau2} \text{funct}(\tau_2 - \tau_0)d\tau$$

A_n and B_n are constants given by Massih

$$K_2 = a/3 - K/(4\pi a^2)$$
$$K_3 = 3/a \ K_2$$
$$1 + K_3 = \sum_{n=1}^{3} A_n \exp(-B_n \tau/a^2), \ n=1,2,3$$

In modifying the original model, the partition of resolved gas and the gas arriving at the boundary at the end of each time step is redefined as follows.

$$\Delta \ \text{Resolved Gas} = F/(1+F) \cdot \Delta G_B$$
$$\Delta G_B = \Delta G_B/(1+F) \qquad (A.6)$$

where F = FITMULT•$[1.84 \times 10^{14} \cdot \text{GRN}/(3\cdot D)]$ where GRN = grain radius in meters, D = diffusion constant in m^2/sec, FITMULT is an adjustable multiplier, and the term in brackets is the original Massih equation for the resolution rate. It should be noted that although F is unitless in Massih's derivation, it does not represent the fraction of retained gas. It is also noted that when the grain boundary gas exceeds the saturation concentration for the boundary, all of the resolved and grain boundary gas is released.

A.2.2 Diffusion Constant

The original diffusion constant is defined over three temperature ranges, as follows:

$$D = 1.09 \times 10^{-17} \exp(-6614/T), \quad T > 1650 \text{ K}$$
$$D = 2.14 \times 10^{-13} \exp(-22884/T), \quad 1381 < T < 1650 \text{ K}$$
$$D = 1.51 \times 10^{-17} \exp(-9508/T), \quad T < 1381 \text{ K}$$

The form of the Massih mid-range diffusion constant has been modified to include burnup enhancement, changed the pre-exponential term to be $2.14 \times 10^{13} \cdot 14$, and changed the activation energy term (Q/R) to be $22884 \cdot 1.15$. This diffusion constant is the only one used at high temperatures (the Massih diffusion constant for temperatures above 1650K is not used). The original Massih low temperature diffusion constant is retained, but the cutoff temperature recommended by Massih is not used. Instead, if the new high temperature diffusion constant is less than the low temperature Massih diffusion constant, the latter is used. The modified and original diffusion constant functions are plotted versus inverse Kelvin temperature in Figures A.1 and A.2 respectively.
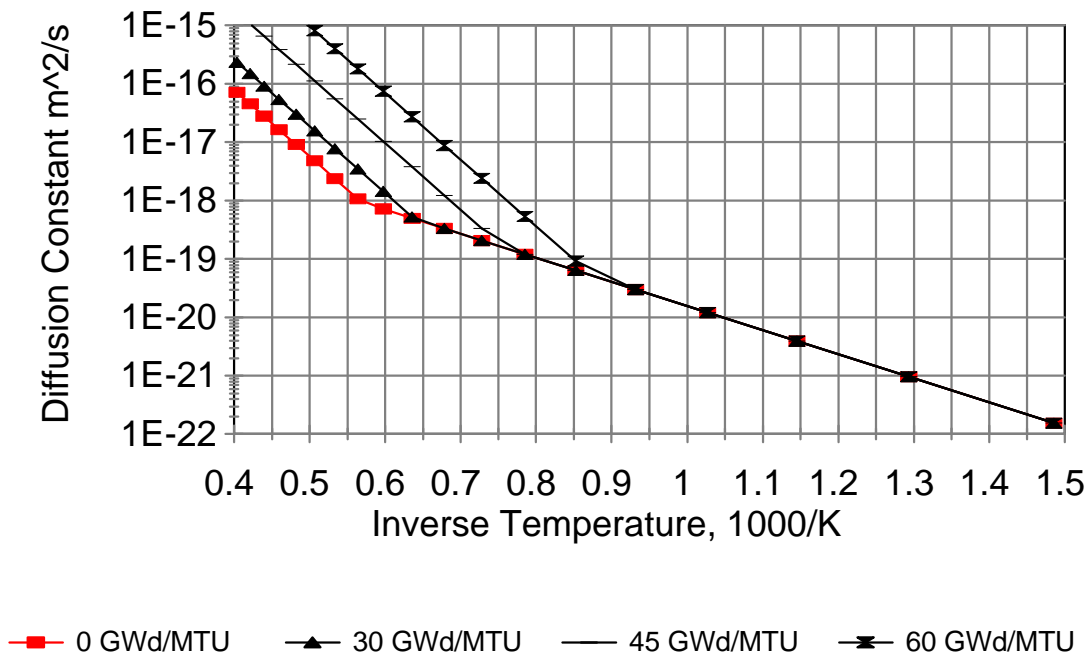
Figure A.1. FRAPCON-3 (Modified MASSIH Model) Diffusion Constant as a Function of Temperature and Burnup
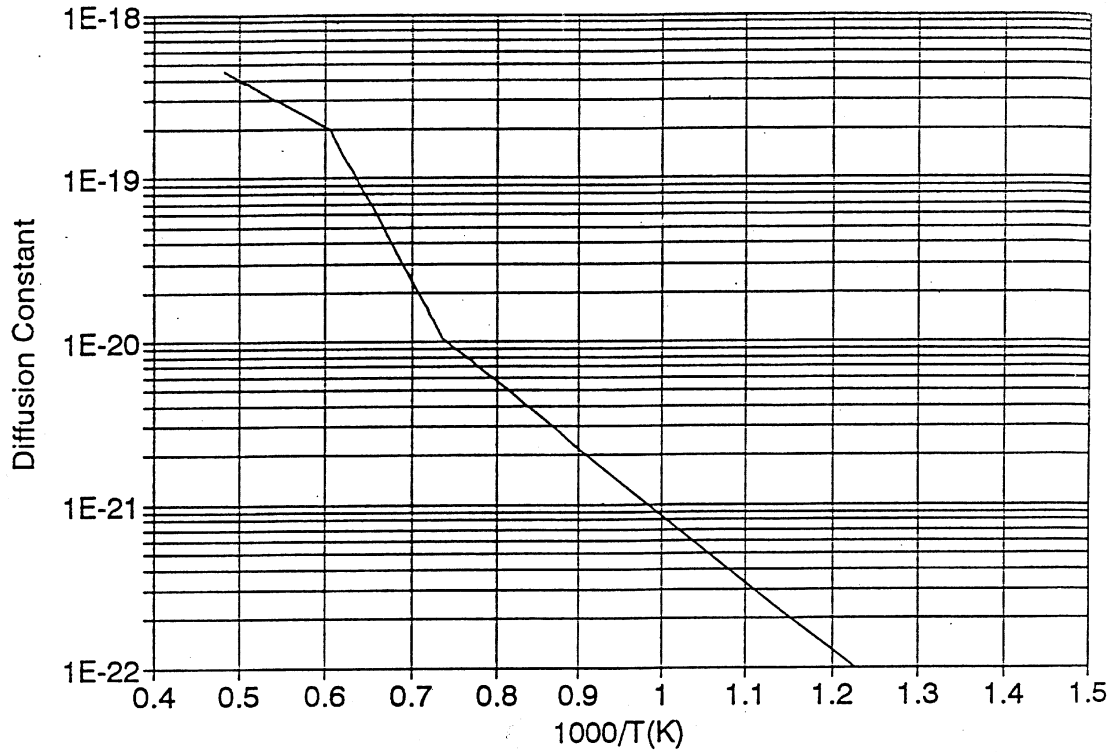
Figure A.2. Massih Diffusion Constant (Original Model)

The burnup enhancement factor is of the form

$$100^{(BURNUP-21)/35}, \text{ where BURNUP = burnup in GWd/MTU}$$

with a maximum value of 20,000 for this enhancement factor.

A.2.3 Gas Release

The gas is accumulated at the grain boundary until a saturation concentration is achieved, at which time the grain-boundary gas is released. The saturation areal density of gas is given by

$$N_s = [(4rF(\theta)V_c)/(3K_BT \sin^2(\theta)] \bullet (2\gamma/r + P_{ext}) \tag{A.7}$$

where θ = dihedral half-angle = 50°
        K_B = Boltzman constant
        γ = surface tension = 0.6 J/m^2
        V_c = critical areal coverage fraction = 0.25
        r = bubble radius = 0.5µm
    $F(\theta) = 1 - 1.5\cos(\theta) + 0.5\cos^3(\theta)$
    P_{ext} = external pressure on bubbles = gas pressure in Pa

    The final modification to the original model is to release both the grain boundary and the resolved gas whenever the saturation condition is achieved, and the grain-boundary gas is released.

A.2.4 Optimized Parameters

    Finally, optimized parameters have been applied, based on comparisons to selected steady-state and transient data:

The activation energy(Q/R) = 1.15 • 22884. = 29060
                                    (high-temperature diffusion)

The resolution parameter = 250.• 1.84E-14 = 1.47E-12

Burnup enhancement factor is of the form

$$100^{(BURNUP-21)/35}, \text{ where } BURNUP = GWd/MTU$$

Multiplier on the diffusion constant = 14.0.
                                    (Applied after all other modifications.)

A.2.5 Burnup Dependence at Low Temperatures

    A burnup dependence has been observed in fuel rods operated at low fuel temperatures to high burnups. At these low temperatures, both the MASSIH thermal release model and the ANS-5.4 low-temperature release model predict less than 1 to 2% release while 4 to 5% FGR values have been measured at burnups of 60 GWd/MTU. As a result, an empirical burnup dependent term for use at low fuel temperatures is added to the MASSIH model. The low temperature burnup dependence is simply

$$F = 7 \times 10^{-5} \, *b + C \tag{A.8}$$

where   F = fractional FGR
        b = burnup, GWd/MTU
        C = 0 at b $\leq$ 40 GWd/MTU
        C = 0.01*(b-40)/10 at b > 40 GWd/MTU and F$\leq$ 0.05

The first term is from the ANS-5.4 low temperature release model and the C term is only applied if burnups exceed 40 GWd/MTU, and axial node FGR is less than 5%.

A.3 References for the FGR Cases

The following reference lists include references for the steady-state and power-ramp FGR cases referred to in Tables 2.1 and 2.2. The correlation between rod numbers and reference documents is shown in Table A.1 for the steady-state cases. All U.S. Department of Energy (DOE) references can be obtained from the National Technical Information Service (NTIS).

Table A.1. Reference Key for Steady-State FGR Cases Used for Model Development

Rod Designation	Program or Experiment	Document Author and Number
111I5	Westinghouse High-Burnup BR-3 Rods (PWR -Type)	Balfour, M.G., WACAP-10238
36i8	"	"
24i6	"	"
28i6	"	"
LFF	AECL Tests (Candu Type Fuel)	Notley, M.J.F., AECL-2662
CBP	"	Notley, M.J.F., AECL-2230
4110-AE2	CEA Tests	Janvier, J.C., CEA-R-3358
4110-BE2	"	"
BNFL Rod DE	Battelle High Burnup Effects Program (BR-3 Rod)	Barner, J.O. DOE/NE/34046-1 (HBEP-61)
IFA-429 Rod DH	NRC/Halden Instrumented Test	Personal communication with Halden Reactor Project

A.4 Bibliography for Assessment Cases

Balfour, M. G., W. C. Chubb, and R. F. Boyle. 1982. *BR-3 High Burnup Fuel Rod Hot Cell Program* Vols. 1 and 2, WCAP-10238. Westinghouse Electric Corporation, Pittsburgh, Pennsylvania.

Balfour, M. G. 1982. *Zorita Research and Development Program*, Vols. 1 and 2, WCAP-10180. Westinghouse Electric Corporation, Pittsburgh, Pennsylvania.

Barner, J. O., M. E. Cunningham, M. D. Freshley, and D. D. Lanning. 1990. *High Burnup Effects Program - Final Report*, DOE/NE/34046-1. Pacific Northwest Laboratory, Richland, Washington.

De Meulemeester, E., N. Hoppe, G. de Contenson, and M. Watteau. 1973. "Review of Work Carried out by BELGONUCLEAIRE and CEA on the Improvement and Verification of the Computer Code with the Aid of In-Pile Experimental Results" *International Conference on Nuclear Fuel Performance*, October 15-19, 1973, British Nuclear Energy, Limited.

Djurle, S. 1985. *Final Report of the Super-Ramp Project*, DOE/ET/34032-1. Studsvik Energiteknils AB, Nykoping, Sweden.

Janvier, J. C., B. de Bernardy de Sigoyer, and R. Delmas. 1967. *Irradiation of Uranium Oxide in Strong Cladding Effect of Initial Diametral Cap on Overall Behavior*, CEA-R-3358, Commissariat à l'Energie Atomic, Paris, France.

Knudsen, P., C. Bagger, H. Carlsen, I. Misfeldt, and M. Mogensen. 1983. *Riso Fission Gas Release Project Final Report*, DOE/ET/34033-1, RISO, Roskilden, Denmark, NTIS.

Lysell, G. and S. Birath. 1979. *The Studvik Inter-Ramp Project Hot Cell PIE Final Report*, STIR -51. Studsvik Energiteknils AB, Nykoping, Sweden.

Notley, M. J. F., R. DesHaies, and J. R. MacEwan. 1966. *Measurements of the Fission Product Gas Pressures Developed in UO$_2$ Fuel Elements during Operation*, AECL - 2662, Atomic Energy of Canada Limited, Chalk River, Canada.

Notley, M. J. F., and J. R. MacEwan. 1965. *The Effect of UO$_2$ Density on Fission Product Gas Release and Sheath Expansion*, AECL - 2230, Atomic Energy of Canada Limited, Chalk River, Canada.

Appendix B

FRAPCON Models Retained Without Modification

A number of MATPRO materials properties models were assessed but have been retained without modification. These are discussed in the following subsections.

B.1 Fuel Thermal Expansion

The thermal expansion strain of the fuel pellets is calculated as a function of temperature and plutonia content in subroutine FTHEXP and corresponds with the model of the same name in MATPRO-11, Rev.1. No data have been found from which to determine a burnup or a burnable poison dependency for fuel thermal expansion. In addition, thermal expansion functions are not expected from mechanistic considerations to change significantly up to currently approved burnup and burnable poison concentration limits. However, due to the anticipated increase in fuel burnup limits in the future, it is recommended that out-of-reactor testing be performed to examine possible effects at very high burnups and burnable poison concentrations.

B.2 Fuel Specific Heat

The specific heat of the fuel pellets is used in FRAPCON-3 in the calculation of stored energy. It is calculated in subroutine FCP as a function of temperature and plutonia content and corresponds with the model of the same name in MATPRO-11, Rev. 1. There is a potential for the specific heat to be influenced by gadolinia additions and by fuel burnup. A correction has been added for gadolinia additions, following the same format as for plutonia additions. No correction is made for burnup, based on the following discussion.

The heat capacity of nonirradiated urania-rare-earth mixtures has been measured for several years at Nagoya University, Japan, using direct heating pulse calorimetry (see Inaba et al.[1987] and Matsui et al. [1992]). For urania-rare earth mixtures simulating fission product accumulations for burnups up to 10 at.%, Matsui found a remarkable "excess heat capacity" (above that of undoped urania) for temperatures from 500 to 1200°C.

However, Lucuta et al. (1991) failed to find a similar increase in specific heat in the same temperature and simulated burnup ranges with SIMFUEL samples, which also simulate burnup via rare-earth additions to urania before sintering. Lucuta's samples simulated burnup up to 8 at.%. In addition, Takahashi and Asou (1993), attempted to confirm Inaba's findings for urania-gadolinia using drop calorimetry and differential scanning calorimetry. They could not reproduce Matsui and Inaba's "excess heat capacity"

and, in fact, concluded that for gadolinia contents up to 10 wt% and temperatures up to 1200°C, the specific heat of the urania-gadolinia mixtures were only slightly less than that of pure urania, i.e., 2 to 3%. They further concluded that the Nuemann-Kopp rule satisfactorily explained the small decrease in heat capacity for urania-gadolinia mixtures.

A similar statement can thus probably be made for high-burnup fuel pellets up to 8 at.% burnup. Thus, the only change to the fuel specific heat due to high burnup is a slight increase (of the order of 2 to 3%) based on gadolinia addition, calculated via the Nuemann-Kopp rule.

B.3 Cladding Thermal Properties

The thermal conductivity and specific heat of the Zircaloy cladding in subroutines CTHCON and CCP, respectively, do not appear to be significantly affected by the neutron fluence associated with extended burnup. No data have been found that indicates such an effect exists. A similar comment applies to the conductivity of the zirconium dioxide corrosion layer that forms on zircaloy cladding; however, there is considerable uncertainty in this conductivity. This oxide conductivity is currently under investigation by several organizations worldwide, and the current value used for oxide conductivity may change in the future based on these investigations.

B.4 Cladding Thermal Expansion

The cladding thermal expansion is calculated in subroutine CTHEXP. It does not correspond with the rather complex, texture-dependent application of single-crystal data recommended in MATPRO-11. Rather, it contains separate correlations for the diametral and the axial expansion data for Zircaloy-4 and Zircaloy-2 tubing presented by D.B. Scott (1965) and J.J. Kearns (1965), and the data for Zircaloy sheet expansion by Mehan and Weisinger (1961). A distinction is not made between the two cladding types.

B.5 Cladding Creepdown

The creep rate of Zircaloy cladding material is calculated in subroutine CREPR and does *not* correspond to the complex strain/stress models recommended in MATPRO-11. The creep rate is a correlation of creepdown data as a function of stress by Ibrahim (1973), with fluence dependence taken from Ross-Ross and Hunt (1968) and an activation energy temperature dependence taken from Fidleris (1968). This creep formulation is currently considered to be acceptable for application to high burnup LWR fuel. This is because the current model has a publicly available database, applies to the two major cladding types used commercially, and provides a reasonable estimate of LWR cladding creepdown based on the FRAPCON-3 assessment against high burnup commercial fuel rod data (Beyer et al. 1997).

B.6 Open-Gap Thermal Conductance, Gas Conductivities, and Thermal Accommodation Effects

The model for heat conductance across a given open fuel-cladding gap does not contain parameters that will be significantly affected by high burnup. The open-gap conductance in modern LWR fuel with helium fill gas pressures of at least 0.4 MPa (room temperature) depends mainly on the conductivity of the fill gas and released fission gases with no explicit burnup dependence.

The gas conductivity subroutine GTHCON was modified to update the pure-gas conductivity equations to those found in MATPRO-11 and to remove the Knudsen-domain (small-gap) correction for accommodation. This correction was never applied in FRAPCON-2 and is not applied in FRAPCON-3; however, accommodation at the gas-solid interface is accounted for by calculating a "temperature jump distance" extension to the gap size. This temperature jump distance is calculated as a function of gas composition, temperature, and pressure as derived from a literature survey by Lanning and Hann (1975), with a multiplier of 1.8 to adjust it to the extensive measurements by Loyalka (1974).

B.7 References

Beyer, C. E., D. D. Lanning, G. A. Berma, and K. J. Geelhood. 1997. *FRAPCON-3: Integral Assessment,* Nureg/CR-6534, PNNL-11513, Vol. 3, prepared for the U.S. Nuclear Regulatory Commission by Pacific Northwest Laboratory, Richland, Washington.

Fidleris, V. 1968. "Uniaxial In-Reactor Creep of Zirconium Alloys,"*J. of Nucl. Mater.*, Vol. 26 pp. 51-76.

Ibrahim, E. F. 1973. "In-Reactor Tubular Creep of Zircaloy-2 at 260 to 300 C,"*J. of Nucl. Mater.* Vol. 46, pp. 169-182.

Inaba, H., K. Naito, and M. Oguma. 1987. "Heat Capacity Measurement of $(U_{1-y},Gd_y)O_2$ from 310 to 1500 K," *J. of Nucl. Mater.*, Vol. 149, pp. 341-348.

Kearns, J. J. 1965. *Thermal Expansion and Preferred Orientation in Zircaloy*, WAPD-TM-472.

Lanning, D. D., and C. R. Hann. 1975. *Review of Methods Applicable to the Calculation of Gap Conductance in Zircaloy-Clad UO_2 Fuel Rod*. BNWL-1984, Battelle Northwest Laboratory, Richland, Washington.

Loyalka, S. K. 1974. "Temperature Jump Distance in a Gas Mixture,"*Physics of Fluids*, Vol. 17, p. 897.

Lucuta, P.G., R. A. Verrall, H. J. Matzke, and H. A. Tasman. 1991. "Microstructural Features of SIMFUEL - Simulated High-Burnup UO_2-Based Nuclear Fuel," *J. of Nucl. Mater.,* vol 178, p. 48-60.

Matsui, T., Y. Arita, and K Naito. 1992. "High Temperature Heat Capacities and Electrical Conductivities of UO$_2$ Doped with Yttrium and Simulated Fission Products." *J. of Nucl. Mate*r., Vol.188, pp. 205-209.

Mehan, R. L., and F. W. Wiesinger. 1961. *Mechanical Properties of Zircaloy-2*, KAPL-2110.

Ross-Ross. P. L., and C.E.L. Hunt. 1968. "The In-Reactor Creep of Cold-Worked Zircaloy-2 and Zirconium-2.5 wt.% Niobium Pressure Tubes," *J. of Nucl. Mater.* Vol. 26, pp 2-17.

Scott, D. B. 1965. *Physical and Mechanical Properties of Zircaloy-2 and Zircaloy-4*, WCAP-3269-41.

Takahashi, Y., and M. Asou. 1993. "High-Temperature Heat Capacity Measurements on (U,GD)O2 by Drop Calorimetry and DSC," *J. of Nucl. Mater.*, Vol. 201, pp. 108-114.